Experimental Investigations on Wickless and Wicked Multi-branch Heat Pipe in Different Orientations

A Thesis Submitted to

Nirma University

In Partial Fulfillment of the Requirements for

The Degree of

Doctor of Philosophy

in

Technology & Engineering

By

Bhatt Anandkumar Ambaprasad

(16EXTPHDE160)

Mechanical Engineering Department
Institute of Technology, Nirma University
Ahmedabad-382481, Gujarat, India

May 2023

Nirma University
Institute of Technology

Certificate

This is to certify that the thesis entitled **Experimental Investigations on Wickless and Wicked Multi-branch Heat Pipe in Different Orientations** has been prepared by **Bhatt Anandkumar Ambaprasad (16EXTPHDE160)** under my supervision and guidance. The thesis is his own original work completed after careful research and investigation. The work of the thesis is of the standard expected of a candidate for Ph.D. Programme in **Mechanical Engineering** and I recommend that it be sent for evaluation.

Date: 15/05/23

Signature of the Guides: Dr. Rajesh N. Patel Dr. Sanjay V. Jain

---

Forwarded Through:

(i) Head, Mechanical Engineering Department

(ii) Dean, Faculty of Technology and Engineering

19-5-23

(iii) Dean, Faculty of Doctoral Studies and Research

To:
Executive Registrar
Nirma University

20/05

Nirma University

Institute of Technology

Declaration

I, **Bhatt Anandkumar Ambaprasad**, registered as Research Scholar bearing Registration No. **16EXTPHDE160** for Doctoral Programme under the Faculty of **Technology and Engineering** of Nirma University do hereby declare that 1 have completed the course work, pre-synopsis seminar and my research work as prescribed under R. Ph.D. 3.5

I do hereby declare that the thesis submitted is original and is the outcome of the independent investigations / research carried out by me and contains no plagiarism. The research is leading to the discovery of new facts / techniques / correlation of scientific facts already known. (Please tick whichever is applicable). This work has not been submitted to any other University or Body in quest of a degree, diploma or any other kind of academic award.

I do hereby further declare that the text, diagrams or any other material taken from other sources (including but not limited to books, journals and web) have been acknowledged, referred and cited to the best of my knowledge and understanding.

Date: 15/05/2023

Signature of the Student

We agree with the above declaration made by the student.

Signature of the Guides: Dr. Rajesh N. Patel | Dr. Sanjay V. Jain

Nirma University
Institute of Technology

Certificate

This is to certify that the thesis entitled **Experimental Investigations on Wickless and Wicked Multi-branch Heat Pipe in Different Orientations** has been prepared by me, under the supervision and guidance of **Dr. R. N. Patel & Dr. Sanjay V. Jain**. The thesis is my own original work completed after careful research and investigation. The work of the thesis is of the standard expected of a candidate for Ph.D. Programme. The final hard bound copy of the thesis is submitted after incorporating all the suggestions / corrections suggested by the referees.

Date: 20/10/2023

Anand A. Bhatt (Student)

Date: 20/10/2023

Dr. R. N. Patel (Guide) **Dr. Sanjay Jain (Jt. Guide)**

Forwarded Through:

(i) **Dr. R. N. Patel**
Dean - Faculty of Technology & Engineering

27-10-23

(ii) **Prof. (Dr.) P. N. Tekwani**
Dean - Faculty of Doctoral Studies and Research

27/10

(iii) **Shri Ramachandran G. Nair**
Executive Registrar, Nirma University

Acknowledgement

I would like to thank all the people who made this doctoral study possible. Mentioning all people who deserve my gratitude without leaving someone out is quite a difficult task, but I will try to incorporate all the names at my level best.

I want to express my sincere gratitude to my supervisor **Dr. Rajesh N. Patel** (Director (i/c), dean, Faculty of Technology and Engineering, Nirma University) for his invaluable guidance, kind cooperation, infallible suggestions, constant encouragement and moral support throughout the research work. I would also like to express earnest thanks to my co-supervisor **Dr. Sanjay V. Jain** (Associate Professor, Mechanical Engineering Department, IT, NU) to trust my ability and to inspire me to work in the field of Heat transfer and Heat Pipes. He has always set high goals to make my research better and more and more fruitful. I am grateful to **Nirma University and management** for granting permission to pursue a Ph.D. and provide all the facilities to carry out my experimental study round the clock.

I am thankful to the members of my research progress committee, **Dr. Bharat Ramani** (Professor & Principal, Shri Labhubhai Trivedi Institute Engineering and Technology, Rajkot) and **Dr. Vikas J. Lakhera** (Professor, Mechanical Engineering Department, IT, NU) for their valuable suggestions and insightful comments given during my all the research progress seminars. I am very much thankful to **Dr. K.M. Patel** (HOD, Mechanical Engineering Department, IT, NU) for their constant motivation and support throughout the tenure of my study as an external PhD candidate.

I am thankful to **Shri. B. J. Patel** (Deputy Registrar, IT, NU) and **Shri. Dinesh Patel** (Assistant Registrar, IT, NU) for all the administrative support. I would also like to thank **Dr. P. N. Tekwani** (Director, DRI & Dean, Faculty of Doctoral Studies and Research) and the staff of the Ph.D. section especially **Ms. A. P. Prashya** and **Mr. Sachin Kikani** for their academic help and indirect support.

Experimental research couldn’t be possible without financial support. I would like to thank **Nirma University** (Project No: NU/PhD/MRP/IT/18-19/934) and **Mechanical Engineering Department** for a financial assistant to undertake this research.

I express my sincere thanks to office and lab staff of Mechanical Engineering Department such as **Mr. Alkesh Patel, Mr. Dharmendra Rathod, Mr. Sanjay Trivedi, Mr. Dharmendra**

Nayak, Mr. Ishwar Patel, Mr. Jayesh Panchal, Mr. Sameer Dave and Ms. Alka Darji for their continuous help during my study. I am also thankful to my students, **Neel Patel, Jaymal Godhaniya, Rohan Pandya, Jas Sahanand, Dipak Vaghela, Jiniyash Ranpriya, Jaimin Sachapara** for their helping hand during my research. I would like to thank **faculty members** of the mechanical engineering department for constant help, support, and motivation. My colleagues, **Dr. Absar Lakdawala, Dr. Shebaz Memon, Dr. Darshit Upadhyay, Prof. Tejas Raval and Prof. Ath Singhal** for their continuous moral support and technical help during my research.

I am also very much thankful to **Mr. Birju Shah and Mr. Devang Modi** for their industrial and manufacturing related support.

I express my gratitude to my father (**Shri A. K. Bhatt**), mother (**Shri N. A. Bhatt**), sister (**Hetal Bhatt**), wife (**Reena**) and my kids (**Krishiva and Mantra**) for their constant support and encouragement. I am also thankful to **God Almighty** for blessings.

At last, I extend my sincere thanks to **all** those who helped me directly or indirectly in the research work.

List of Figures

List of Tables

Contents

Abstract

In the recent years, due to miniaturization in electronics and space application systems, significant reduction in the size of electronics devices and circuits have been observed which subsequently increases the cooling requirement of heat transfer device. In an electronic circuit of laptops, supercomputers with multiple CPUs, spacecraft etc., it is required to arrange the cooling system for multiple heat loads in the smallest possible space in view of power saving opportunities. Heat pipes have been proven to be highly effective and simple cooling devices for electronics and spacecraft applications. Conventional heat pipes work on single source and single sink methodology. One source is in contact with an evaporator of heat pipe which absorbs heat and this heat is carried away to the condenser using working substance and rejected to the heat sink. However, the concept of single heat pipe for multiple heat source is the emerging idea in the research community as far as the space constrain and compactness is concerned.

In order to use single heat pipe for multiple heat source in electronics and space applications, a multibranch heat pipe with two evaporators and a condenser is developed. In the present study, initially, the experimental investigations are carried out on a wickless multi-branch heat pipe in gravity assisted mode. The start-up and dynamic characteristics are studied with different filling ratios (range: 40 - 70%), with equal heat loads (range: 0-200 W) and unequal heat loads (range: 0 -100 W) on evaporators. The results are analyzed in terms of temperature variation in axial direction, thermal resistance and heat transfer coefficient for a multi-branch thermosiphon heat pipe (MBTHP). It is found that the optimal filling ratio depends on the applied heat load under tested condition. In a thermosiphon mode, the heat pipe is capable of transporting maximum heat load of 210 W and maximum heat flux of 20.31 W/cm^2 with the maximum evaporator temperature lower than 100 °C. The minimum wickless thermal resistance of heat pipe is found to be 0.21 °C/W at 50% filling ratio and 160 W and maximum total heat transfer co-efficient is found as 6.33 kW/m^2 °C.

Moreover, a multibranch heat pipe with two evaporators and a condenser is developed with 20 internal grooves as a wick structure. Experimental investigation is carried out for axially grooved multibranch heat pipe (AGMBHP) by considering various parameters to obtain the best possible operating condition. AGMBHP is investigated for different filling ratios (range: 75% to 200%) in horizontal orientation for equal heat loads (0-240 W) and unequal heat loads (0-120 W) on evaporators. Heat pipe is tested for dynamic characteristic for optimum filling ratio range of 125% and 150%. Further, condenser cooling flowrate analysis is carried out to understand the performance of heat pipe. AGMBHP is capable to transmit 240 W heat load with a minimum resistance of 0.192 °C/W in horizontal orientation. The optimum condenser cooling water flowrate is found to be 5 ml/s under tested conditions. AGMBHP is capable to provide effective thermal conductivity as high as 31,824 W/m°C which is quite suitable for electronics cooling.

Further, experimental study is performed by considering four novel types of orientations i.e. (a) horizontal orientation (HO) (b) gravity assisted orientation (GAO) (c) anti-gravity orientation (AGO) and (d) compound orientation (CO) for AGMBHP with 20 grooves. Results are analyzed in terms of start-up characteristics and total heat transfer coefficient at different heat loads. Evaporator and condenser thermal resistances are calculated and analyzed for better understanding. It is found that the horizontal orientation results in the highest overall heat transfer coefficient (2.72 kW/m^2°C at 240 W) and comparatively lower evaporator temperatures (less than 100°C at 240 W). Maximum effective thermal conductivity is also achieved by horizontal orientation. It also resulted in lowest evaporator resistance (0.157 °C/W) and lowest condenser resistance (0.114 °C/W). Phenomena of temperature jump is observed, understood and elaborated for compound orientation.

Finally, the comparative investigation is carried out on multi-branch heat pipe with 20, 16 and 12 numbers of axial grooves by keeping the remaining parameters constant. Results are analyzed in terms of thermal resistance; convective heat transfer coefficient and start-up temperature rise for the optimum filling ratio of each individual heat pipe. It is found that the choice of optimum number of grooves depends on the amount of heat to be transported and the duty of heat pipe for a given application. However, for the representative heat load of 240 W, heat pipe with 20 number of grooves has been proven to be optimum with the lowest temperature rise of evaporator and the lowest overall temperature variation in axial direction.

Keywords: Heat pipe, multi branch, multi heat source, electronics cooling, axial grooves, orientation study, thermosiphon

Chapter 1

Introduction

Technology associated with heat pipe and its importance is presented in this chapter. The working principle of heat pipe and importance of different components is discussed. Major thrust areas of application are included in the chapter. Moreover, research motivation, research gap and organization of the thesis are elaborated in this part.

1.1 Background of the Study

At present, numerous modern applications demand a simple, effective, compact as well as reliable heat transfer solutions to transfer heat with high precision. Heat pipes have gained significant importance and popularity in this advanced era of high-power electronics, fast computing, space explorations and heat recovery.

1.1.1 Working principle of heat pipe

Heat pipe is basically heat transport devices by means of phase change of working fluid. The original idea of heat pipe was first discovered by Gaugler [1] in 1944 but the need of heat pipes in cooling requirements arose after almost 18 years in 1962 suggested by Trefethen [2]. However, it was George Grover [3] who gave the name “Heat Pipe” and used the sophisticated yet very simple version of heat pipe in their existing space program at Los Alamos National Laboratory, New Mexico [4] [5]. Heat pipes are very simple devices for transporting heat to large distances without much significant loss. Such characteristic of heat pipes makes them highly appreciable in broad areas of research and development as well as vast fields of applications.

Heat pipe consists of mainly three sections namely evaporator section, adiabatic section and condenser section. A required quantity of working substance is filled inside the heat pipe to undergo phase change by absorbing heat from the evaporator section and rejecting the same to the condenser section. Heat pipes are normally accommodated with porous structure inside the pipe wall in order to generate capillary for the return of liquid from the condenser section to the evaporator section. Such a porous structure is known as the wick structure. If the return of working substance is operated by gravity, heat pipes are generally known as thermosiphon heat pipe. However, in the space applications where gravity is absent, the wick structure becomes necessary for continuous circulation of the working substance. Moreover, as the wick structure provides enhanced capillary and higher heat pumping capacity, modern applications of heat pipes are nowadays provided with suitable wick structure[6]. The operating principle of the heat pipe is described in figure 1.1.

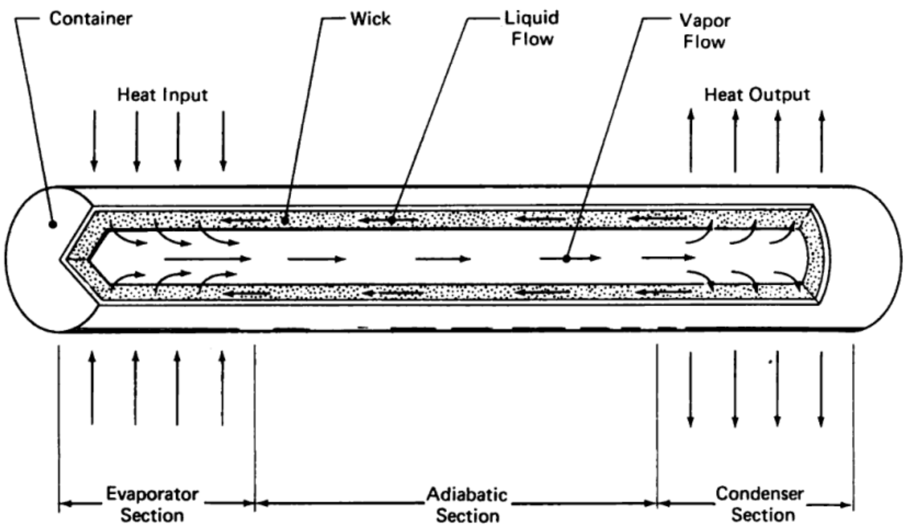

Fig.1.1 Operating principle of heat pipe [5]

1.1.2 Wick structure

As stated earlier, the wick structure is an important component as far as rate of boiling and condensation cycle of heat pipe is concerned. In many cases wicked heat pipes are superior compared to wickless heat pipes. The wick structure provides enhanced capillary which results in higher heat pumping rate and faster mass flow rate of working substance through any section of heat pipe [7]. It provides the required flow passage for the returning liquid and accommodates the heat flow through liquid vapor interface. Modern heat pipes apply various types of wicks in their operation. Wick structures are broadly classified (not limited to) in three categories. (1) wire mesh screen (2) sintered wick (3) grooved wick. Figure 1.2 shows the photograph of different types of wicks used commonly.

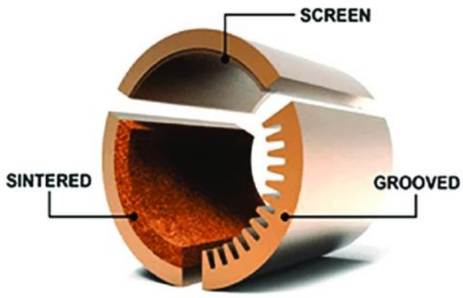

Fig. 1.2 Various types of wick structure [8]

1.1.3 Application areas of heat pipe

Heat pipes are simple yet very effective heat transport devices operated on the principle of phase change heat transfer. Due to the involvement of boiling and condensation, it provides very high heat transfer rates. Initially the applications of heat pipe were limited to aerospace industries. However, in recent years many researchers have found immense potential in different areas of heat transfer and applicability of heat pipes in modern engineering devices for cooling purpose. Some of the impactful areas are elaborated in brief.

Modern Computer Systems

Modern computer CPU and GPU need high cooling requirements due to fast operating speed and it is increasing continuously. Heat pipes are used to convey the heat produced by computer processors from load point to the environment.

Industrial Applications

Solar energy in the form of radiation is absorbed in the solar collectors. In evacuated tube collectors, solar energy is conveyed from absorber plate to water through multiple heat pipes. They are widely used in solar thermal water heating systems. Trans-Alaska pipeline system uses heat pipe in the support system of the pipe line containing oil to conduct heat generated by oil turbulence. Finned heat pipe systems have been used in the greenhouse application [4].

Energy Conservation

Immense possibilities lie in the area of heat recovery and energy conservation as the fuel prices continuously increases. Heat pipes have been proving to be the best tool due to high effectiveness in the area of energy conservation. Number of researchers and designers are finding innovative applications of heat pipe in the area of waste heat recovery in the form of heat pipe heat exchanger [9].

Spacecraft

Heat pipes have gained irreplaceable importance due to its capability of heat transport in the absence of gravity. They have been used in the temperature flattening as well as temperature control in spacecraft circuit cooling as well as cooling of space nuclear power sources.

Cooling of Electronic Components

The widest application area of heat pipes has been found in the cooling of electronics devices. Electronics components such as transistors, semiconductor devices and integrated circuit packages are nowadays accommodated with heat pipes for the cooling purpose. Heat pipes are the first choice for an electronic circuit designer for the heat dissipation. In modern era, where large number of heat loads are located on a single circuit board, sufficient cooling has become the most significant task [10].

1.2 Research Motivation

Though the technology associated with heat pipe is well proven and significantly developed, the demand of industries like high performance electronics, space, energy recovery and renewables are continuously increasing. High speed computer systems and high-performance electronic systems need constant improvements. The processors of cell phones and computer systems are becoming more and more powerful day by day. The reliability of such devices is largely dependent on its cooling requirements. Insufficient heat dissipation may lead over heating of the circuit which results in device failure. Moreover, the modern electronics and computing devices are getting more and more compact which results in large heat fluxes to be transmitted in a small available space in order to maintain the desired temperature. Compact size of a circuit board or integrated circuit contains large number of heat dissipation sites. The cooling technology associated with these large number of heat loads demands continuous improvement in cooling devices.

Conventionally, in electronics circuits and devices, one heat pipe is used to cool one heat source. However, due to increasing demand of high-performance, fast computing processors and run for compactness of system results in multiple heat loads in a small available space. Moreover, in space programs where available space is very small for the payload and electronics instrumentations, simultaneous cooling is required for more than one heat dissipating sites. Use of multiple heat pipes for each individual heat load do not serve the purpose of compactness wherever there is a space constrain. There has been an increasing interest in the last few years to use single heat pipe to absorb heat from multiple heat source. Number of researchers have started working in the area of heat pipe working under the influence of multi heat load evaporators. Indeed, it is necessary to understand the effect of various parameters on the operating condition of heat pipe applied with multiple heat loads. Authors have found a huge void in this area of heat pipe which motivated us to investigate on a heat pipe with multiple heat loads.

1.3 Scope of Work

Heat pipe is a simple device used to transport the desired amount of heat in order to maintain the temperature of an electronics circuit constant. However, the parameters affecting the performance of heat pipe are not as simple as the principle of operation of heat pipe. Moreover, in a conventional heat pipe with one heat source and one heat sink, the performance parameters are limited. In case of heat pipe with multiple heat sources, novel parameters are required to be investigated in order to predict the performance of the heat pipe. Moreover, in a heat pipe with multi evaporators, the distribution of heat load as well as distribution of the working substance becomes significant. [11]. A thermosiphon is the basic heat pipe operated by the effect of gravity [12]. The working substance returns back from the condenser to evaporator by means of gravity effect. A thermosiphon heat pipe when provided with multiple heat sources, the results obtained can be benchmarked for the development of the wicked heat pipe with multiple heat sources.

In a space mission, axially grooved heat pipes are more popular due to excessive vibration effects. Axially grooved heat pipes are used for cooling of electronics components as well as cooling of control devices in space missions [13]. Moreover, the behaviour of axially grooved heat pipe with multiple heat loads, under the influence of different parameters is a void area to be investigated. Filling ratio of the working substance in a heat pipe is one of the most significant parameters to be investigated [14]. Optimum filling ratio in heat pipe is capable to deliver optimum performance. The performance of heat pipe is largely dependent on different orientations. [15]. In case of heat pipe with multiple heat loads, orientation of heat pipe is completely different than a straight cylindrical heat pipe. Thermal resistance analysis becomes significant while deciding the performance of heat pipe. Moreover, in an axially grooved heat pipe with multiple heat loads, number of grooves plays an important role in the performance [16]. Generally, the heat pipe should absorb maximum heat flux while keeping the temperature of the sensor and simultaneously the thermal resistance, minimum in an electronics application. Moreover, heat pipes are also subjected to continuous variation in heat loads during its operation. The dynamic response of heat pipe with multiple heat loads gives the idea about the practicality of its performance.

Moreover, from the design and manufacturing stage to operation of the heat pipe, the condenser cooling requirement should be kept as low as possible for the power saving opportunities. From the proper design and experimental study, parametric study on above mentioned factors is to be investigated in order to obtain the optimum performance of heat pipe with multiple heat loads.

1.4 Organization of the Thesis

The thesis brings out the experimental investigation on the heat pipe with two heat sources and multiple branches. A “T” shaped heat pipe has been designed, developed and investigated for different heat loads. To investigate the performance of multi-branch heat pipe, an experimental set-up is developed suitable to multi source heat pipe. The water-cooled condenser is designed and applied as a heat sink. The details of the experimental set-up and investigations are elaborated in the subsequent chapters.

Chapter 2 presents the literature review of the heat pipe technology and objectives of the current study. It includes the significance of heat pipes in electronics and space applications and importance of various parameters in the performance of heat pipe operation.

Chapter 3 deals with the experimental studies of basic multi-branch thermosiphon heat pipe (MBTHP). The effect of different filling ratio, different heat loads on both evaporators (equal and unequal), thermal resistance, different vacuum level, overall heat transfer coefficient and steady-dynamic characteristics are elaborated in detail. The performance of MBTHP is optimized by considering above mentioned parameters.

Chapter 4 deals with the axially grooved multi-branch heat pipe (AGMBHP) with 20 number of axial grooves. The effect of different filling ratio, different heat loads on both evaporators (equal and unequal), thermal resistance, overall heat transfer coefficient and steady-dynamic characteristics are elaborated in detail. The performance of AGMBHP is optimized by considering above mentioned parameters. Moreover, AGMBHP and its performance is compared with MBTHP in terms of thermal resistance and effective thermal conductivity.

Chapter 5 includes the effect of different types of novel orientations of AGMBHP with optimum filling ratio and optimum condenser cooling water flowrate condition.

Chapter 6 elaborates the comparative study of AGMBHP having 20,16 and 12 number of axial grooves. The performance of AGMBHP is optimized in terms of numbers of grooves.

Chapter 7 presents the conclusions of the current study and the scope of further research.

Chapter 2

Literature Review

This chapter presents the historical progress of heat pipes, their types and heat transport limitations in a heat pipe. It also includes discussion on various parameters affecting the operation of heat pipes. The development of heat pipes for multi-heat source and their operation of working are also included in this chapter.

The heat pipe is proven to be one of the most reliable cooling technologies in many industrial and electronics applications. In modern era, where high speed computing and electronics sensors are increasingly getting miniaturized, large number of heat sources get concentrated in a very limited space. The multi-source heat pipe technology can be effective cooling technique for these devices. In this chapter, the technological progress and performance parameters of heat pipe are discussed. Moreover, the primary research performed by various researchers in the area of multi-source heat pipes is also presented.

2.1 Historical Development

As mentioned earlier, the concept of heat pipe was first introduced by Gaugler [1] in 1944 and patented as a lightweight heat transfer device which was a very basic version of heat pipe. During that time period, this technology did not require such a passive heat transfer device and much attention was not given to it [4]. Trefethen [2], in the form of patent application suggested the same device in 1962 and then by Wyatt [17] in 1963, after that, heat pipes once again came into the limelight. George Groove [3] and his coworkers at Los Alamos National Laboratory independently investigated the same concept for space program in 1964 after that heat pipes became more popular. Due to passive cooling characteristics and high heat transport capacity, heat pipes became much smaller compared to heat exchangers to handle high heat fluxes.

Early applications of heat pipes were limited to space based thermionic energy conversion systems, operating at more than 1500 K temperature [4]. Deverell and Kemme [18] in 1964 reported 410 W/cm^2 radial heat flux and 4 kW/cm^2 axial heat flux in their Ag-Ta heat pipe operating at 2273 K temperature. Grover [19] summarized the compatibility and life cycle studies of different combinations of heat pipe wall and working substance fluid in his work in 1964. Kemme [20] in 1966, conducted a study on characterizing Potassium and Sodium heat pipes with different wick structures and limitations of heat pipe in starting and operation [21].

Heat transfer via capillary movement of fluids refers to the process of a liquid flowing in a narrow space without the assistance of any external forces like gravity. The pumping action of surface tension forces may be sufficient to move liquids from a cold temperature zone to a high temperature zone. The subsequent return in vapor using a difference in pressure as the driving force, at the two temperatures and transferring heat from the hot to the cold zone. Such a closed system, requiring no external pumps, may be of particular interest in space reactors in moving heat from the reactor core to a radiating system. In the absence of gravity, the forces must only be such as to overcome the capillary and the drag of the returning vapor through its channels [3].

2.2 Operating Limitations to Heat Transport in a Heat Pipe

There are several restrictions that must be taken into consideration during design process for proper functioning of the heat pipe. Heat pipe should be able to handle the required heat flux in the given environment and the type of application. These limitations placed on the performance of heat pipes are described in following passages as summarised in Fig. 2.1.

1. Viscous limit: At low temperatures when the vapor pressure is also low, viscous resistance on the vapor flow may be more significant than inertial forces. Due to the reduced circulation of working fluid in this condition, the heat pipe's ability to transport heat is also constrained.

2. Sonic limit: The vapor velocity leaving the evaporator may equal to or exceed the speed of sound at low vapor pressures. In that case, the condenser pressure cannot be decreased beyond the limit. In other words, a vapor flow is choked which restricts the flowrate of working substance.

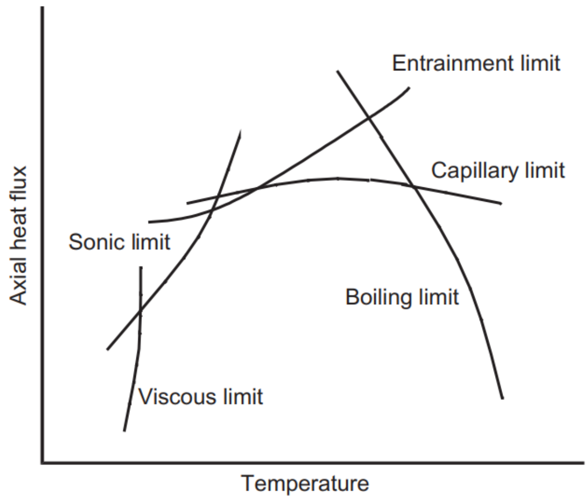

Fig. 2.1 Operating limits to heat transport in a heat pipe [3].

3. Capillary limit: A capillary structure can only enable circulation of a particular fluid to a limited extent. This limit is determined by the characteristics of working fluid and the permeability of wick structure.

4. Entrainment limit: The liquid in the wick, which flows against the vapor flow direction, experiences a shear stress from the vapor flow. Small liquid droplets are entrapped in the flow of vapor when the shear force is more than the liquid's resistive surface tension (Kelvin-Helmholtz instabilities). The liquid entrainment speeds up the flow of fluid but not the transfer of heat through the pipe. If the capillary force is unable to handle the increased flow, the wick in the evaporator may become dry.

5. Boiling limit: The nucleate boiling, which results in vapor bubbles in the liquid layer, may happen at high temperatures. The wick pores may be blocked by the bubbles, which will reduce vapor flow. Additionally, the presence of bubbles reduces heat transfer through the liquid layer, limiting the amount of heat that can transfer from the shell of heat pipe to the liquid via conduction alone.

2.3 Heat Pipes: Types and their Features

Various types of heat pipes have been designed and tested by the researcher community. The design of heat pipe depends on the type of duty and area of application. Some of the types of heat pipes and their special features are discussed here.

(a) Thermosiphon Heat Pipe: A thermosiphon or a wickless heat pipes are the most fundamental types of heat pipe which doesn’t require any wick structure for the return of liquid from condenser section to evaporator section. The liquid return is carried by gravity action. It becomes necessary to keep the condenser plane upper than the evaporator plane in order to execute proper liquid flow from sink to source. Thermosiphons are ordinary metal pipes with working substance filled inside for the phase change at desired pressure [12]. They are very simple in construction and easy to manufacture. However, their application is limited due to insufficient heat transport capacity for a given size. The obvious reason being the absence of capillary forces and dependency on gravity effect. Hence, these types of heat pipes do not find their application in space. However, due to their simplicity, they are still popular in passive heat transport devices in solar and electronics applications.

(b) Variable Conductance Heat Pipes (VCHP): The VCHP differs from other forms of heat pipes due to a special characteristic as shown in Fig. 2.2. It is frequently referred to as a particular variant known as the gas controlled or gas-loaded heat pipe. It is capable to keep a device at a constant temperature regardless of the amount of heat the device is producing. VCHPs are currently employed in a wide variety of applications, which include tasks like precise temperature calibration and standard electronics temperature control, as well as thermal control of satellite systems [21]. A sharp interface between working fluid vapour and the non-condensable gas was observed. As a result, the non-condensable gas effectively blocked off the condenser section it occupied, preventing any local heat transfer.

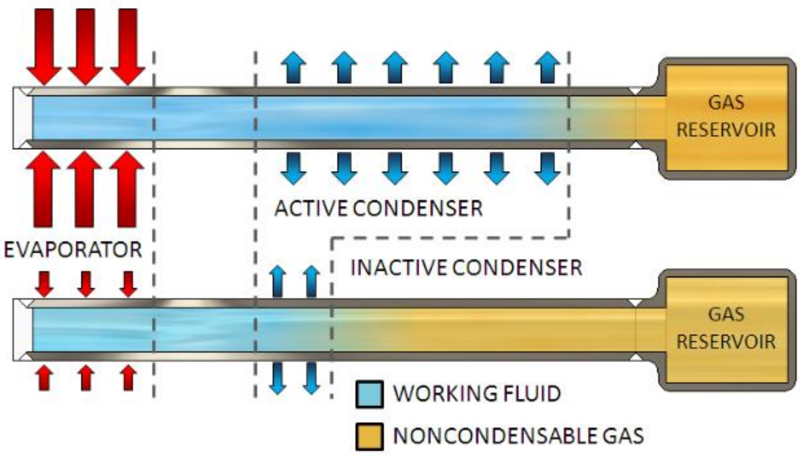

Fig. 2.2 Working of variable conductance heat pipe [22].

Significantly, it was found that the non-condensable gas interface moved along the pipe in response to the thermal energy carried by the working fluid vapour. It was therefore concluded that the gas interface could be strategically positioned to regulate the temperature of the heat input section within precise ranges.

(c) **Pulsating (Oscillating) Heat Pipe (PHP):** The pulsating or oscillating heat pipe consists of a capillary-diameter tube that is partly filled in with the working fluid and evacuated. The working of pulsating heat pipe (PHP) is presented in Fig. 2.3. A PHP typically consists of a capillary-sized serpentine channel that has been emptied and filled with the working fluid partially. Slugs of liquid and vapour bubbles are formed due to surface tension effects.

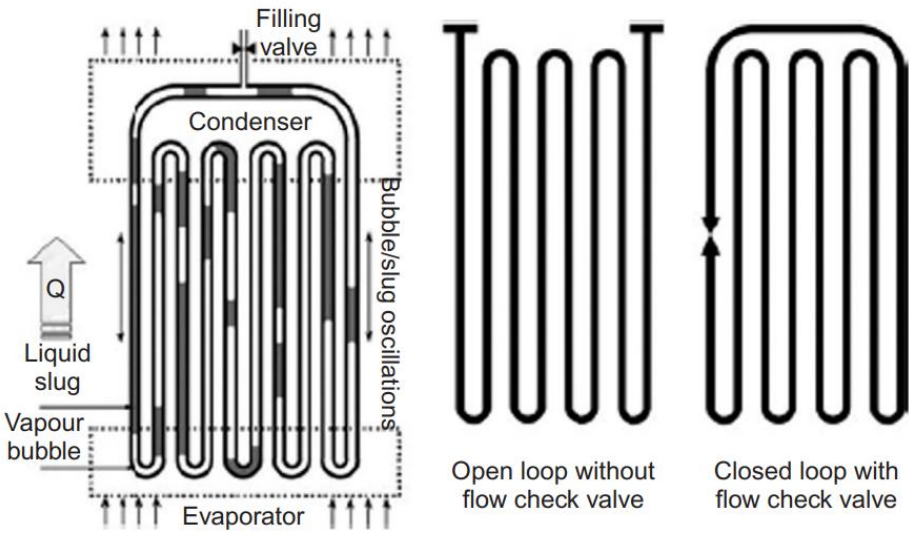

Fig. 2.3 Schematic diagram of PHP [6], [21].

In PHP, the vapour pressure is increased by the evaporation of working fluid in the evaporator zone increasing the size of bubbles. As a result, the liquid is pushed toward the condenser. When the condenser is cooled, the vapour pressure decreases and bubbles condense in that area of the heat pipe. The oscillating motion in the tube is caused by the expansion and contraction of bubbles in the evaporator and condenser sections, respectively [4]. Due to the fluid circulation that is superimposed upon the loop's oscillations, performance of closed-loop pulsating heat pipe (CLPHP) is better than open-loop devices.

It is reported that the addition of check valves could lead to further performance gains. But, intrinsic small size of the device, results in installation of such valves is challenging and expensive.

(d) Loop Heat Pipe (LHP) and Capillary Pumped Loop (CPL): The capillary head in the wick, which is adequate to counteract the pressure drop caused by the liquid and vapour flow and the gravitational head, is what allows a heat pipe to function as shown in Fig. 2.4. The wick must stretch the full length of a normal heat pipe in order for the system to function with the evaporator above the condenser in a gravitational field. The hydraulic resistance is directly proportional to the wick length and inversely proportional to the square of the pore radius. However, the capillary head P_c is inversely proportional to the effective pore radius of the wick but does not of length. Thus, if one wants to increase the length of a heat pipe against gravity, a reduction in pore radius is necessary to provide the required capillary head. However, this results in an increase in the liquid pressure drop. The contradictory effects of reducing the pore size of the wick limit the length at which heat pipes operating against gravity can be successfully designed. In similar way, the requirement for the liquid to flow through the wick restricts the total length of the conventional wicked heat pipe. [21]

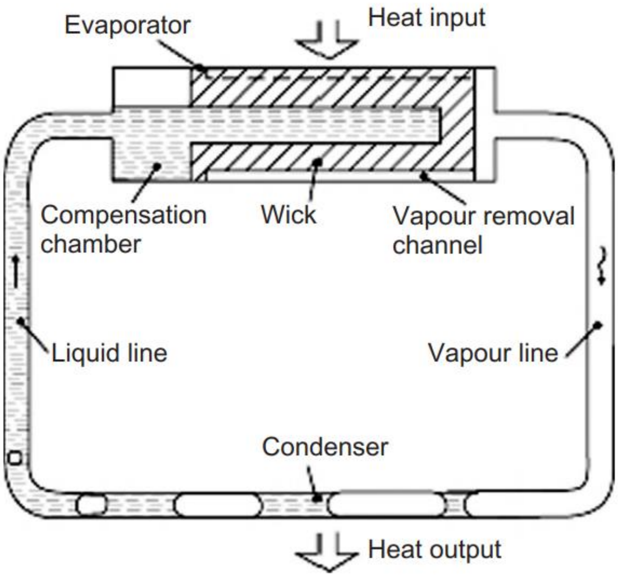

Fig. 2.4 Operating principle of loop heat pipe (LHP) [9], [10]

The inherent difficulty of combining a long wick with a small pore radius in a typical heat pipe led to the development of LHPs and CPLs. In transient state, there is enough liquid to fill the liquid and vapour lines, the condenser section, and the evaporator section. There is also enough liquid in the compensation chamber and evaporator to saturate the wick. Fluid evaporates from the surface of the wick when a heat load is applied to the evaporator. But, because the wick exhibits a significant thermal resistance, the temperature and pressure in the compensation chamber are lower than those in the evaporator. The wick's capillary force stops the vapour from moving from the evaporator to the compensation chamber. The liquid is displaced from the vapour line and the condenses. It returns to the compensation chamber with the increase in pressure differential between the evaporator and the compensation chamber.

(e) Rotating Heat Pipe: In a rotating heat pipe, the condenser and evaporator are separated by direction of rotation axis as shown in Fig. 2.5. Like the conventional heat pipes, it is also divided in three regions viz. evaporator region, adiabatic region and condenser region. The liquid flows from the condenser region to evaporator region by the centrifugal force of rotation i.e., $r\omega^2$.The component $r\omega^2 \sin\alpha$ along the direction of wall causes the liquid to push towards evaporator region to provide necessary capillary as shown in Fig. 2.5 [4] The centrifugal force is the most important parameter in this type of heat pipe in order to decide the different regions. Moreover, centrifugal force is developed by the rotational speed. These heat pipes are applied in the gas turbines for the blade cooling in order to prevent the blades from overheating and thermal stresses.

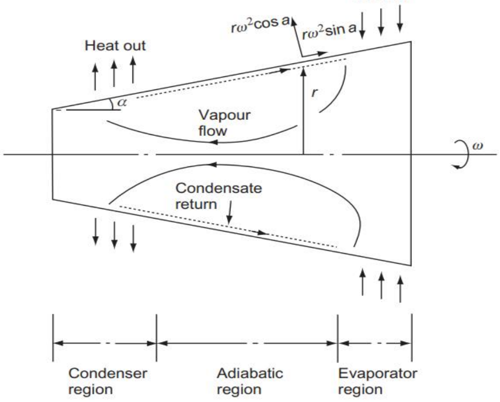

Fig. 2.5 Operating principle of rotating heat pipe[6], [10].

2.4 Cooling of Electronics and Space industry

All the significant types of heat pipes discussed above, are classified as per their working principle, operating condition and their need in a particular application. However, in the modern era, there is a continuous demand of improvisation in the heat pipe technology due to more and more complex systems. In the past few years, miniaturization in electronics and space thermal control systems caused significant reduction in the size of electronics devices and circuits which subsequently increased the thermal duty on cooling devices [23]. Various heat pipes have been proven to be effective, efficient and simple devices for electronics and spacecraft thermal cooling applications [24]. In the recent years, technology associated with heat pipes have shown significant and rapid advancements as far as size, shape, types and heat transport capability are concerned [25]–[27]. Conventional heat pipes work on single source and single sink methodology. One source is in contact with an evaporator of heat pipe which absorbs heat and this heat is carried away to the condenser using working substance and the same is rejected to the heat sink. Modern heat pipes are the extended versions of the basic types of heat pipes discussed above as per the applications [28]. In the electronics, high speed computing and semiconductor devices, despite of being impressive progress in the last few years, the future challenges in the thermal management are still serious. Figure 2.6 shows maximum heat flux and power dissipation for microprocessor chips in past couple of decades [29].

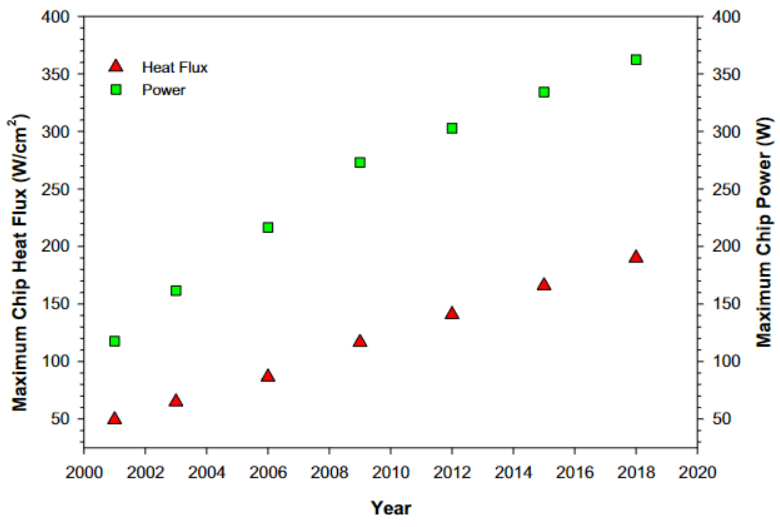

Fig. 2.6 Maximum heat flux and power dissipation for microprocessor chips [29]

As a result of the miniaturization in electronic industry, medium-scale integration (MSI) with 50–1000 components per chip, large-scale integration (LSI) with 1000–100,000 components per chip, and very large-scale integration (VLSI) with 100,000–10,000,000 components per chip emerged in the 1960s, 1970s, and 1980s, respectively [29]. Researchers are trying to decrease the size and increase the speed of semiconductor devices for better performance. This results in high operating temperatures and power densities, as well as poor performance and a short lifespan for the electronic devices. Component and device temperatures keep rising if heat rejection is not equal to or more than the rate of heat generation. This drastically decreases the reliability and performance resulting in device failure [29].

Moreover, modern devices contain multiple heat dissipating sites in a very small area as far as electronics applications are concerned. It includes servers with processors, memory modules, chipsets, power supplies and voltage regulators. Processors are the most stringent heat generating units for cooling due to very high heat fluxes. Individual processor heat loads have become between 140 and 190 W in normally operating servers and between 210 and 300 W in high performance computing (HPC) applications by the year 2020 [30].

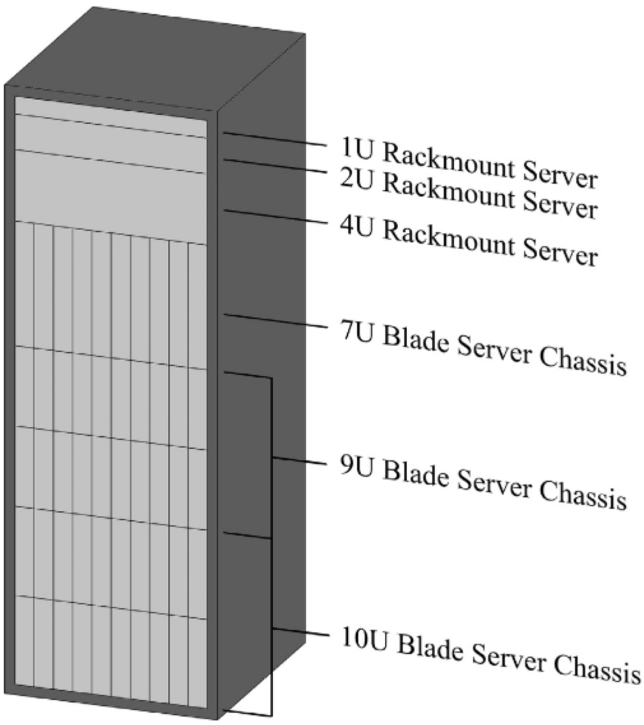

Fig. 2.7 Common types of servers with different size [30].

Moreover, electronic gadgets today contain a growing number of heat sources due to ongoing advancements in downsizing and integration. A computer might have several CPUs, for instance, and several high-power chips might be packaged on the same PCB. A heat dissipation technique using several heat pipes is typically used for these multi-heat source systems [31].

From the above discussion, it is understood that there is an immense need to investigate the possibilities of heat pipes having multiple heat sources. Such type of heat pipes can accommodate multiple heat sources simultaneously allowing the space constrain limitations. The purpose of miniaturization and integration along with high power heat dissipation can be served by the heat pipe having multiple heat loads. Few researchers have started working in the area of heat pipes with multiple heat loads in the last few years [32]–[36] Albeit, limited work has been performed on a single heat pipe with multiple heat sources. Moreover, for a conventional heat pipe, it is found that the performance of heat pipe depends on many parameters like filling ratio, maximum heat flux capacity, thermal resistance, maximum start-up temperature, start-up time, cooling requirements, dynamic response, quick starting ability etc. The influence of these parameters and their effect of a heat pipe with multiple heat sources is again another unexplored area. In a nutshell, the parametric study on a heat pipe with multiple heat sources is necessary at this point of time to understand its performance for future applications.

2.5 Recent Development in Multi Heat Source Heat Pipes

As discussed earlier, few researchers have started working in the area of multi-heat source heat pipe and electronics cooling. Their contribution is described in the following sections in brief.

Wang et al. [25] investigated the potential of multiple heat pipes in CPU cooling and found 66.2% fan power saving with multiple heat pipes in comparison with conventional heat sink. Although, whenever available space constrain may not allow user to accommodate multiple number of heat pipes as in case of electronics and spacecraft applications for individual source, it becomes necessary to rethink and redesign the thermal management system. Continuous evolution of miniaturization pushes the heat pipe technology towards more and more challenging heat transport duties. A few investigators have started working on the multiple heat source thermal management problems in last few years.

Tang et al. [32] investigated on a conventional heat pipe having multiple heat sources and provided with cooling at both the ends as shown in Fig. 2.8. Heat pipe was intended for the application of the spacecraft. The investigation was carried out on the performance of grooved heat pipe by placing two water coolers at both ends of the heat pipe and multiple numbers of heat sources in the middle. Authors considered the effects of different water flow rates (1.5-3.5 lit/min), heat inputs (5-60 W) and power distributions. It was concluded that under variable heat load, temperature of each section becomes steady without much variation and it became operational in a short period with higher heat carrying capability compared to the heat pipe operated conventionally.

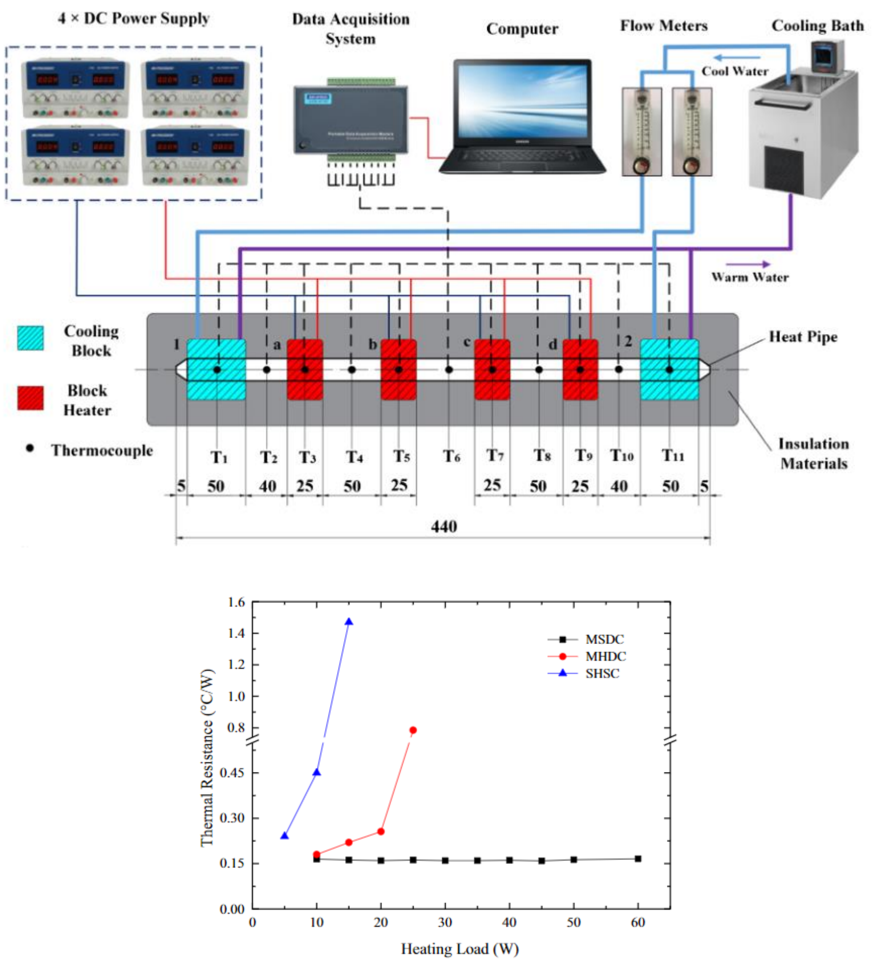

Fig. 2.8 Schematic diagram of multi-source double end cooling set-up and variation in thermal resistance [32].

Lower thermal resistance was reported in case of MSDC (multi-source double end cooling) than MHDC (middle heat source double cooling) and SHSC (single heat source and single cooling).

Boo et al. [37] investigated on a copper heat pipe having wire screen mesh as a wick structure with distilled water as a working substance with 100% and 120% fluid charge ratios based on the volume of wick void. It was kept at 45° inclination with gravity assisted mode. Multiple and varying heat loads were applied using five heat sources placed along the heat pipe length. The performance of heat pipe was optimized for the parameters like fluid ratio, uniform heat load and thermal resistance.

Han et al. [38] developed a novel flat plate heat pipe with multiple sources capable of transporting high heat flux with the lowest thermal resistance of 0.103 °C/W for three heat loads and 4.5 m/s cooling air velocity and 90° inclination. The heat pipe was able to convey 400 W heat with 65 °C maximum temperature. However, due to number of condensing zones and large number of fins, the size of heat sink was significantly large.

Laura et al. [34] investigated on a novel loop heat pipe with multiple heat source arrangements for electronics cooling. The miniature heat exchangers were provided and two condensers with refrigerant R245fa as a working substance. Their goal was to compensate multiple heat sources with variable heat and temperature duty.

Okutani et al. [39] developed looped heat pipe with two evaporators and wick structure with high porosity. The stability of heat pipe was tested by applying equal loads (40/40 W) and variable loads (0/50 W). It was found that the complexity and cost related to a loop heat pipe should also be considered along with its heat transport capacity.

Wang et al. [14] performed the experiments to understand the effects of filling ratio (10-60%) and types of working fluid on the operation of miniature heat pipe. It was concluded that miniature heat pipe with 20% filling ratio gave better performance since thermal resistance was the least among all the filling ratios and the heat pipe having working fluid as methanol provided the better performance compared to acetone and R141b.

Sedighi et al. [40] suggested a pulsating heat pipe (PHP) with an extra branch. It was used to improve the circulation of working fluid by creating secondary bubble pump. Experiments were conducted on the performance of conventional PHP and PHP with an extra branch by varying inclination angles and filling ratios. The analysis concluded that by using filling ratios of 40% and 70%, performance of the novel PHP was found better than the conventional PHP in the vertical orientation. The thermal resistance decreased up to 29% in comparison with PHP for inclination angle of 30° and 60° and an additional branch improved the thermal operation of PHP in the horizontal orientation since pulsating heat pipe cannot work in the horizontal position.

Pastukhov et al. [41] designed and developed an ammonia-based loop heat pipe for the cooling of multiple heat loads. Two heat loads were kept on liquid channel and one on vapour channel. The maximum heat load capacities were observed to be up to 120 W for main evaporator, 34 W total for both liquid line evaporators and 9 W for vapour line evaporator.

Liu et al. [42] prepared experimental setup for flat plate oscillating heat pipe with dual serpentine and multi-heat source for electronics application. Experiments were conducted for various angle of inclination and heat loads with uniform heat power located at the middle of heat pipe and air cooling at the end. Authors found that heat pipe works steadily under all inclination angles from 0° to 90°, temperature in between 41°C to 46°C, with respect to increment in the heat load. Authors found that its overall thermal conductivity was much higher than the average value. The overall performance of heat pipe concluded its application in electronics cooling with number of heat sources.

Zhang et al. [43] developed axial swallow tailed micro grooved heat pipe with multiple evaporators and looped water-cooled condenser section as shown in Fig. 2.9. It was found that heat pipe had better isothermal conductance with low temperature difference between evaporator and adiabatic portion. As heat load increased, the temperature gradient also increased between adiabatic to evaporator section and adiabatic to condenser section. For the same length of heat pipe, steady temperature was found to be dependent on the length of the condenser section. The layout of the heat sources significantly affected the optimum working of heat pipe. The maximal heat transmission capability enhanced with decreasing distance between heat source and heat sink while the length of the evaporating and condensing section remained constant. The input power reached the limit of heat transfer, the temperature at the beginning of the evaporating section increased sharply. Whereas, the heating power reached the maximum heat transport capacity and the heat source was away from the starting, the temperature at the source site was higher than the typical operating temperature. The heat pipe was able to reach a new steady state.

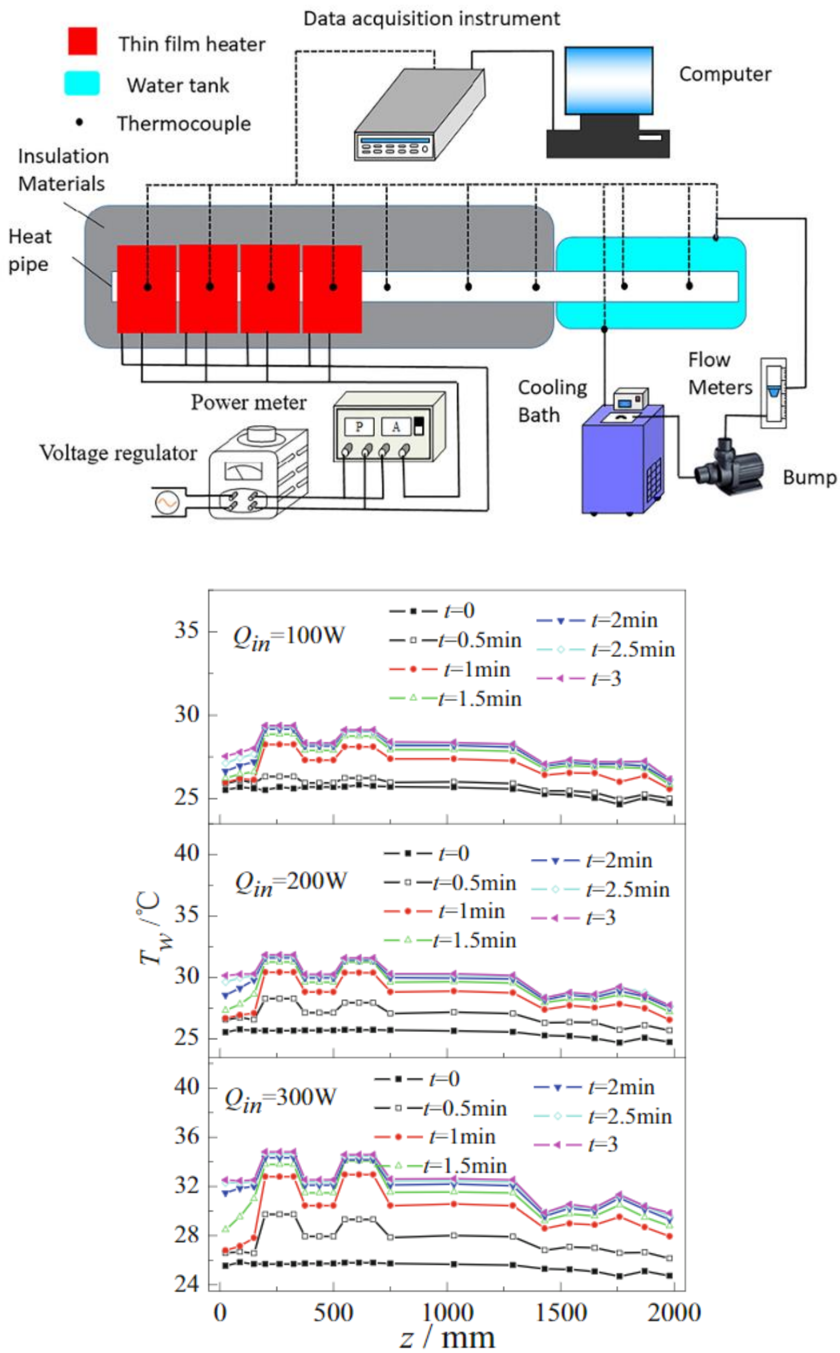

Fig. 2.9 Schematic diagram of multi-source set-up and transient axial distribution no.2 and no.4 heat sources during start-up [43]

Mashaei et al. [44] proposed numerical model for the analysis of cylindrical heat pipe with multiple heat sites by applying Al_2O_3 nanofluid as a working substance. In their study, volume fraction of nanofluid was taken as 0, 2.5, 5 and 0.075% with heat load of 14, 28, 56 and 112 W respectively. It was observed that if volume fraction is 5% and heat load is 112 W, the thermo-hydraulic performance was improved in all the cases.

Porosity of wick structure and size of particle also influenced the performance when different volume fractions of the nanofluid were considered. When more volume of nanofluid was employed, the thermal resistance of heat pipe reduced significantly.

Huang et al. [45] proposed and developed flexible Y shaped heat pipe with one branch as evaporator and two branches as air cooled condensers. Results showed that flexible branch heat pipe had a higher heat load and cooling capability compared to the straight heat pipe. From their analysis, it was concluded that if the operating temperature was set as 60 °C, then maximum heat load of the heat pipe was around 25 W, which was 92% higher than the straight one. When filling ratio was kept as 45%, the performance of heat pipe in anti-gravity orientation was found comparatively better.

Nguyen et al. [46] designed and produced dual flat evaporator heat pipe. Wick structure was made by hydrophilic polytetrafluoroethylene porous membranes with water as a working fluid. Experiments were performed for six different orientations within heat source temperature limit of 130 °C and natural convection condensation. Heat pipe worked satisfactorily between 40 W to 140 W in each orientation. Experimental analysis concluded that the minimum thermal resistance was 0.34 °C/W at 140 W.

Zied et al. [47] developed experimental setup for axially grooved heat pipe and its network conduction model for simulation of heat transfer in wall. Temperature sensors were placed vertically and horizontally for measurement of temperature gradient at evaporator section. Top grooves of evaporator section got burnout compared to the bottom grooves due to gravity effect and resulted in increase in the operating temperature. When operating temperature was increased then puddle expansion took place at the bottom grooves.

Anand [13] performed experiments for axially grooved heat pipe with different working fluids such as methane, ammonia and ethane. It was found that when there was undercharge of working fluid, heat transport capability decreased due to less volume of liquid compared to nominal charge. The wetting angle at groove surface was found to be independent from gravity but dependent on heat flux. When evaporator heat flux was increased, apparent contact angle became higher causing lower capillary pressure at grooves and dry out occurred.

Huang et al. [48] proposed and investigated “L” shaped copper heat pipe with ethanol as a working substance. Their investigation comprised of comparison of various types of wicks with grooves, partially hybrid mesh and fully hybrid mesh grooves. It was found that the partially hybrid mesh wick outperformed the other two wicks at evaporator section under the tested conditions.

Jiang et al. [49] developed phase change flattening process for the fabrication of axially grooved heat pipe. Authors used elasto-plastic FEM simulation for the analysis of stress and strain distribution during flattening process. It was found that vapour pressure inside grooves is the key factor during the flattening process.

Liu et al. [36] developed a large area cryogenic loop heat pipe for space optical telescope as shown in Fig. 2.9. It had 1 m^2 of heat exchange area but average temperature performance was found to be lower than 5 K. Heat pipe was capable to start-up and operate normally under anti-gravity condition. The large area multi-heat source heat pipe was having working range around 80 K to 120 K.

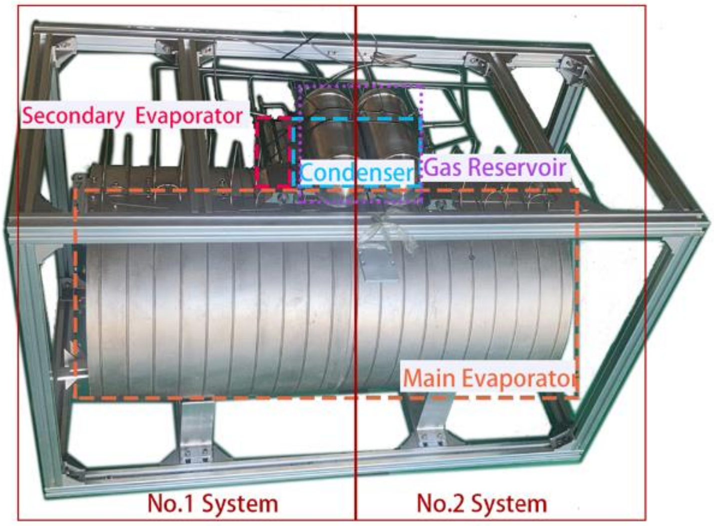

Fig. 2.10 Photograph of cryogenic loop heat pipe (CLHP)[36].

Subedi et al [50] presented the theoretical investigation on heat pipe with multi-heat source and heat sink. Authors considered the flat micro heat pipe and provided the analytical solution based on modified liquid pressure drop. The analytical model was presented based on the effect of mesh wick geometry on the maximum heat transfer rate. The mesh wick fiber diameter, fiber separation distance and wick thickness were identified with the model as key parameters which influenced the heat transfer rate of flat micro heat pipes (FMHP).

Biao et al. [35] addressed the heat dissipation issue of many heat sources by the design of a heating region of 190 mm x 90 mm huge flat-plate loop heat pipe as shown in Fig.

2.11 and briefly discussed the design process. The heat transfer between the compensation chamber and the ambient was improved by heat dissipation fins, placed on the rear side of the compensation chamber. Fins were composed of aluminum alloy. Acetone was used as the working fluid, and stainless-steel wire mesh served as the porous wick. As a heat source, six ceramic heating blocks were used. The findings demonstrated that the system could operate regularly between 20 W and 140 W while maintaining a heating surface temperature of less than 90°C. The experiment involved altering the conditions for heat dissipation on both the condenser and evaporator sides. The system equilibrium temperature difference generated by the air ventilation of the condenser was changed when the heat load was kept as 120 W and the ambient temperature remained constant. It was found to be smaller than the heat dissipation of the evaporator under the same circumstances. The minimal thermal resistance of 0.032 °C/W was reached at the heat load of 120 W, and the evaporator's thermal resistance dropped as the heat load increased.

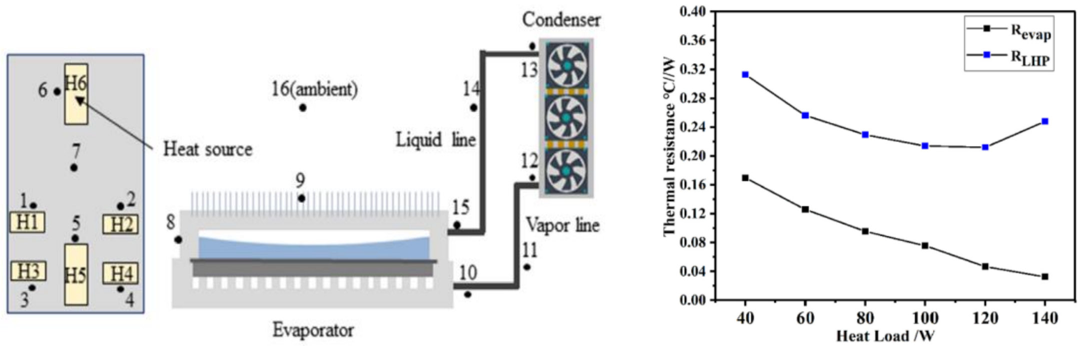

Fig. 2.11 Schematic diagram of the test set-up and dependance of thermal resistance on heat load [35]

Tong et al. [51] experimentally investigated on a novel loop heat pipe with multiple evaporators for high power thermal devices. Three flat disc evaporators were applied with three separate vapor lines as shown in Fig. 2.12. Author studied about the interaction, tilt angle and variable heat loads for these vapor lines. The gravity-assisted angle changed the non-uniformity of the liquid distribution, which had an impact on the startup procedure. The greatest performance was increased for tilt angle θ=2° by 77% compared to the gravity-assisted tilt θ =10°. The peak load was approached up to 300 W. The findings of the current study reported the broaden use of loop heat pipes with flat surfaces to address problems, involving multiple heat sources.

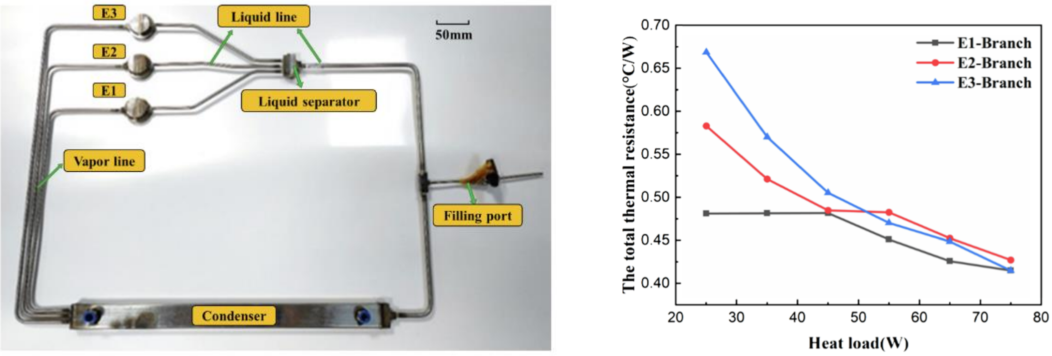

Fig. 2.12 Flat disc multi evaporator loop heat pipe (ME-LHP) and dependance of thermal resistance on heat load [51]

Valentine et al. [52] designed and developed a three leg multi-channel heat pipe to understand the two-phase heat transfer by experimental, theoretical and numerical approach. The Volume of Fluid (VOF) technique and Lee model were applied in order to simulate the heat pipe operation with ANSYS Fluent. The influence of the condenser's boundary condition, saturation temperature, and mass transfer coefficient were investigated. Several types of Lee models employing user defined function (UDF) were examined. Major limitations of the Lee model for the simulation of heat pipes were identified for the first time. In light of the Lee model's slow physical meaning and ease of manipulation, it was argued that model was unable to accurately estimate the temperature of a heat pipe.

Cai et al. [33] developed multi-branch heat pipe with multi-heat source evaporator section as shown in Fig. 2.13. Authors used copper sintered powder as a wick material. The heat pipe was comprised of three branches, two for evaporator section and one for air cooled condenser section. From the experimental analysis, it was found that filling ratio made impact on the heat transport capability of heat pipe. Optimum filling ratio was obtained between 75% to 100%. The heat pipe was capable of transporting maximum 200 W heat load and minimum thermal resistance of 0.04 °C/W was obtained (Fig. 2.14) at 160 W heat load, with maximum peak temperature of 110 °C.

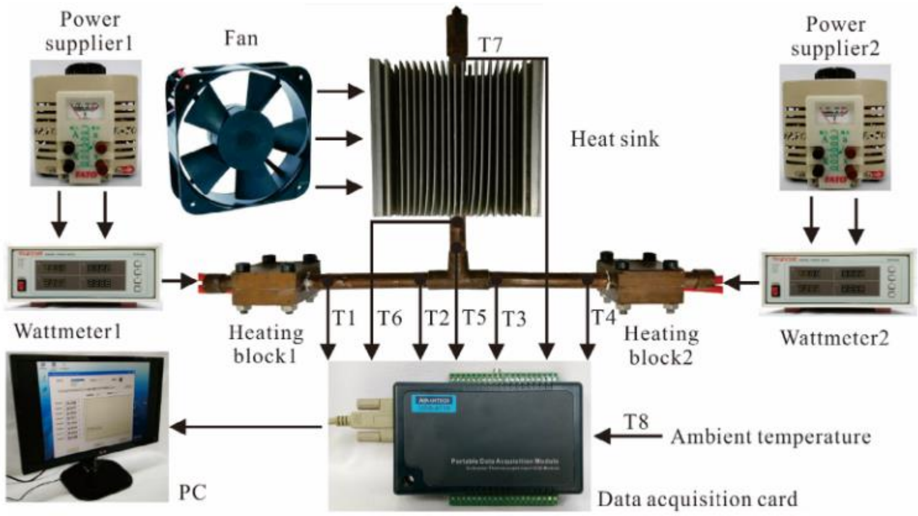

Fig. 2.13 Schematic diagram of multi-branch sintered heat pipe set-up[33]

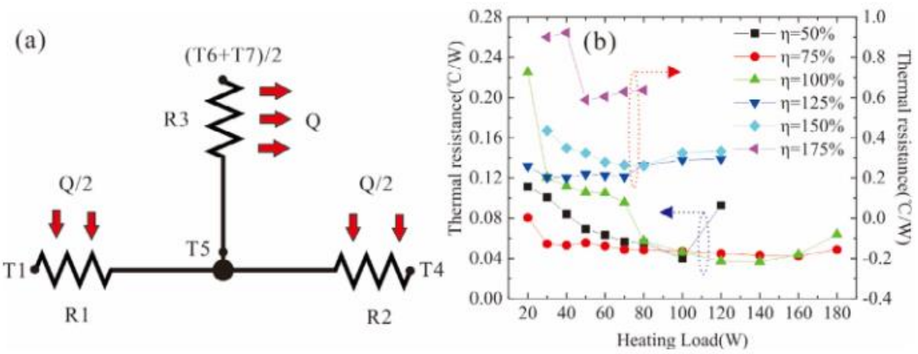

Fig. 2.14 (a) Thermal resistance network (b) Variation in thermal resistance with respect to heat load [33].

Zhong et al. [53] proposed multi-branch heat pipe (MBHP) with dual heat sink on longer branch and single heat source on shorter branch with sintered wick as shown in Fig. 2.15. The investigations were carried out for MBHP by changing various orientations and various particle sizes of copper powder in the sintered wick. The maximum heat transport capacity and the minimum thermal resistance were found to be 80 W and 0.042 °C/W respectively among all the orientations. MBHP with 75-100 μm particle size of copper powder and gravity assisted orientation (GAO) resulted in better performance compared to other particle sizes and orientations respectively as shown in Fig. 2.16.

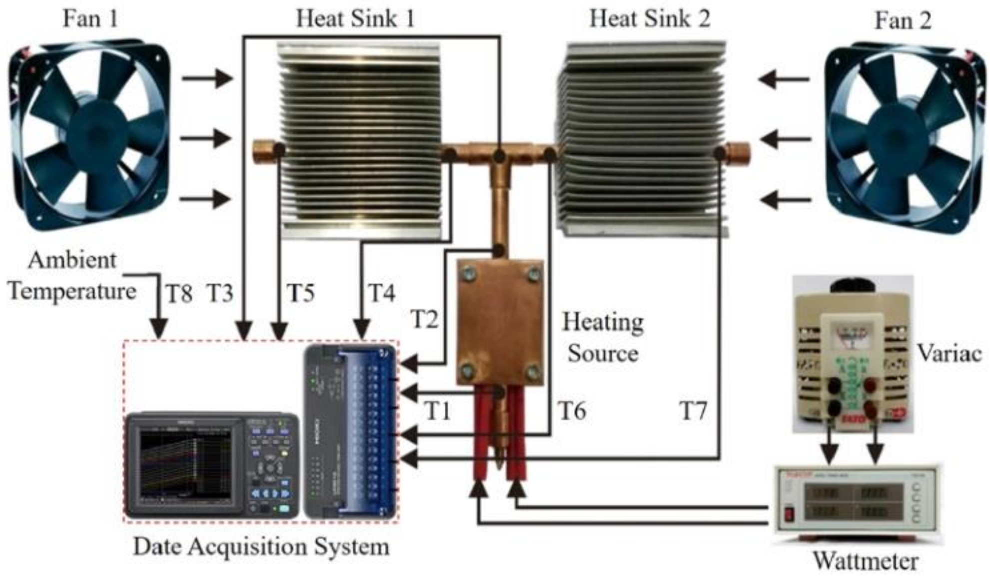

Fig. 2.15 Schematic diagram of multi-branch heat pipe orientation study[53]

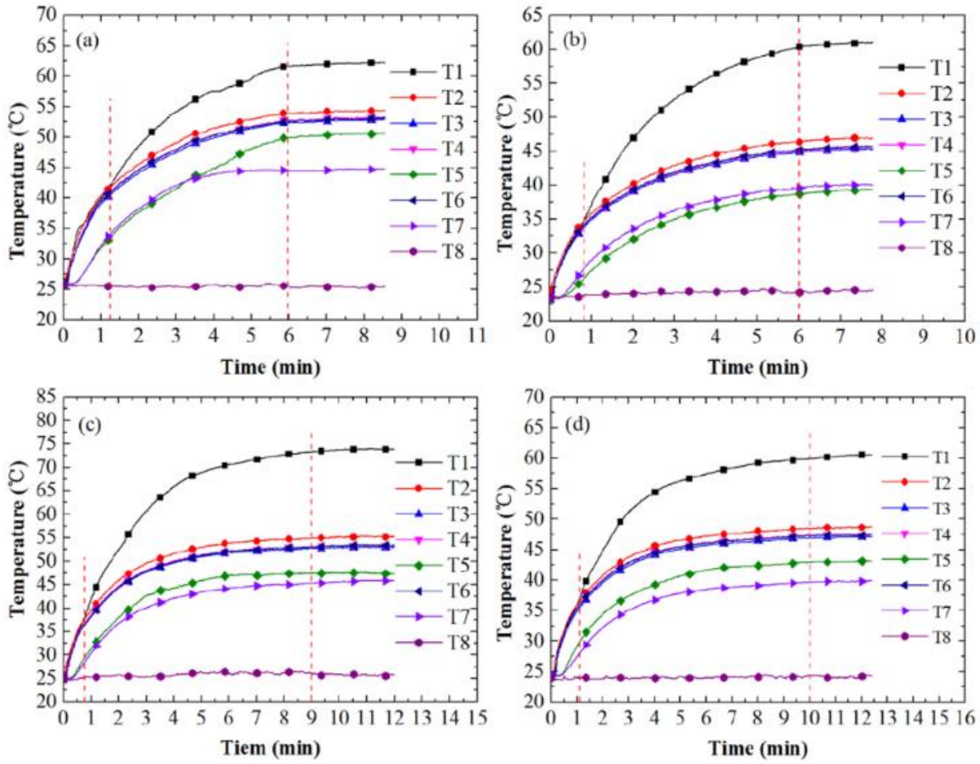

Fig. 2.16 Start-up characteristics of (a) GAO (b) AGO (c) HO (d) CPO[53].

2.6 Limitations and Recommendation

The above discussed literature of experimental and numerical study on heat pipes with multiple heat sources revealed that the performance of heat pipe having multiple heat loads is encouraging. However, limited research is available in the multi-branch heat pipe as mentioned in Chapter 1. Moreover, it is understood that an unconventional experimental set-up is required to be developed to investigate the effect of various parameters as far as heat pipe with multiple heat sources are concerned. No research has been performed by any author on a thermosiphon heat pipe with multiple heat sources and multiple branches. In case of conventional heat pipes, sintered wicks are very common. However, in case of multi-branch heat pipe, manufacturing of sintered wick is very difficult process. Moreover, in spacecraft electronics and thermal cooling, sintered wick is not suitable due to excessive vibrations [32]. Moreover, very limited study is available on multi-heat source heat pipe with different orientations. Specifically in a multi-branch heat pipe, it is important to define and investigate the effects of different orientations like both evaporators under gravity, one evaporator under gravity, both evaporators under anti-gravity etc. Moreover, axial grooves are proven to be better option as far as space and electronics cooling is concerned [54]. The manufacturing of axial grooves is comparatively easy and provides reasonably good capillary force [55]. However, investigation on optimum number of axial grooves in a multi-branch heat pipe is another area to be explored. In a conventional cylindrical straight heat pipe, the effect of different parameters is quite different than a multi-branch heat pipe having "T" geometry and with multiple heat sources. All the required performance parameters should be investigated from the scratch in a multi-branch heat pipe with axial grooves [56].

Moreover, From the literature review, it was understood that the optimum filling ratio was one of the most important parameters to be determined at the initial stage before putting the heat pipe in use. It was observed that the optimum filling ratio resulted in optimum performance of heat pipe [57]. Moreover, very few researchers have explored the effect of vacuum level on the performance of an unconventional heat pipe. When a heat pipe with multiple heat sources is subjected to variable heat loads, which is a usual case applied to electronics cooling, its performance gives the idea of practicality of heat pipe. In a multi-branch heat pipe, due to multiple evaporators and variable heat loads, the effect of temperature and thermal resistance can be understood when applied to different vacuum levels. From the literature review, it was observed that the multi-branch heat pipe with multiple evaporators is subjected to operate under dynamic conditions, the stability of operation of heat pipe provides the actual operating range and its applicability in actual condition [58]. The thermal resistance, heat transfer coefficient and effective thermal conductivities are the important performance parameters to be investigated in case of multi-branch heat pipe. The effectiveness of heat pipe as a heat transport device is decided by these parameters [59].

2.7 State of the Art of the Current Work

The technological advances in the field of heat pipe demands continuous improvisation in the design and applications. Heat pipes and their performance evaluation techniques are experimental, numerical, analytical and theoretical in nature depending upon the area of application [60]. Heat pipes have found their way in the fields of building construction, energy sectors of the buildings and building envelopes as well. Heat pipe integrated building structure can utilise the low-grade energy in efficient way to improve indoor thermal comfort environment [61]. The current scenario in the transportation sector resulted the developments of electric vehicles so rapidly that the cooling of battery module of an automobile vehicle and its thermal management is a major task for a heat transfer engineer today. Li-ion and Li-polymer batteries are not the only choice in transportation sector but also popular in electronics devices, satellites and aerospace [62]. The widely accepted maximum allowable temperature range in the cell to cell and module to module is set at 5 ℃ [63].

In electronics and space thermal cooling system, cylindrical heat pipes have become more popular due to its ease of operation and installation [64], [65]. Thermal resistance and heat transfer coefficients are the key investigating parameters in the performance of heat pipe [66] in electronics applications. CPU and data centre cooling has become one of the most common problem in the current scenario. The conventional air-cooling systems have number of short comings like lower heat transfer coefficient and excessive power usage. Cooling by liquids is one of the choices for IT equipments. However, the higher flow resistance for liquids while passing through the skin of equipment is a major drawback of the system. This leads to higher pressure drop and excessive power usage. [67]. Out of the conventional vapour compression system, thermo-electric system and heat pipes, the later has been proven to be best in all the aspects in electronics cooling [68]. For the effective thermal management of electronics components researchers have started coupling the phase change material (PCM) along with heat pipe [69] [70] [71]. Since the development of integrated circuit industry, it was first proposed by Moore's law in 1960 [72], that the integration of IC doubles every 18 months. Although being an empirical relation, its accuracy has been proven from years and widely used to guide the semiconductor industry [73]. Study shows that approximately 55% of failures in electronics industry is due to variation in temperature of the circuit beyond its design criteria [73]. Heat Pipes have been started to be used in data centres, a facility that incorporates information technology equipments, telecommunication and data storage system for digital processes [74] for cooling and maintaining the temperature. As in case of data centre cooling, multiple components are to be cooled with limited space available. In mobile electronics devices and cooling of computer servers, multiple heat liberating sites are present in a very small space [75]. Loop heat pipes (LHP) [76] and pulsating heat pipes (PHP) [77] have shown promising results in electronics cooling. Recently, many researchers have started investigating this problem of cooling multiple heat sources with single heat pipe [11], [32]–[35], [50], [52], [53], [78], [79]. Multi-evaporator loop heat pipes have shown significant progress in the multi heat source cooling in both electronics and spacecraft applications [80]. Multi heat source loop heat pipes have shown applications in the cooling of deep space telescope in cryogenic temperature range in the absence of gravity as well [78]However, the complexity and cost associated with loop heat pipe is comparatively high [33], [56] [81]. Deng et. al. [82] investigated a flat heat pipe with multi heat source configuration to meet the cooling demand of 5G base stations. The performance was optimised in terms of filling ratio, inclination angle, heat source and power distribution. It was found that 30° inclination and 20% filling ratio resulted in reduction of thermal resistance and temperature rise by 15.3% and 10℃ respectively. The study suggested the importance of optimum working parameters in the operation of heat pipe. A comparative investigation between single and multiple heat sources was performed by Li [83]. The study concluded that the multiple heat source heat pipes have good start-up performance and great potential for applications. Thermal resistance of heat pipe is the most important performance parameter to be investigated before the actual application [84] . It represents the approach of given design and configuration of heat pipe near to ideal working state. Effective thermal conductivity is another significant parameter to represent the combined effect of conduction and boiling from a heat pipe [85] [86] [87].

Multi-branch heat pipe is simple in construction, installation and operation. It is basically the extension of simple cylindrical heat pipe and its performance parameters are the most significant operating characteristics of a device before putting it in use [88] [89]. However, the investigation of all the performance parameters for multi-branch heat pipe is still an unexplored area. After successful completion of the study, the community may get benefited from the results and optimum operation of MBHP. These will be useful further in experimental, numerical, mathematical and theoretical study for the heat pipe community.

2.8 Objectives of the Work

In light of the above discussions, the following objectives are laid down for the present study:

1. To explore the effect of different parameters on the performance of multibranch thermosiphon heat pipe (MBTHP) like filling ratio, vacuum level, equal and un-equal heat loads and dynamic loading and optimise the same.
2. To investigate the performance of axially grooved multi branch heat pipe (AGMBHP) by considering various parameters with similar geometry and optimise its working condition and its comparison with MBTHP.
3. To understand the effect of different orientations on the performance of AGMBHP and recommend an optimum orientation.
4. To analyze the effect of different number of axial grooves on the performance of axially grooved multi-branch heat pipe (AGMBHP) and to understand its effects on the thermal resistance, heat transfer coefficient and temperature distribution.

2.9 Diagram of Methodological Approach

Following diagram represents the strategy adopted in order to successfully overcome the above-mentioned objectives. A diagram of methodological approach indicates all the input parameters under consideration in the present study. It shows the output parameters in form of various results and their analysis leads towards the fruitful conclusions as an optimum operating condition of multi branch heat pipe.

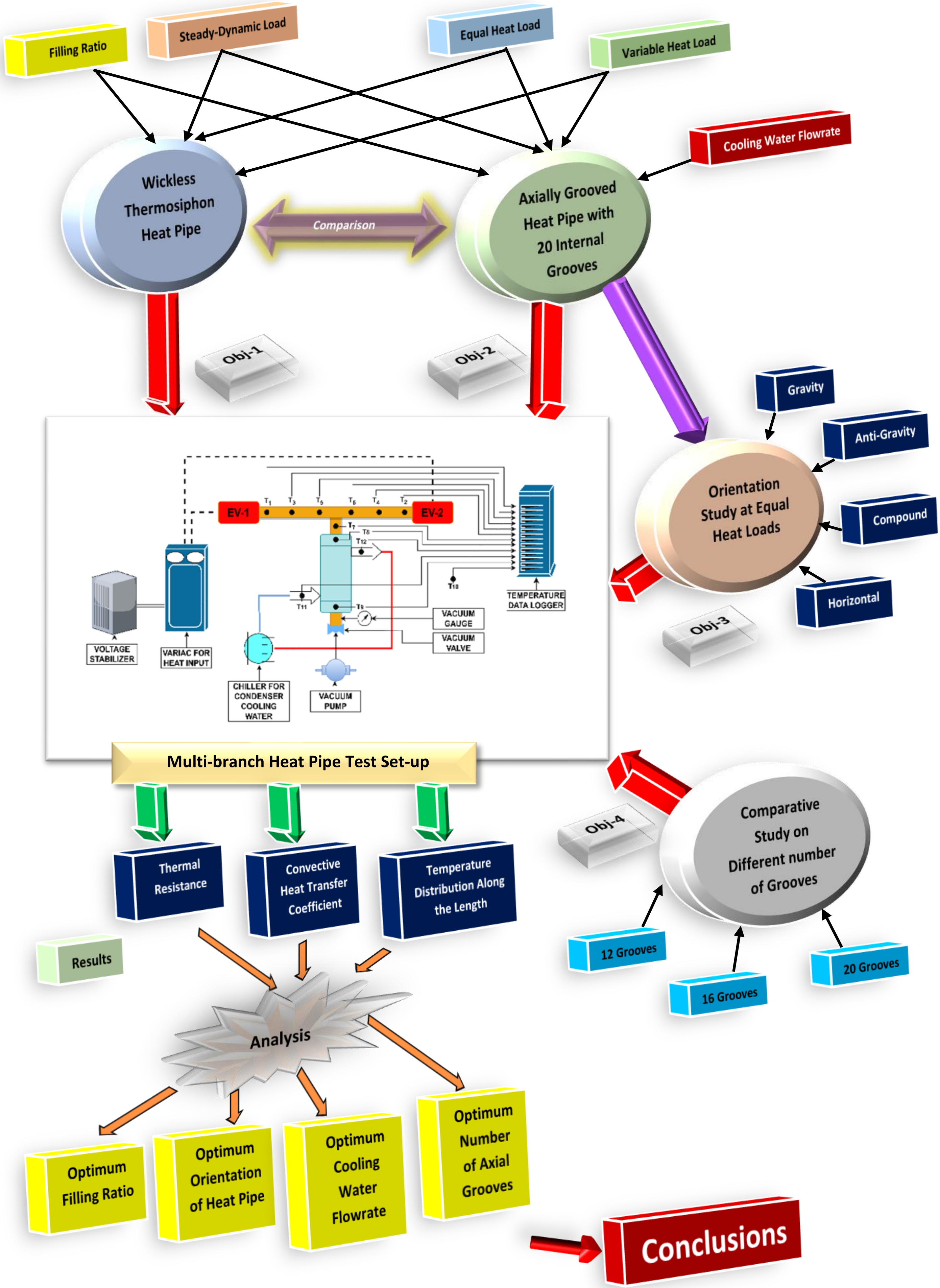

Filling Ratio
Steady-Dynamic Load
Equal Heat Load
Variable Heat Load
Cooling Water Flowrate
Wickless Thermosiphon Heat Pipe
Comparison
Axially Grooved Heat Pipe with 20 Internal Grooves
Obj-1
Obj-2
Gravity
Anti-Gravity
Compound
Horizontal
Orientation Study at Equal Heat Loads
Obj-3
EV-1
EV-2
TEMPERATURE DATA LOGGER
VACUUM GAUGE
VACUUM VALVE
VOLTAGE STABILIZER
VARIAC FOR HEAT INPUT
CHILLER FOR CONDENSER COOLING WATER
VACUUM PUMP
Multi-branch Heat Pipe Test Set-up
Obj-4
Comparative Study on Different number of Grooves
12 Grooves
16 Grooves
20 Grooves
Thermal Resistance
Convective Heat Transfer Coefficient
Temperature Distribution Along the Length
Results
Analysis
Optimum Filling Ratio
Optimum Orientation of Heat Pipe
Optimum Cooling Water Flowrate
Optimum Number of Axial Grooves
Conclusions

2.10 Closure

This chapter comprises of review of electronics and space thermal cooling and their importance in research and development. The commercial demand for multi-heat source heat pipe and their need in today's era is elaborated. It also includes the information about different types of heat pipes and modifications needed to cope up with the development of miniaturization. The available literature of multi-heat source heat pipe and various performance parameters are discussed. The motivation behind the present research in the particular area is again explained in this section.

Chapter 3

Parametric Study on Multi-Branch Thermosiphon Heat Pipe (MBTHP)

This chapter describes the experimental investigation on multi-branch thermosiphon heat pipe (MBTHP) and the effect of various parameters on the performance of heat pipe. The experimental set-up and its specifications, and experimental procedure are elaborated and based on the parametric study, some important findings are presented.

This chapter describes the investigation of T-shaped multi-branch heat pipe with two evaporators on longer branch and one condenser on shorter branch in gravity assisted mode. A water-cooled condenser is used with constant flow rate of water. The start-up as well as dynamic characteristic are studied with various filling ratios with equal and unequal heat loads on evaporators. The results are presented in terms of temperature variation in axial direction, variations in thermal resistance and convective heat transfer coefficient, maximum heat transport capacity etc.

3.1 Experimental Set-up and Specifications

The experimental setup was developed at the Heat Transfer Laboratory of Mechanical Engineering Department at Nirma University. The setup consisted of the multi-branch heat pipe (T-shape), two heaters, heat exchanger provided over the condenser portion, two variable auto-transformers, temperature sensors, data logger, etc. Figure 3.1 illustrates the schematic diagram of the experimental setup along with heat pipe dimensions and temperature sensor locations.

The multi-branch thermosiphon heat pipe (MBTHP) used in the study was made up of copper and comprised of three sections namely two evaporator sections, one condenser section and one adiabatic section. Two heaters were placed on the either side of the horizontal branch of heat pipe, working as evaporators and one water cooler was placed on the vertical branch working as condenser. The length of each of the branches of heat pipe was kept as 100 mm. The outer and inner diameters of the heat pipe were 9 mm and 7 mm respectively. As a working fluid, pre-determined quantity of deionized water was filled inside the heat pipe (based on the required filling ratio) after necessary evacuation process. A vacuum pump was used to create a required level of vacuum inside the heat pipe. The major specifications of MBTHP set-up are given in table 3.1 and its photographs are shown in Fig. 3.2. In order to control the heat input individually for both the evaporators, two separate variable auto-transformers were used. The entire heat pipe testing assembly was wrapped with glass wool insulation to minimize the heat loss to the surrounding.

In order to measure the temperatures at various locations along the heat pipe, twelve numbers of RTD sensors were used as shown in Fig. 3.1. The temperatures of evaporator sections were measured at three locations on either side along the length (T_1, T_2, T_3, T_6, T_7, T_8) and two sensors were provided on the adiabatic section (T_4, T_5). Two sensors (T_9, T_{12}) were provided to measure the temperature of the condenser section. Two sensors (T_{10}, T_{11}) were used to measure cooling water temperature at inlet and outlet respectively. Thermal conductive grease was applied on the temperature sensors before mounting them on the heat pipe to minimize the contact resistance. All the temperature readings were automatically recorded and stored by the temperature data logger at an interval of 10 seconds.

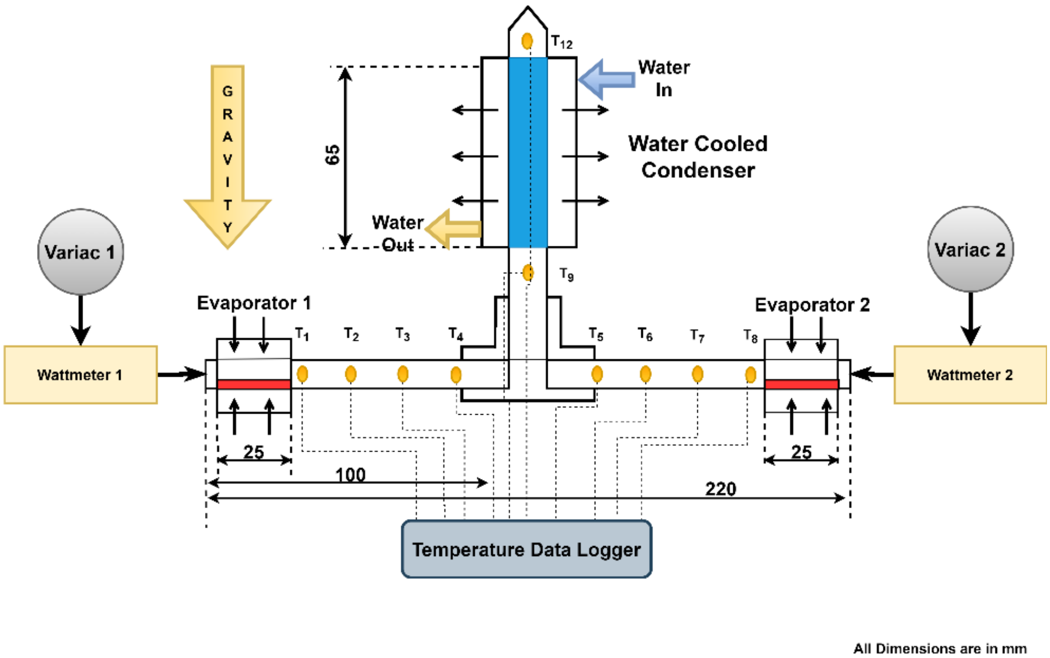

Fig. 3.1 Schematic diagram of test set-up for MBTHP.

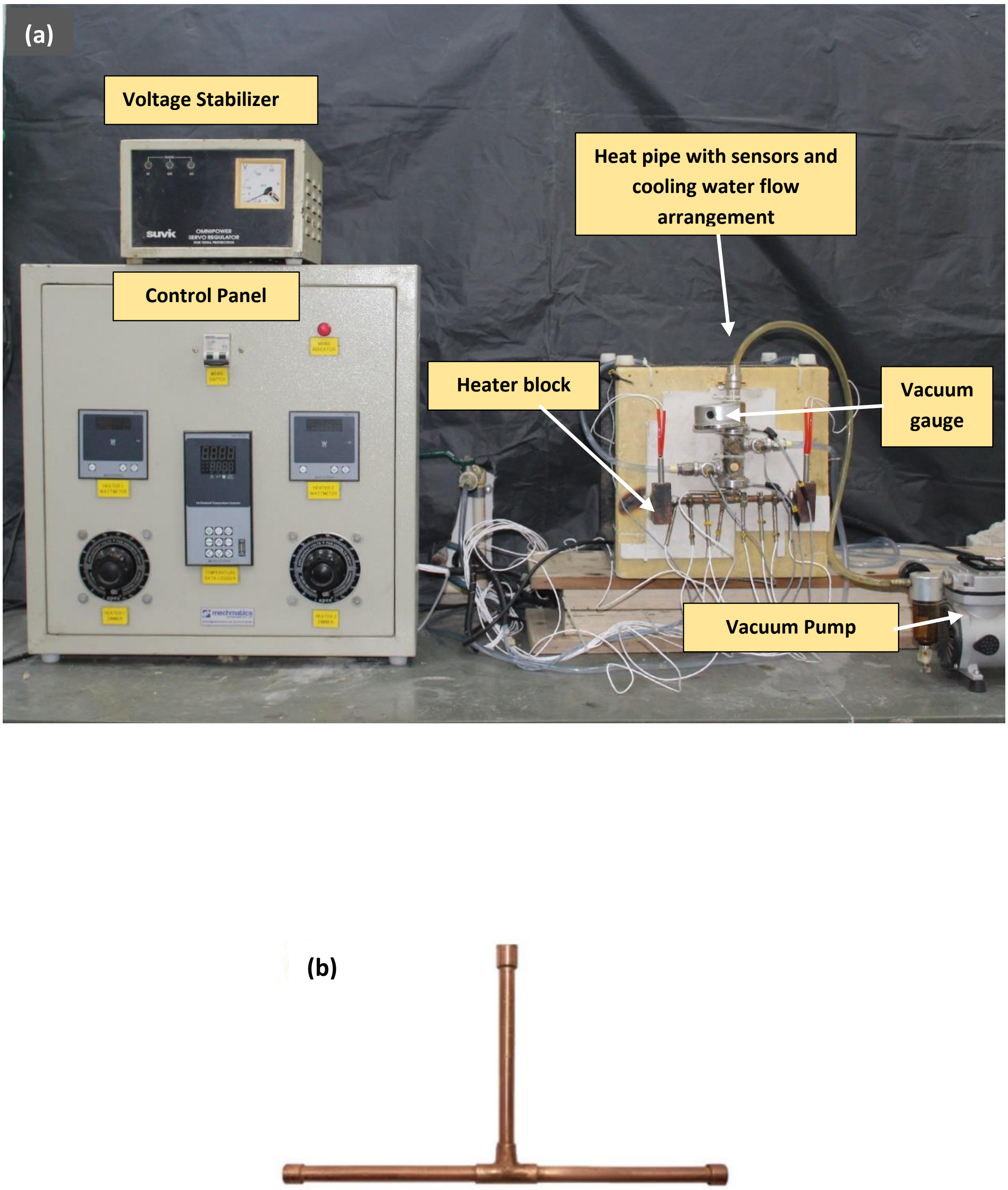

Fig. 3.2 Photographs of (a) Experimental setup (b) Multi-branch heat Pipe.

Table 3.1

Major specifications of experimental setup

Component	Specifications
Heat pipe	Material : Copper OD : 9 mm ID : 7 mm Overall size : Horizontal branch: 220 mm Vertical branch: 125 mm
Working fluid	Deionized water
Evaporator	Length : 25 mm Numbers : 2
Condenser	Length : 100 mm Number : 1
Water heat exchanger	ID : 50 mm Length : 65 mm
Temperature sensors	Type : RTD, PT-100 Accuracy : $\pm$ 0.1°C Numbers : 12
Temperature data logger	Make : Multispan Model : MS-5716RU-M1 No. of Channels : 16 Resolution : 0.2 °C
Heaters	Type : Cartridge Numbers : 2 Rating : 110 W Independent variable autotransformers ($\pm$ 1 W)

3.2 Experimental Procedure

Initially, the heat pipe was evacuated up to a vacuum level of -710 mm of Hg as higher vacuum provides large value of latent heat of working substance which increases heat pumping capacity of heat pipe for given quantity of working substance. As far as latent heat is concerned, molecules require larger value of heat in order to undergo phase change from liquid to vapour at lower pressure compared to higher pressure. At lower pressures, molecules have larger mean free path compared to higher pressure thus it requires extra value of heat to be given to reduce the mean free path and ultimately the conversion of liquid into vapour is the process of decreasing the mean free path by providing latent heat [90]. Then after, the heat pipe was charged with deionized water before sealing it as per the predetermined filling ratio (i.e., 40%, 50%,60%,70%). It was estimated that the height of liquid pool in horizontal branch depends on the filling ratio. In case of 70% filling ratio, entire horizontal branch was filled with liquid in addition to 20 mm more in vertical branch. Subsequently, for 40%, 50% and 60% FR, height of liquid pool was found approximately 4.2 mm, 5.2 mm and 6.3 mm respectively in horizontal branch. Further estimation suggested approximately 6.86 mm, 6.12 mm and 4.2 mm width of fluid layer for 40%, 50% and 60% FR respectively. The above estimation indicated boiling inside the heat pipe rather than thin film evaporation. After installing the heat pipe in the setup, both the heaters and all the temperature sensors were mounted on the heat pipe. In the present study, experiments were performed with different heat inputs in the range of 20 W to 210 W. Based on the requirement, different heat inputs were given to evaporator sections by heaters placed on it. Throughout the experimental analysis, a constant cooling water flow rate of 3.14 lit/min was maintained. All the temperature readings were recorded in the data logger at an interval of 10 seconds. All the connections in the heat exchanger were checked for the leakages.

All the measuring instruments were calibrated before putting in use. In order to obtain the total uncertainty in temperature measurement, various parameters considered were (a) accuracy of temperature sensor PT-100 (b) resolution of temperature data logger (c) accuracy of cartridge heater and its digital indicator (d) heat loss through 1 cm thick glass wool insulation. Calculating all the uncertainties for the total experimental uncertainty in temperature measurement was estimated maximum 7.71% in accordance with the procedure given by Kline et al. [91] using square formula by assuming approximately 50% heat loss through insulation. Relative uncertainty of thermal resistance and convective heat transfer coefficient were also calculated. Maximum relative uncertainty in resistance and convective heat transfer coefficient were found out to be 5 % and 5.1 % respectively considering accuracy in temperature sensor is $\pm$ 0.1°C.

3.3 Performance Parameters

The fluid filling ratio (η) of working substance was defined as

$$\eta = \frac{v_w}{v_t} \times 100\ \% \tag{3.1}$$

Where, v_w = volume of water to be filled inside the heat pipe (ml) and v_t = total inner volume of heat pipe (ml).

Heat flux (q) for the multi-branch heat pipe was calculated by the following equation

$$q = \frac{Q}{F_A\, 2\pi D_i l_e} \tag{3.2}$$

Where, D_i is inner diameter of heat pipe and Q is total heat power (W) on both the evaporators. l_e is length of each evaporator and F_A is area fraction.

In calculation of heat flux, only wet area was taken into consideration for finding its value. Wet surface area of heat pipe depends on the filling ratio. For 40%, 50%, 60% and 70% filling ratio, 0.62, 0.79, 0.94 and 1.0 were the area fractions (F_A) respectively out of total possible heat transfer surface area.

Thermal resistance of heat pipe is a significant performance parameter. The resistance network diagram for MBTHP is shown in Fig. 3.3. It can be seen that; two evaporators are in parallel connection and a condenser is in series connection to evaporators.

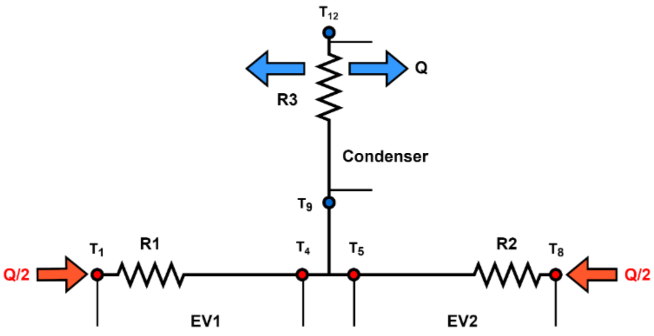

Fig. 3.3 Thermal resistance network in MBTHP.

The resistances (R_1 and R_2) of individual evaporators (EV_1 and EV_2) were calculated as follows,

$$R_1 = \frac{2\,(T_1 - T_4)}{Q} \tag{3.3}$$

$$R_2 = \frac{2\,(T_8 - T_5)}{Q} \tag{3.4}$$

An equivalent resistance for two evaporators (R_{evap}) was evaluated as follows,

$$R_{evap} = \frac{R_1 R_2}{R_1+R_2} \tag{3.5}$$

The condenser resistance (R_{cond}) was determined as follows,

$$R_{cond} = \frac{(T_9 - T_{12})}{Q} \tag{3.6}$$

Total thermal resistance of heat pipe was calculated by

$$R_{total} = \frac{T_{evap} - T_{cond}}{Q} = \frac{\left(\frac{T_1+T_8}{2}\right) - T_{12}}{Q} \tag{3.7}$$

Technically, resistances R_1 and R_2 can only be considered in parallel connection if equal heat load is applied on both the evaporators and their evaporator temperatures are identical. The calculation of thermal resistance is made for steady characteristics for equal heat loads to make the analysis simple.

Also, during calculation of thermal resistances, it was assumed that the temperatures T_1 and T_8 provided the evaporator temperatures, as they were located nearest to the heater block on heat pipe. Due to curvature effect of cylindrical heat pipe, it was difficult to insert temperature sensors exactly on the evaporator surface. This limitation resulted in slightly lower thermal resistance than the actual value.

The evaporator convective heat transfer coefficient (h_e) and the total heat transfer coefficient of heat pipe (h_T) were calculated using following equations [92]

$$h_e = \frac{Q}{A_{se}\,(T_e - T_{sat})} \tag{3.8}$$

$$h_T = \frac{Q}{A_{se}\,(T_e - T_c)} = \frac{Q}{A_{se}\left[\left(\frac{T_1+T_8}{2}\right) - T_{12}\right]} \tag{3.9}$$

Where, Q = total heat power (W), A_{se} = surface area of evaporator heat transfer surface (m^2) as per filling ratio, T_e and T_c are evaporator and condenser temperatures (°C) respectively. T_{sat} is the saturation temperature with respect to final vacuum pressure when heat pipe reaches to steady state.

Uncertainty in temperature U_T using square formula was calculated as per following,

$$U_T = \sqrt{\left(\frac{dT}{T_{avg}}\right)^2 + \left(\frac{dW_{heater}}{Q}\right)^2 + \left(\frac{dT_{data\ logger}}{T_{avg}}\right)^2 + \left(\frac{dQ_{insulation}}{Q_{insulation}}\right)^2} \tag{3.10}$$

Relative uncertainty in Thermal resistance of heat pipe was calculated using following equation

$$\frac{dR}{R} = \sqrt{\left(\frac{d(\Delta T)}{\Delta T}\right)^2 + \left(\frac{dQ}{Q}\right)^2} \tag{3.11}$$

Relative uncertainty in convective heat transfer coefficient was calculated by

$$\frac{dh}{h} = \sqrt{\left(\frac{d(\Delta T)}{\Delta T}\right)^2 + \left(\frac{dQ}{Q}\right)^2 + \left(\frac{dA}{A}\right)^2} \tag{3.12}$$

3.4 Results and Discussion

In this section, the effects of fluid filing ratio are discussed on the performance of MBTHP. The start-up characteristic is presented with equal and unequal heat loads on the evaporators. The dynamic characteristic of heat pipe is plotted at different heat loads. The temperature variation along the axial direction of heat pipe as well as the variations in thermal resistances and heat transfer coefficients are also discussed.

3.4.1 Effect of fluid filling ratio

The filling ratio is one of the most important parameters affecting the thermal performance of the heat pipe. In the present study, for the wickless heat pipe, filling ratio was considered as the ratio of filled volume of working fluid to the total inside volume of the heat pipe. It is required to optimize the filling ratio because the smaller filling ratio may result in an early dry-out of the heat pipe at higher heat inputs, whereas an excess amount of filling ratio may prevent the vapour flow path [12]. In this study, the experiments were performed with four different filling ratios viz. 40%, 50%, 60% and 70%. The total heat load Q was taken as the summation of heat supplied to the left (Q_L) and the right (Q_R) evaporators.

The effects of different filling ratios viz. 40%, 50%, 60% and 70% on the evaporator and the condenser temperatures at an equal values of Q_L and Q_R (i.e. 10 W, 20 W,…up to 100 W each on both evaporators are shown in Fig. 3.4 (a-d). It was found that, with an increase in the heat load, the surface temperature of the evaporator and the condenser increased. Moreover, the temperature difference between the evaporator and the condenser also increased as practically it was not possible to obtain a zero thermal resistance. With a filling ratio of 40% (Fig. 3.4(a)), the maximum heat transfer rate without dry-out was found as 120 W and the corresponding values of the peak temperature and the maximum heat flux were found as 70 °C and 17.6 W/cm^2 respectively. With the further increase in the heat load beyond 120 W, the peak temperature (T_1 and T_8) increased quickly which was the indication of the dry-out in the heat pipe. Similar trends of the evaporator and the condenser temperatures were found with the filling ratio of 50% as shown in Fig. 3.4(b). In this case, the maximum heat transfer rate (without dry-out), the peak temperature and the maximum heat flux were found as 160 W, 75 °C and 18.41 W/cm^2 respectively.

For the lower filling ratio (up to 50%) with an increase in the heat load, boiling of water and generation of vapour occurred at comparatively high rate. The presented heat pipe geometry was such that in which liquid working substance from the condenser could be visualized to fall under the effect of gravity and distributed in two horizontal branches by the push of back-coming fresh condensed water. However, in this motion of liquid return, it also encountered vapour from the opposite direction. Basically, at lower filling ratio, there could not be enough amount of liquid to guarantee the continuous circulation for given heat power, even after sufficient condensation. Another possible reason for dry-out could be entrainment of condensed liquid into vapour at liquid-vapour interface. The vapour drag force could be so strong over the opposing liquid, so water evaporated before reaching to evaporator section [12]. which resulted in the evaporator surface temperature (T_1 and/or T_8) increased rapidly by conduction heat transfer as shown in Fig. 3.4 (a and b). For 40% and 50% filling ratios, dry-out of heat pipe occurred at 130 W and 180 W respectively.

The variations of evaporator and the condenser temperatures with the filling ratios of 60% and 70% are shown in Fig. 3.4 (c-d). It was seen that; in these cases, the heat pipe could work up to a relatively higher heat loads in comparison with the previous cases. For 60% and 70% filling ratios, heat pipe was capable of absorbing 210 W heat load with 20.31 and 19.1 W/cm^2 heat flux respectively. This attributed to the fact that at higher filling ratios (beyond 50%), sufficient water was available in the evaporator section for the phase conversion for a relatively higher heat loads than that at the lower filling ratios. Hence, the heat pipe was able to work up to higher heat loads without dry-out. At very high filling ratios (and for high heat loads as well), excessive volume of vapour generation hindered the return flow of condensed water and local dry-out in the evaporator caused the temperature rise. Indeed, this happened in case of 70% filling ratio where the maximum temperature was found as 105 °C at 200 W, which was relatively higher compared to the maximum temperature of 94 °C corresponds to 60% filling ratio.

In the present study, the experiments were performed with the maximum filling ratio of 70% because at very high filing ratio (beyond 70%), the excess water present in the evaporator section might obstruct the flow path of vapour and it could affect the heat transfer rate of the heat pipe. Moreover, the maximum heat load was kept limited to 200 W, as generally, it is considered as the representative value of heat load in the high-performance electronics cooling [93], [94].

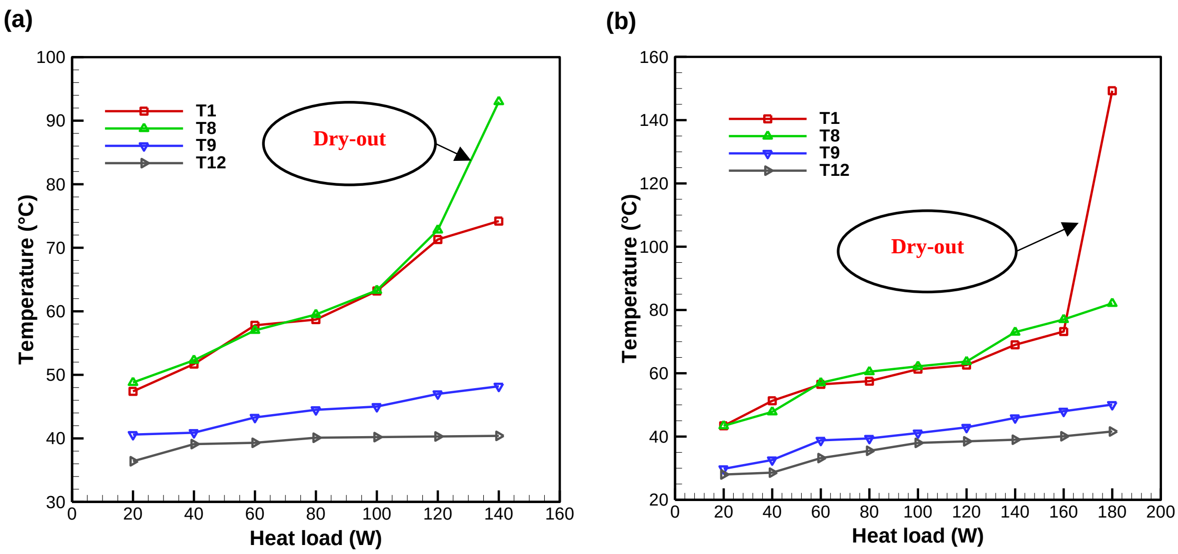

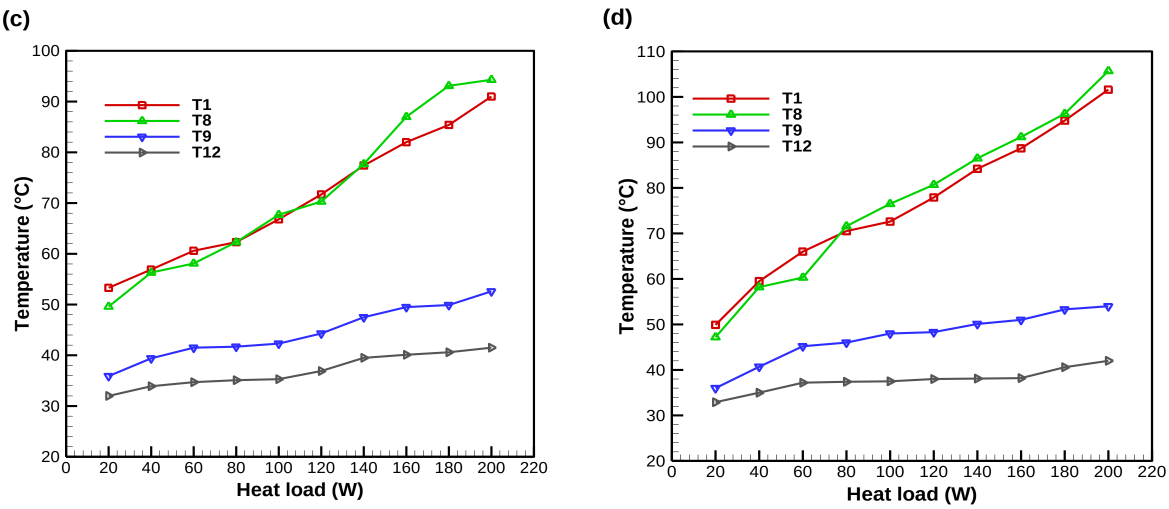

Fig. 3.4 Thermal performance of MBTHP with different filling ratios: (a) 40% (b) 50% (c) 60% (d) 70%.

3.4.2 Analysis of thermal resistance

One of the methods of studying the effect of the filling ratio on the heat pipe performance is to evaluate the total thermal resistance between evaporator and the condenser. Total thermal resistance of heat pipe was calculated using eqs. (3.7). The separate thermal resistances of evaporator and condenser sections were calculated using eqs. (3.5) and (3.6) respectively as described above. Variation in total thermal resistance, evaporator thermal resistance and condenser thermal resistance with respect to the heat load at different filling ratios are shown in Fig. 3.5 (a-b-c). It was found that the total thermal resistance varied from maximum (overall) 0.99 °C/W to minimum (overall) 0.21 °C/W (Fig. 3.5(a)).

It was found that the evaporator thermal resistance (Fig. 3.5(b)) varied from the maximum of 0.22 °C/W to the minimum of 0.10 °C/W with 40% filling ratio, 0.55 °C/W to 0.08 °C/W with 50% filling ratio, 0.32 °C/W to 0.049 °C/W with 60% filling ratio and 0.22 °C/W to 0.10 °C/W with 70% filling ratio. The sudden increment in the thermal resistance at 130 W and 180 W indicated the dry-out of evaporator section corresponding to 40% and 50% filling ratio respectively. It was observed that for the lower values of heat loads, thermal resistances were very large compared to higher heat loads in all the cases. With an increase in the heat load, the vapour generation rate, pressure and the movement of working fluid also increased, which gradually decreased the resistance of the heat pipe. However, an increment of heat load beyond a certain limit might cause evaporator dry-out due to local attainment of the boiling limit. Moreover, in the normal working range of 60 W to 200 W, the evaporator resistance was found lower than 0.15 °C/W for all the filling ratios (excluding the dry-out with filling ratio of 40% and 50%). For 60% filling ratio, the minimum evaporator thermal resistance was achieved as 0.049 °C/W at 60 W heat load. Furthermore, at the maximum heat load of 210 W, the evaporator resistance was found as 0.081 °C/W.

It is clear from Fig. 3.5 (c) that the condenser thermal resistance gradually decreased with an increase in the heat load. The maximum condenser resistance was found below 0.2 °C/W for all the filling ratios. The evaporator dry-out occurred at 130 W and 180 W with 40% and 50% filling ratio respectively but there was no sign of dry-out phenomena in the condenser section which indicated sufficient cooling of vapour in condenser. The average value of condenser resistance was found lower than that of average evaporator resistance and also no effect of evaporator dry-out was detected in the condenser resistance.

Point of minimum total thermal resistance was achieved at 50 % filling ratio and 160 W heat load in Fig. 3.5(a). So, this combination of heat load and filling ratio could be considered as optimum for proposed heat pipe under tested condition.

(a)

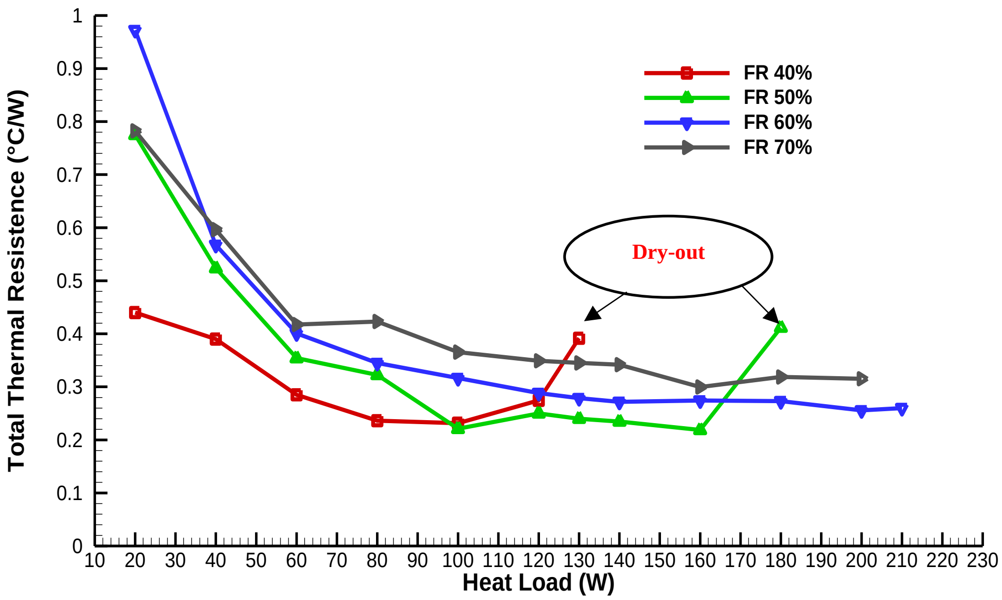

(b)

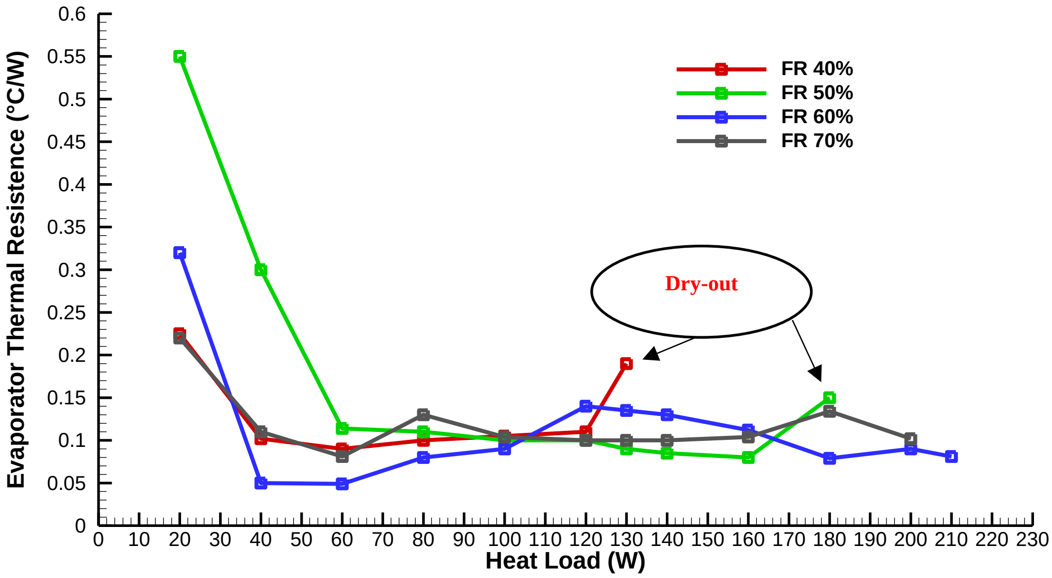

(c)

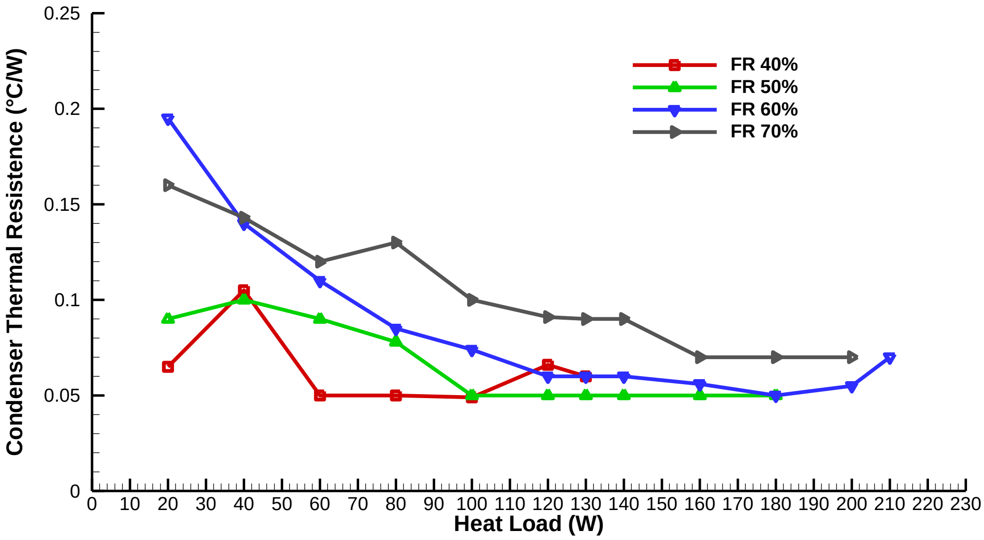

Fig. 3.5 Thermal resistance variation at various heat loads with different filling ratios (a) Total (b) Evaporator (c) Condenser

Thermal resistance for given filling ratio of heat pipe can be visualized as how effectively the working substance absorbs the given amount of heat and undergoes phase change rather than wall conduction. Large thermal resistance means large fraction of wall conduction and poor phase change. It is a well-established fact that at small value of heat load, rate of vapour generation is small which may slower down the phase change (evaporation-condensation) cycle and increases thermal resistance. The same can be observed in Fig. 3.5 at low value of heat loads for all filling ratios.

Further, if quantity of working substance was more than the optimum, for given small value of heat load, then the phase change might be further poor in order to heat large bulk of working substance. Which was the case observed in Fig. 3.5 (a) for 60% and 70 % filling ratio. However, surprisingly, at 20 W heat load, total thermal resistance for 70% filling ratio was less than 60%. As it was discussed earlier, from the calculations of liquid pool height, for 70% filling ratio, entire horizontal branch of heat pipe was completely filled with water. This might lead the whole circumferential heating of water compared to partially filled at 60% FR which could result in lower thermal resistance for 70% filling ratio at earlier stages of heat inputs. The same was observed in evaporator resistance as well in Fig.3.5 (b). Although, at higher heat loads, large quantity of liquid restricted the vapour flow which subsequently increased the thermal resistance for 70% filling ratio.

In case of evaporator resistances in Fig. 3.5 (b), up to 60 W heat load (low heat load) 40% and 70% resistances were almost identical and comparatively lower. As per the previous discussion, the participating heat transfer area was different for different filling ratios. In case of 70% FR, whole circumferential area was available for heat dissipation, made the phase change process effective in horizontal branch so did the evaporator resistance even at lower heat loads. Whereas for 40% FR, participating area was minimum but at the same time, required quantity of working substance was also sufficient for low value of heat load which made the evaporator resistance comparatively lower. However, for 50% filling ratio, the combination of lesser participating heat transfer area and more than sufficient quantity of working substance, both didn't make the condition suitable for lower heat loads (up to 60%) which subsequently resulted in higher thermal resistance in evaporator.

3.4.3 Start-up characteristic

(a) With equal heat loads on the evaporators at different filling ratios

In the present study, the start-up characteristics of MBTHP were plotted for predefined filling ratios earlier. The characteristics were plotted at different values of heat loads at an interval of 20 W until dry-out occurred. From the start-up characteristics performance data points, where $\frac{dT}{dt} \approx 0$ for all the sensors, the heat pipe was considered in steady state condition, where $\frac{dT}{dt}$ is change in temperature with respect to time. The starting point where above condition was satisfied, and further repeated from that point onwards, was the start-up time in the paper. However, in this section four important cases viz. 40% FR - 60 W, 50% FR - 60 W, 60% FR – 140 W and 70% FR – 140 W are discussed in Fig. 3.6 (a-d) The summary of the remaining cases is also presented in Fig. 3.7. The start-up temperature rise was considered as the temperature difference of evaporator (average of T_1 and T_8) at starting and at the steady-state condition after a specific heat input.

Figure 3.6 (a-b) shows the start-up characteristics at the same heat input with the different filling ratios i.e., 40% FR - 60 W and 50% FR - 60 W. It was seen that the start-up of the MBTHP was smooth and steady and the start-up time for MBTHP was below 15 minutes in both the cases. It was observed that the variation in the condenser outlet temperature (T_{12}) was negligible in all the cases. It indicated the proper condensation of vapour in the condenser section. Although, higher temperature variation between evaporator and condenser was due to the large cooling medium flow rate and large length of the condenser. With the filling ratio of 40%, the start-up temperature rise and the start-up time of MBTHP were found to be 13.1 °C and 12 min, 21.2 °C and 13.5 min and 26.9 °C and 14 min corresponding to the heating loads of 20 W, 60 W and 100 W respectively. Similarly for 50% filling ratio, the start-up temperature rise and the start-up time were found to be 15.7 °C and 12 min, 23.2 °C and 12.5 min, 33.3 °C and 24 min and 38.4 °C and 24.5 min corresponding to the heating loads of 20 W, 60 W, 100 W and 140 W respectively.

Figure 3.6 (c-d) shows the start-up characteristics at the same heat input of 140 W with the filling ratios of 60% and 70%. For 60% filling ratio, the start-up temperature rise and the start-up time were found as 23.3 °C and 16 min, 26.5 °C and 15 min, 36 °C and 14.5 min, 41.6 °C and 14 min and 56.4 °C and 13.5 min at the heating loads of 20 W, 60 W, 100 W, 140 W and 180 W respectively. Similarly, for 70% filling ratio, the start-up temperature rise and the start-up time were found as 26.2 °C and 17 min, 29.1 °C and 16 min, 40.1 °C and 14 min, 51.5 °C and 13.7 min and 61.4 °C and 13 min at the heating load of 20 W, 60 W, 100 W, 140 W and 180 W respectively.

From the comparison of the start-up characteristics of 60% and 70% filling ratios (Fig. 3.6 (c-d)), it was observed that for the same heat load of 140 W and with equal cooling requirements, 60% filling ratio resulted in smaller temperature rise. The maximum evaporator temperature was also found lower in case of 60% filling ratio. Although, in both the cases, maximum evaporator temperature was observed to be lower than 100

°C which is a common requirement in electronics cooling [94]. The minimum start-up temperature rise was found with FR of 40% corresponds to heat load of 100 W and with FR of 50% with the heat load of 120 W and 140 W. Whereas for the higher heat loads in the range of 140 W to 200 W, the minimum start-up temperature rise was found with FR of 60% which validated the thermal performance of MBTHP discussed in Fig. 3.4.

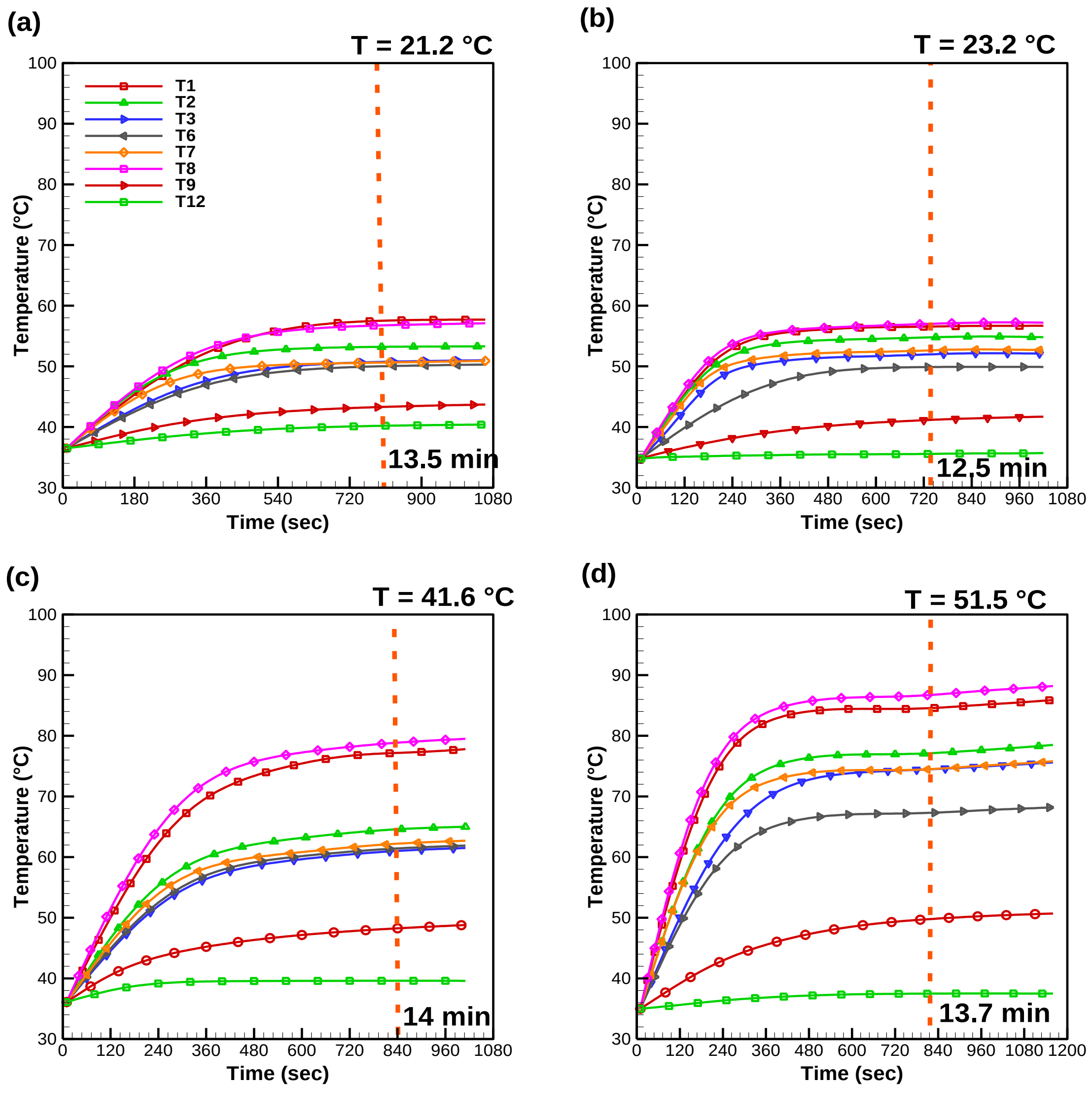

Fig. 3.6 MBTHP start-up characteristics for various filling ratios and heat loads (a) 40% and 60 W (b) 50% and 60 W (c) 60% and 140 W (d) 70% and 140 W

Figure 3.7 indicates the evaporator temperature rise before and after steady state of MBTHP is reached at various heat loads and at different filling ratios. From the diagram, it was observed that temperature rise of evaporator was dependent on filling ratio. For lower filling ratio, small value of temperature rise was observed. As the filling ratio was increased, for the same heat load, temperature rise was also increased.

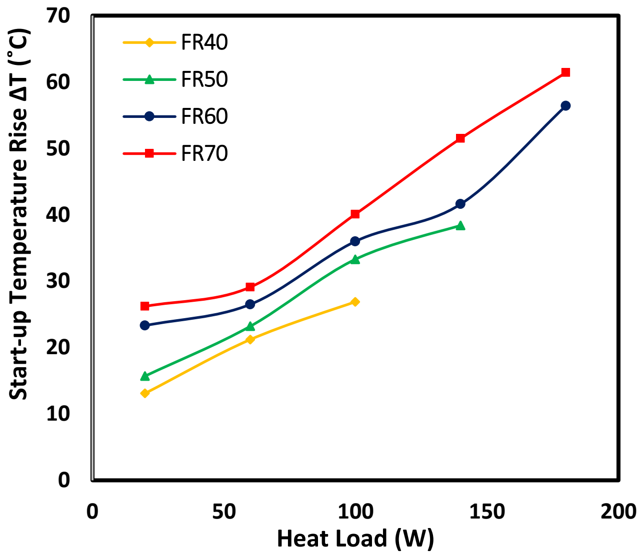

Fig. 3.7 Summary of final and initial temperature difference of evaporator at different heat loads and filling ratios.

From the steady characteristics (Fig. 3.6 and Fig. 3.7), it was understood that for the same heat load, lower filling ratio resulted in lower temperature rise due to less quantity of working substance was required to be heated and phase change was immediate so did the evaporation-condensation cycle. This happened up to a specific heat load before dry-out.

(b) With variable heat loads on the evaporators at 60% filling ratio

In this set of experiments, the transient characteristics of heating were studied with the variable heat loads on the evaporators. The experiments were performed with 60% filing ratio and a combined heat load of 100 W. The vacuum level was kept slightly higher i.e. - 650 mm of Hg to check the dependency of the maximum temperature on the vacuum. The start-up characteristic of heat pipe subjected to five different combinations of the heat loads viz. 0 W - 100 W, 90 W - 10 W, 80 W - 20 W, 70 W - 30 W and 60 W - 40 W are shown in Fig. 3.8 (a-e). It was observed that with the variable heat loads on the evaporators, the heat pipe took maximum 15 minutes to reach to the steady state condition. The peak temperature and the maximum start-up temperature rise were found well below 95 °C and 60 °C respectively in all the cases, which was the representative range in a high-performance electronics package [94]. The corresponding values with an equal heat load of 100 W (i.e., 50 W - 50 W) on the evaporators were found as 72 °C and 37 °C respectively. The values of the peak temperature and the start-up temperature rise were found to be slightly higher with the unequal loads in comparison with an equal load on the evaporators. This could be attributed to the fact that, with a lower pressure (i.e., higher vacuum) inside the heat pipe, the boiling point of working fluid was relatively lower hence a small amount of heat input may initiate the boiling- condensation cycle and the temperature increment ceased. It was understood from Fig. 3.8 that in these set of experiments, both the evaporators were having large temperature difference due to unequal loads. As the difference between heat loads between two evaporators decreased, temperature difference also decreased. The maximum evaporator temperature was lowest in case of 60-40 W heat load (figure 3.7 (e)) compared to all the other heat load combinations. This can be understood due to the fact that the heat load distribution was more even in this case compared to all the other combinations. However, from these experiments, it was concluded that the proposed mode of heat pipe worked satisfactorily with equal as well as unequal heat loads on the evaporators at both the vacuum levels.

(a) (b)

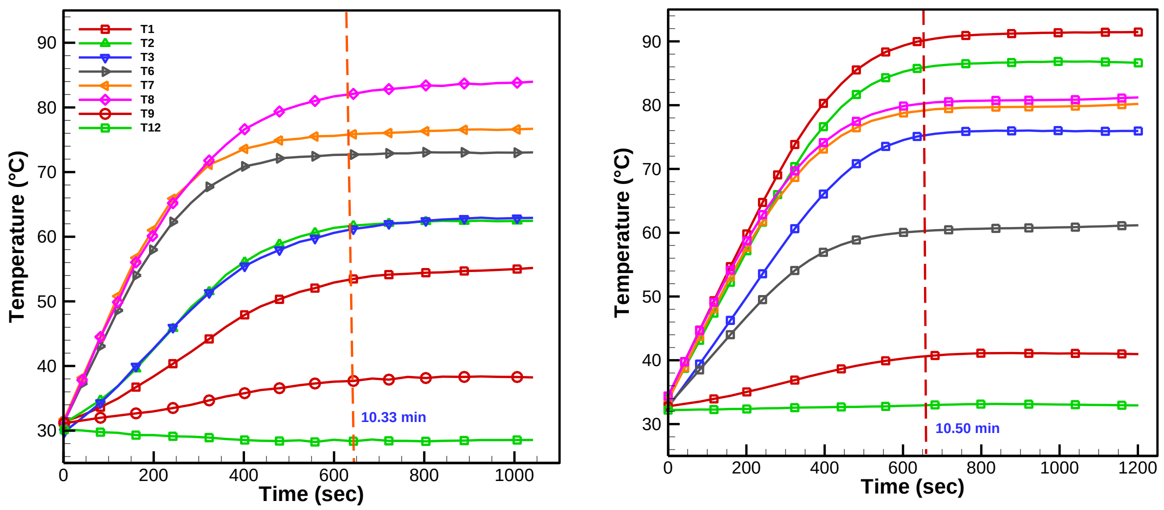

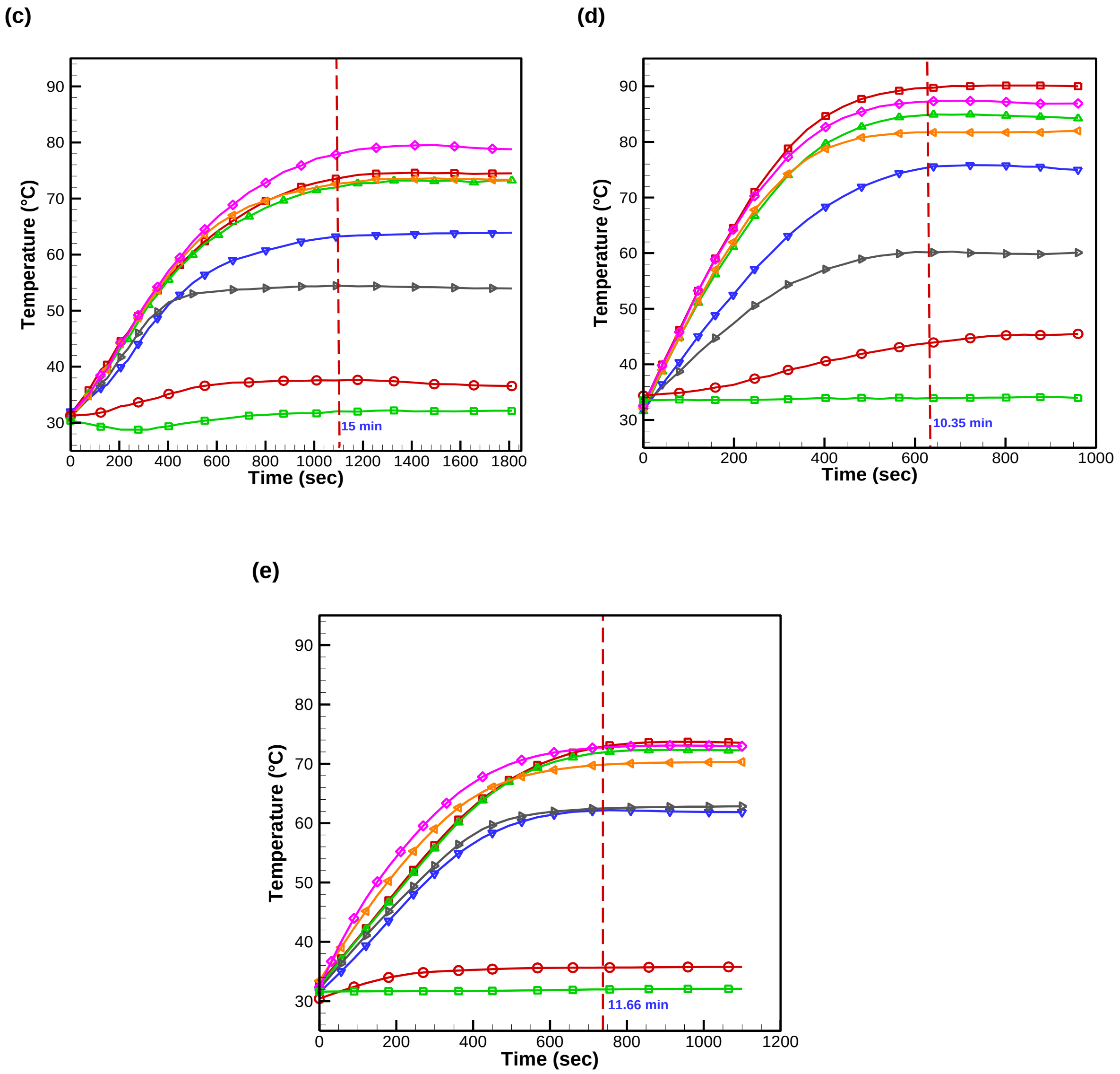

Fig. 3.8 Start-up characteristics of MBTHP with 60% filling ratio with variable heat load on evaporator (a) 0-100 W (b) 90-10 W (c) 80-20 W (d) 70-30 W (e) 60-40 W.

3.4.4 Dynamic characteristics

The dynamic response of the heat pipe is defined as the behavior of heat pipe under continuous progressive increase in the heat load immediately after reaching to a steady state condition at a particular heat load [58]. In this set of experiments, MBTHP was subjected to the heat load from 0 W to 210 W in a step of 30 W each, equally on both the evaporators for 60% and 70% filling ratios. After each step of 30 W, once the steady state was reached, total 30 W increment was applied on both the evaporators (15 W each) and the variations in the temperature trend were observed.

The dynamic characteristics were plotted with the filling ratios of 60% and 70% in the heat load range of 0 W to 210 W as shown in Fig. 3.9 (a-b). The temperatures of the similar locations, on the either side of the evaporators, may not remain exactly same due to minor uncertainty in both the evaporators. Hence, the temperatures of the similar locations were averaged for the single value representation in Fig. 3.9.

Initially, when the heat input was increased from 0 W to 30 W, all the temperatures increased and reached to the steady state condition. The peak temperature and the temperature rise were found as 50.3 °C and 15.9 °C for the filling ratio of 60% and 56.4 °C and 22 °C for the filling ratio of 70%. A temperature jump can be observed at a temperature of 59 °C at a heat load of 30 W with 70% filling ratio. This phenomenon particularly occurs at low heat input and high filling ratio [95]. The reason behind the temperature jump could be non-uniform heating of one of the evaporators due to unequal return of condensate in the evaporators, uneven surface finish etc.[33]. When both the evaporators received different quantity of working substance, the evaporator with a larger quantity of working substance remained colder compared to another evaporator which resulted in unequal temperature of the evaporators [95]. With the higher heat loads, the problem of temperature jump was negligible because in that case more quantity of vapour was generated which in turn returned with a high pressure inside the heat pipe thereby minimized the effect of unequal condensate distribution. Indeed, in case of 70% filling ratio, entire evaporator was flooded which resulted in temperature jump at lower value of heat load.

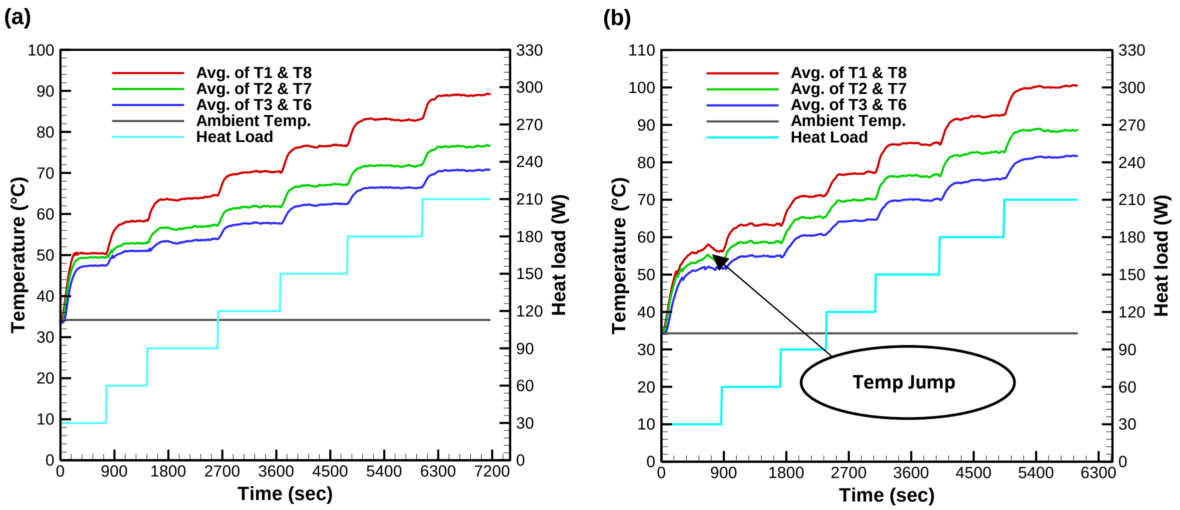

Fig. 3.9 Dynamic characteristics of MBTHP with heat load ranging from 0 to 210 W (a) 60% filling ratio (b) 70% filling ratio.

The values of the peak temperatures and the temperature rise obtained for different heat loads ranging from 0 to 210 W for 60% and 70% FR are summarized in table 3.2. It can be seen that, for 60% filling ratio, the peak temperatures as well as the temperature differences were found to be lower compared to that with 70% filling ratio for all the heat loads except for 30 W - 60 W. In case of 30 W - 60 W heat load, the temperature rise was found as 8.3 °C and 7.1 °C with FR of 60% and 70% respectively. This may be due to the fact that the heat pipe redeemed itself from the temperature jump effect. At this operating point, the heat pipe temperature was already higher due to the temperature jump effect at the heat load of 30 W. When 60 W power was applied, the heat pipe did not show much temperature rise because of re-adjustment and diminishing effect of temperature jump at higher load [95].

Table 3.2

Dynamic response of MBTHP at filling ratios of 60% and 70%

Heat Load	**Peak temperature (°C)**		**Temperature rise (°C)**	
	60% FR	**70% FR**	**60% FR**	**70% FR**
0-30 W	50.3	56.4	15.9	22
30-60 W	58.6	63.5	8.3	7.1
60-90 W	64.6	71.3	6	7.8
90-120 W	70.4	77.2	5.8	5.9
120-150 W	76.6	85.2	6.2	8
150-180 W	83.2	93	6.6	7.8
180-210 W	89.1	100.5	5.9	7.5

From the dynamic characteristics, it was observed that for 60% and 70% filling ratios, the heat pipe was able to function satisfactorily in the thermosiphon mode in the dynamic heat load range of 0 to 210 W. The maximum peak temperature was found below 95 °C and 105 °C with filling ratio of 60% and 70% respectively. For many military electronics applications, the temperature below 125 °C is considered as a reliable operating condition [96]. However, from the current study, 60% filling ratio was considered to be better compared to 70% filling ratio because it could transport up to 210 W heat load, with the lower peak temperature (10 °C lower) without any effect of temperature jump.

3.4.5 Temperature distribution along the length

The temperature distributions along the length of multi-branch heat pipe at different heat loads with different filling ratios are shown in Fig. 3.10 (a-d). In order to study the temperature distribution along the length of the heat pipe, T- shaped heat pipe was considered to be an equivalent straight heat pipe in order to understand the temperature variation in different sections. In order to convert the T-shaped heat pipe into the straight heat pipe, the temperatures of the similar sections of both the evaporators were averaged and marked on a straight line (as shown in Fig. 3.10 (a-d)). Among the previous studies, similar approach was applied by Kim et.al. [92] and obtained similar trends of temperature distribution.

It was observed that the temperature decreased along the length of the heat pipe in all the cases. As expected, the maximum temperature was found in the evaporator section, decreased along the adiabatic section and then decreased further along the condenser section.

At 20 W heat load with 40% filling ratio, the heat pipe was subjected to a minimum temperature variation along the length. At lower filling ratio, faster vapour generation rate made the heat pipe quick responsive. However, for higher filling ratio, more heat was required to generate vapour which subsequently made the heat pipe slow respondent and increased the axial conduction loss through the wall surface which in turn increased the temperature variation along the length. Temperature distribution along the length of heat pipe also validated the results described in Section 3.4.1.

(a)

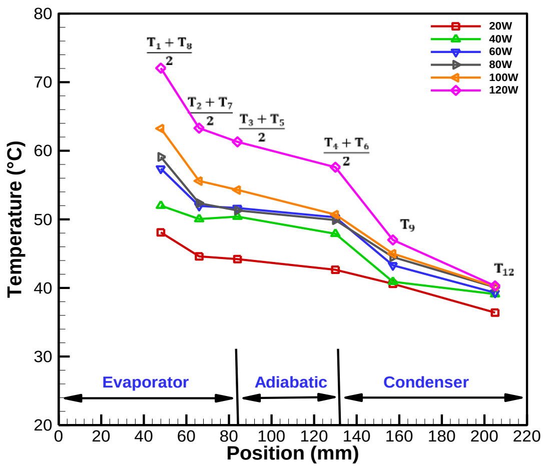

(b)

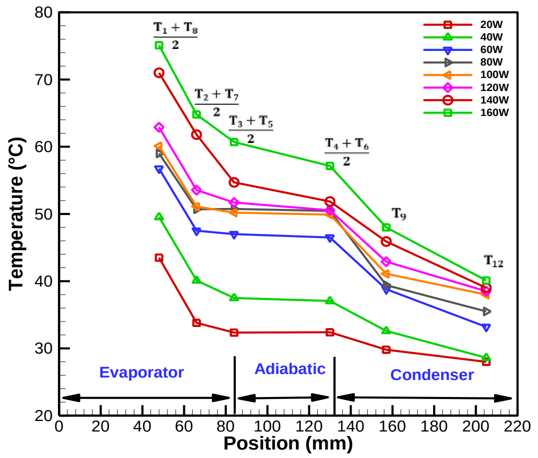

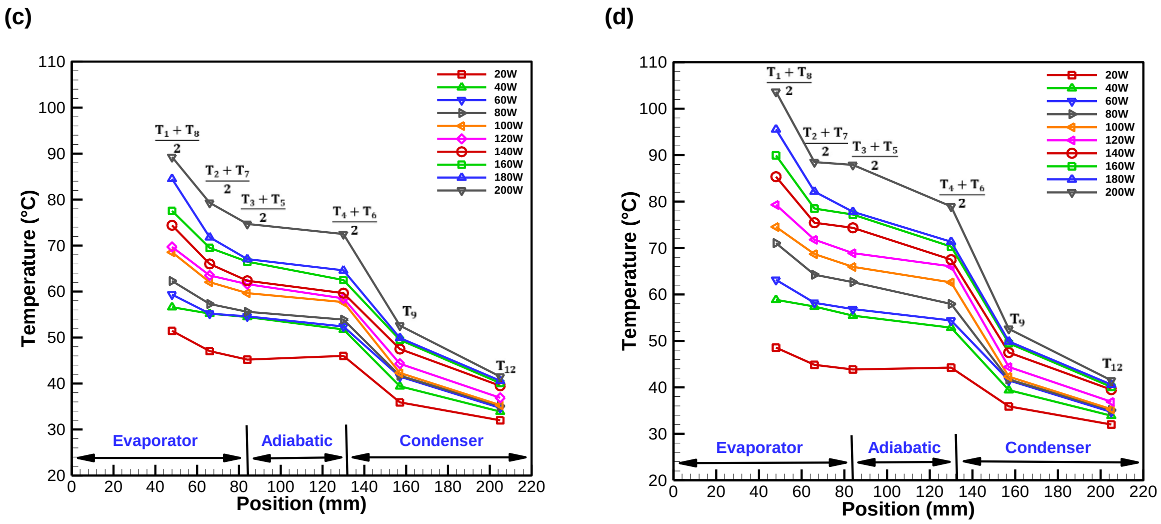

Fig. 3.10 Temperature distributions along the length at different heat loads with filling ratio of (a) 40% (b) 50% (c) 60% (d) 70%.

3.4.6 Variation in the heat transfer coefficient

The evaporator heat transfer coefficients and total heat transfer coefficients of heat pipe were calculated using eqs. (3.8) and (3.9) respectively. Figure 3.11 (a-b) shows the variation of the evaporator and the total heat transfer coefficients at different heat loads with different filling ratios. As the heat load was applied on heat pipe, the pressure inside heat pipe also increased gradually due to vapour generation. Once heat pipe reached to steady state, some high value of pressure (compared to starting pressure/vacuum) was reached which could be termed as steady state pressure. This steady state pressure also increased with respect to applied heat load. As indicated in Fig. 3.2, a vacuum gauge was connected at the end of condenser of heat pipe which gave the final steady pressure/vacuum. The respective saturation temperature (T_{sat}) was used to calculate heat transfer coefficient at evaporator for given heat load [92]. It was observed that the heat transfer coefficient gradually increased, reached to maximum and then suddenly decreased at dry-out in case of 40% and 50% filling ratio. The dry-out in a thermosiphon heat pipe basically indicated the shifting of boiling regime from the nucleate to the film boiling [12] in evaporator. The maximum heat transfer coefficients for complete heat pipe and evaporator, were found to be 6.33 kW/m^2°C and 12.22 kW/m^2°C for 40% FR, 5.26 kW/m^2°C and 12.24 kW/m^2°C for 50% FR, 3.78 kW/m^2°C and 7.35 kW/m^2°C for 60% FR and 3.03 kW/m^2°C and 4.86 kW/m^2°C for 70% FR.

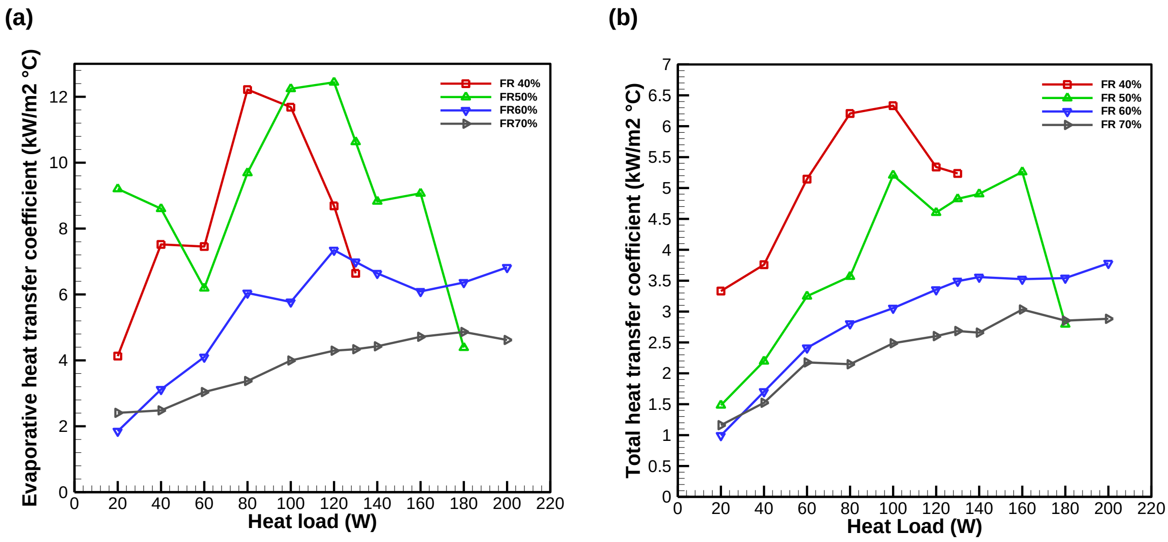

Fig. 3.11 Variations in heat transfer coefficients with heat loads with different filling ratios (a) Evaporator (b) Total.

The analysis concluded that 40% filling ratio provided highest value of convective heat transfer coefficient (6.33 kW/m^2°C) at 100 W heat load compared to other filling ratios for heat pipe. However, in case of evaporator, for 50% filling ratio and 120 W heat load, convective heat transfer coefficient was maximum. From Fig. 3.11 (a), it was evident that evaporator heat transfer coefficients were maximum for particular heat load for each filling ratio. This was due to the fact that for each quantity of working substance, a particular heat load provided the most effective phase change in evaporator. However, actual pressure in evaporator was slightly higher than that measured by the vacuum gauge near condenser which resulted in slight variation than the plotted value. Maximum total heat transfer coefficients (Fig. 3.11 (b)) also depend on optimum heat load for given filling ratio, similar to evaporator. Total heat transfer coefficient data validated the results obtained for total thermal resistance of heat pipe (Fig. 3.5(a)) and vice a versa as both could be visualized as inversely proportional to each other.

3.5 Closure

In the present study, experimental investigations were carried out on the wickless multi-branch thermosiphon heat pipe (MBTHP) with different filling ratios in the wide range of heat loads. The start-up characteristic with equal and variable heat loads on evaporators were analyzed. The dynamic response of MBTHP was investigated. The temperature distribution in the axial direction, thermal resistances of heat pipe, evaporator and condenser along with heat transfer coefficients were also analyzed. The major observations drawn from the study are as follows:

In the heat load range of 50 W to 100 W, 40% filling ratio (FR) showed minimum thermal resistance. From 100 W to 160 W, 50% FR, provided better results and for 160 W to 210 W, 60% FR was found more suitable. The maximum temperature was found to be lower than 100 °C which was very favorable requirement in the electronics cooling. Maximum heat flux values in MBTHP were found to be 17.6 W/cm^2, 18.41 W/cm^2, 20.31 W/cm^2 and 19.1 W/cm^2 corresponding to filling ratios of 40%, 50%, 60% and 70% respectively under tested conditions.

In the next chapter, the effect of axial grooved wick structure on the performance of multi-branch heat pipe is investigated and the same is compared with MBTHP in terms of effective thermal conductivity, thermal resistance and condenser cooling requirement of heat pipe.

The following paper is based on this chapter:

Bhatt, A.A., Jain, S.V., Patel, R.N, 2022, Experimental Investigation on Performance Analysis on Wickless Thermosiphon Heat Pipe with Two Heat Sources and Multiple Branches", ASME J. Therm. Sci. Eng. Appl., **14,** P. 101006.
doi: https://doi.org/10.1115/1.4054163

Chapter 4

Parametric Study on Axially Grooved Multi-Branch Heat Pipe (AGMBHP)

This chapter describes the experimental investigation on axially grooved multi-branch heat pipe (AGMBHP) with 20 numbers of grooves and the effects of various performance parameters. The experimental set-up, heat pipe specifications and experimental procedure are elaborated along with important findings of the work.

This chapter elaborates the investigation on "T"-shaped multi-branch heat pipe with two evaporators on longer branch and one condenser on shorter branch having axially grooved wick. A water-cooled condenser is used with constant flow rate of water. The start-up and dynamic characteristics are studied with different filling ratios with equal and unequal heat loads on evaporators. Cooling water flow rate is also varied to understand its effect on thermal resistance. The results are presented in terms of temperature variation in axial direction, thermal resistance, heat transfer coefficient and effective thermal conductivity.

4.1 Experimental Set-up and Specifications

The experimental setup includes "T" shaped axially grooved multi-branch heat pipe (AGMBHP), two copper blocks inserted with cartridge heaters, tube in tube heat exchanger over condenser portion, two independent variable auto-transformers, ring type temperature sensors, data logger etc. Figure 4.1 illustrates the schematic diagram of the experimental setup along with heat pipe dimensions and temperature sensor locations. Similar experimental set-up was used by authors in their previous work [97]. The axially grooved multi-branch heat pipe (AGMBHP) used in the study was made up of copper. Heat pipe was comprised of three sections namely two evaporator sections, one condenser section and one adiabatic section. Axial grooves (20 nos.) with 0.6 mm width and 0.6 mm depth were cut precisely to work as a wick structure for capillary. Total groove volume in the heat pipe is approximately 2.18 ml in terms of filled working substance. Omur et al. [98] described in his algorithm that 20 number of grooves in the heat pipe provides maximum heat transport capacity. Special care was taken while fabricating the grooves to keep the liquid channel constant through condenser region to evaporator region. This confirmed the continuous flow of working substance without any path break in unconventional “T” shaped heat pipe. Two rectangular copper blocks were used as heaters on the either side of the horizontal branch of heat pipe, worked as evaporators. Cartridge heaters were inserted at one end of copper block and at the other end, heat pipe was inserted up to 25 mm inside to supply heat load in evaporator. One water heat exchanger was placed on the vertical branch worked as a condenser. The length of each of the branches of heat pipe was kept as 100 mm. The outer and inner diameters of the heat pipe were taken 9 mm and 7 mm respectively. As a working fluid, predetermined quantity of deionized water was filled inside the heat pipe (based on the required filling ratio) after necessary evacuation process. A vacuum pump was used to create a required level of vacuum inside the heat pipe. Figure 4.2 (a) shows the photograph of the experimental set-up. Figure 4.2 (b) shows the horizontal position of heat pipe along with temperature sensors and water connections. Figure 4.2 (c) shows the internal grooves of heat pipe. Figure 6.1 (e) shows the internal groove dimensions. (pg.no. 106). The major specifications of AGMBHP set-up are given in table 4.1. In order to control the heat input individually for both the evaporators, two separate variable auto-transformers were used. The entire heat pipe testing assembly was wrapped with glass wool insulation to minimize the heat loss to the surrounding while performing the experiments.

In order to measure the temperatures at various locations along the heat pipe, nine numbers of resistance temperature detector (RTD) sensors were used as shown in Fig. 4.1. The temperatures of evaporator branches were measured at two locations on either side along the length (T_1, T_3 and T_2, T_4) and three sensors were provided on the adiabatic section (T_5, T_6, T_7). Two sensors (T_8, T_9) were provided to measure the temperature of the condenser section at inlet and outlet. Two sensors (T_{11}, T_{12}) were used to measure cooling water temperature at inlet and outlet respectively. One sensor (T_{10}) was used to measure the ambient temperature. Thermal conductive grease was applied on the temperature sensors before mounting them on the heat pipe to minimize the contact resistance. All the temperature readings were automatically recorded and stored by the temperature data logger at an interval of 15 seconds.

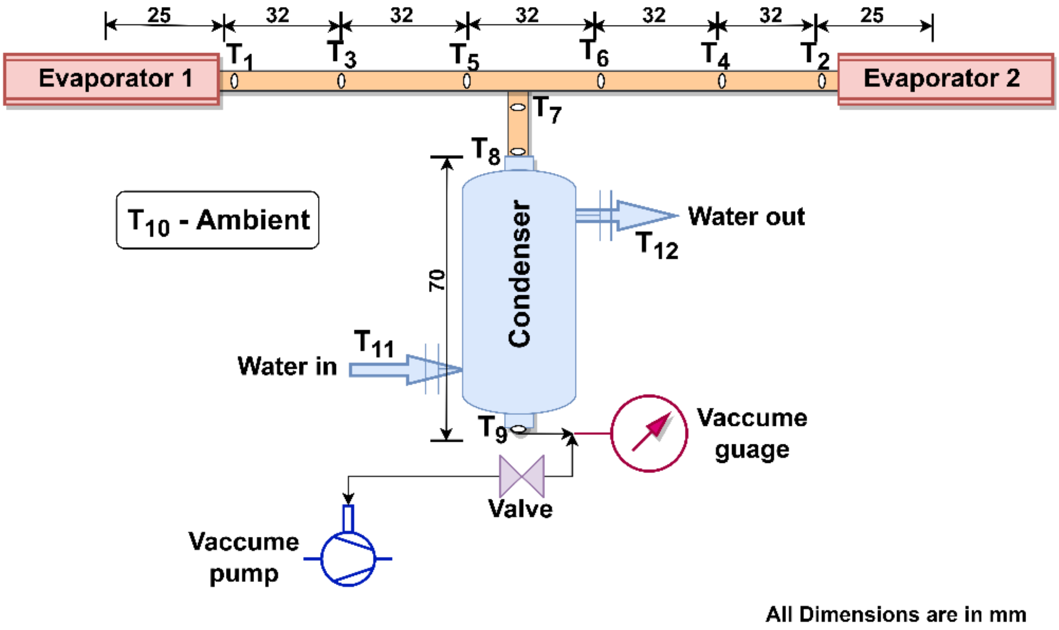

Fig. 4.1. Schematic diagram of test set-up for AGMBHP.

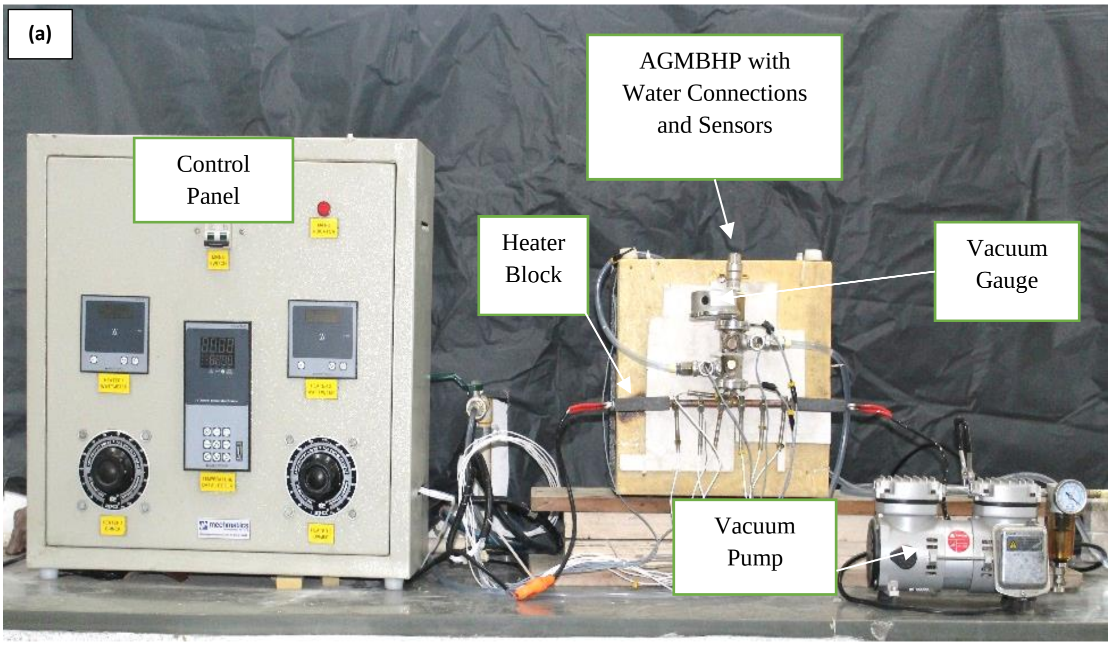

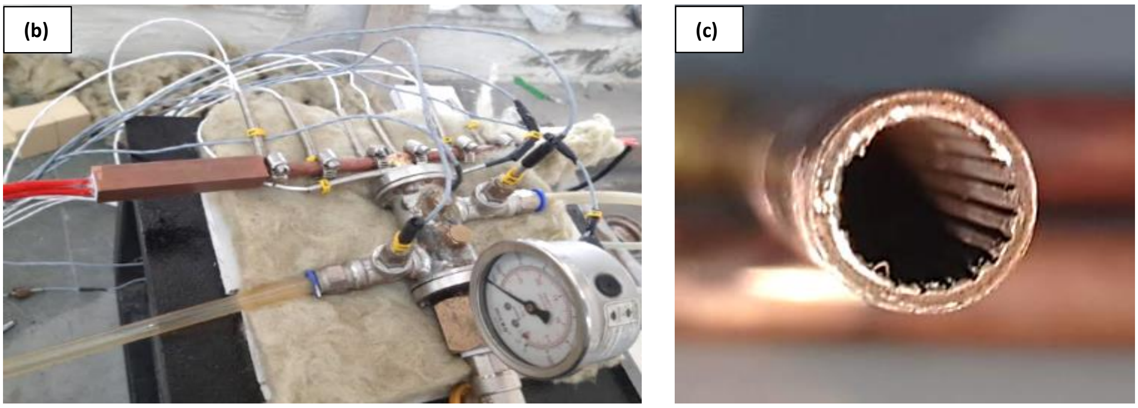

Fig. 4.2 Photographs of (a) Experimental setup (b) Closed view of heat pipe in horizontal position (c) Internal view of axial grooves (20 no.).

Table 4.1

Major specifications of experimental setup

Component	Specifications
Heat pipe	Material: Copper OD: 9 mm ID: 7 mm Overall size: Horizontal branch: 210 mm Vertical branch: 110 mm
Wick Structure	Type: Axially grooved Size of groove: 0.6 mm width and 0.6 mm depth along the length No. of grooves: 20 Shape of grooves: Rectangular
Working fluid	Deionized water
Evaporator	Length: 25 mm Number: 2
Condenser	Length: 70 mm Number: 1
Water heat exchanger	ID: 50 mm Length: 65 mm

4.2 Experimental Procedure

Heat pipe was initially evacuated up to high vacuum. High vacuum provided lower boiling point of working substance so as high heat pumping capacity due to large value of latent heat. After the necessary evacuation process, heat pipe was charged with deionized water before sealing it as per the predetermined filling ratio (i.e., 75%, 100%, 125%, 150%, 175%, and 200%). In case of grooved heat pipe, the filling ratio is defined as the percentage volume of water with respect to total groove volume. When all the axial grooves (liquid channels) were completely filled with water throughout the heat pipe, the filling ratio was considered as 100%. Accordingly, all the filling ratios were accurately calculated and used for experimentations. After the necessary charging process, a constant initial vacuum level of -700 mm of Hg was fixed throughout all the experiments. Initially all the experiments performed for the determination of optimum filling ratio, were in horizontal orientation of heat pipe. Once the optimum filling ratio was obtained, orientation study and cooling flow rate investigations were performed on optimum filling ratio only.

Once, installation of heat pipe in the setup was done, both the heaters and all the temperature sensors were mounted on the heat pipe. In the present study, experiments were performed with different heat inputs in the range of 20 W to 240 W. Based on the requirement, different heat inputs were given to evaporator sections by heater blocks placed on it. Throughout the experimental analysis, a constant cooling water flow rate of 5 ml/s was maintained until and unless it is mentioned. All the connections in the heat exchanger were checked for the leakages.

All the temperature readings were recorded in the data logger at an interval of 15 seconds. All the measuring instruments were calibrated before putting in use. In order to obtain the total uncertainty in temperature measurement, various parameters like (a) accuracy of temperature sensor PT-100 (b) resolution of temperature data logger (c) accuracy of cartridge heater and its digital indicator and (d) heat loss through glass wool insulation were considered [97]. Calculating all the uncertainties for the total experimental uncertainty in temperature measurement was estimated maximum 5.5 % in accordance with the procedure given by Kline et al. [91] using square formula. While calculating the uncertainty in temperature measurement, it was considered that maximum 30 % heat loss occurred through the thermal insulation. Relative uncertainty of thermal resistance and convective heat transfer coefficient were also calculated. Maximum relative uncertainty in thermal resistance and convective heat transfer coefficient were found to be 5 % and 5.1 % respectively by considering an accuracy in temperature sensor as $\pm$ 0.1ºC.

4.3 Performance Parameters

Different parameters used to evaluate the performance of heat pipe are described in this section.

The fluid filling ratio (η) of working substance was defined as per eq. (4.1)

$$\eta = \frac{20\ (v_g)}{v_w} \times 100\ \% \tag{4.1}$$

where, v_w = volume of water to be filled inside the heat pipe for required filling ratio (ml), v_g = volume of water that can be filled in one groove (ml) and No. of grooves = 20

Heat flux (q) for the multi-branch heat pipe was calculated as per eq. (4.2)

$$q = \frac{Q}{20 \times (w + 2h) \times 2l_e} \tag{4.2}$$

where, w is the width of each groove equals to the height of the groove (0.6 mm) and Q is total heat power (W) on both the evaporators and l_e is length of each evaporator.

In the calculation of heat flux, only wet projected area (heat flow is radially inward) was taken into consideration for finding its value. Moreover, it was considered that under steady state condition, all the grooves, in evaporator region were completely saturated with working substance irrespective of filling ratio. The maximum heat flux transferred by heat pipe was found to be 133.3 kW/m^2 under the tested condition.

Thermal resistance of heat pipe is a significant performance parameter. The resistance network diagram for AGMBHP is shown in Fig. 4.3. It was seen that; two evaporators were in parallel connection and a condenser was in series connection.

The thermal resistances (R_1 and R_2) of individual evaporators (EV_1 and EV_2) were calculated as follows,

$$R_1 = \frac{2\ (T_1 - T_5)}{Q} \tag{4.3}$$

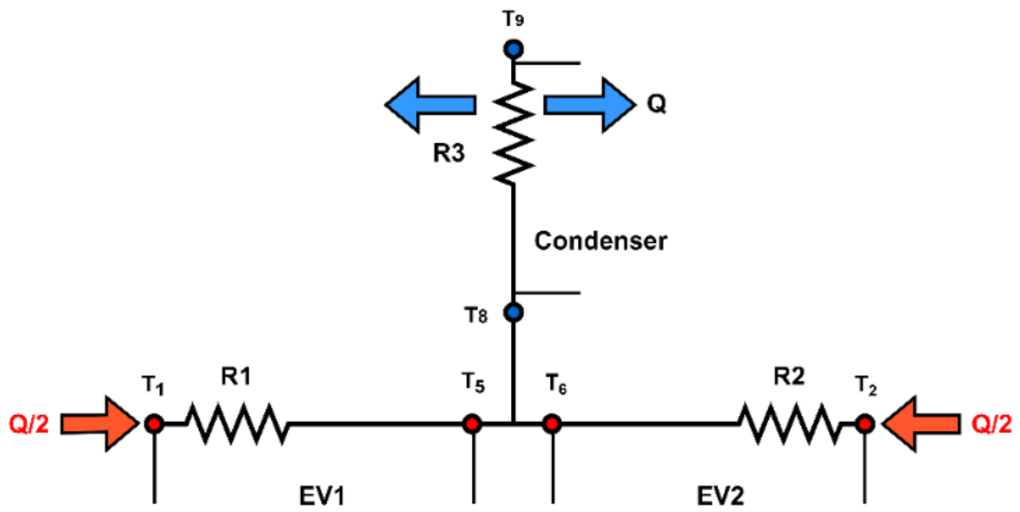

Fig. 4.3 Thermal resistance network in AGMBHP.

$$R_2 = \frac{2\,(T_2 - T_6)}{Q} \tag{4.4}$$

An equivalent resistance for two evaporators (R_{evap}) was calculated as follows,

$$R_{evap} = \frac{R_1 R_2}{R_1 + R_2} \tag{4.5}$$

The condenser resistance (R_{cond}) was determined as follows,

$$R_{cond} = \frac{(T_8 - T_9)}{Q} \tag{4.6}$$

Total thermal resistance of heat pipe was calculated as per eq. (4.7)

$$R_{total} = R_{evap} + R_{cond} \tag{4.7}$$

However, during calculation of thermal resistances, it was assumed that the temperatures T_1 and T_2 were the evaporator temperatures, as they were located nearest to the heater block on heat pipe. Due to curvature effect of heat pipe surface, it was difficult to insert temperature sensors exactly on the evaporator inside the heater block.

The result being slightly lower thermal resistance reported than the exact value. Also, thermal resistance in adiabatic section was considered negligible due to identical temperatures of T_5, T_6 and T_7.

The total convective heat transfer coefficient (h_T) was calculated as per eq. (4.8) [92] under the steady state condition of heat pipe

$$h_T = \frac{Q}{A_{se}\,(T_e - T_c)} = \frac{Q}{A_{se}\left[\left(\frac{T_1+T_2}{2}\right) - T_9\right]} \tag{4.8}$$

where, Q = total heat power (W), A_{se} = total surface area of evaporator heat transfer surface (m^2) A_{se}=20 $(w + 2h)\ 2l_e$ where, T_e And T_c are evaporator and condenser temperatures (°C) respectively.

The uncertainty in temperature (U_T) was calculated using the square formula as per eq. (4.9)

$$U_T = \sqrt{\left(\frac{dT}{T_{avg}}\right)^2 + \left(\frac{dW_{heater}}{Q}\right)^2 + \left(\frac{dT_{data\ logger}}{T_{avg}}\right)^2 + \left(\frac{dQ_{insulation}}{Q_{insulation}}\right)^2} \tag{4.9}$$

The relative uncertainty in thermal resistance of heat pipe was calculated as per eq. (4.10)

$$\frac{dR}{R} = \sqrt{\left(\frac{d(\Delta T)}{\Delta T}\right)^2 + \left(\frac{dQ}{Q}\right)^2} \tag{4.10}$$

The relative uncertainty in convective heat transfer coefficient was calculated as per eq. (4.11)

$$\frac{dh}{h} = \sqrt{\left(\frac{d(\Delta T)}{\Delta T}\right)^2 + \left(\frac{dQ}{Q}\right)^2 + \left(\frac{dA}{A}\right)^2} \tag{4.11}$$

4.4 Results and Discussions

In this section, the effects of fluid filing ratio are discussed on the performance of AGMBHP. The start-up characteristic is described with equal and unequal heat loads on the evaporators. Thermal resistance and its variation is elaborated. The dynamic characteristic of heat pipe is plotted at different heat loads. The temperature variation along the axial direction of heat pipe as well as the variations in heat transfer coefficients are also discussed. Effect of cooling water flow rate and its consequences are also discussed for optimum filling ratio.

4.4.1 Effects of fluid filling ratio

Filling ratio is considered as a significant performance parameter in the working of heat pipe. Performance of heat pipe is largely dependent on the quantity of working substance required for pumping heat from source to sink. Hence, in the present study, as discussed earlier, filling ratio was defined as the ratio of volume of water filled in the heat pipe to the volume of grooves when completely filled. It was necessary to determine the optimum value or range of filling ratio for which heat pipe could work satisfactorily for the given wide range of heat load. Less than required quantity of filling ratio might result in dry-out at comparatively low value of heat load whereas excess quantity of working substance would obstruct the vapour flow path [12].

In the present study, six filling ratios (75%, 100%, 125%, 150%, 175%, and 200%) were taken into consideration for the experimental study. Both the evaporators were given equal heat load on both the sides and steady state was attained. Results were plotted in terms of steady state temperature for different heat loads at different filling ratios for both the evaporators. Figure 4.4 (a-f) shows the effect of different filling ratios on the temperatures of both the evaporators and condenser at equal heat loads (i.e., 20 W, 40 W…up to 120 W each on both evaporators). Moreover, in the present study, maximum heat load was kept limited to 240 W due to its applications in space and electronics cooling as generally it was considered as the representative value of heat load [94]. It was observed that, with an increase in heat load, the surface temperature of evaporator and condenser increased. However, for the representative heat load up to 240 W, it was always desirable to attain minimum temperature for a given heat load. As practical devices like heat pipes are not ideal, they always give some non-zero thermal resistance and so does the temperature difference exist between the source and the sink.

As shown in Fig. 4.4 (a-b), with 75% and 100 % filling ratio, heat pipe dried out at 160 W and 180 W respectively. Sudden rise in temperature (here T_1) in any of the evaporator was the indication of dry-out as shown in the diagram. From Fig. 4.4 (c), it was observed that for 125 % FR, dry out occurred at 220 W heat load. In case of 150 %, 175 % and 200 % filling ratio, no dry-out was observed up to representative heat load of 240 W. However, in these cases, variation in surface temperature was observed at evaporator even at same heat load. For 240 W heat load, the maximum surface temperatures were found to be 99.7 ˚C, 111.6 ˚C and 119.2 ˚C for filling ratio 150 %, 175 % and 200 % respectively.

Insufficient quantity of working substance in heat pipe limited the heat transport capacity which resulted in early dry-out. When the vapour formation rate in evaporator was higher than the vapour condensation rate in condenser, required quantity of working substance could not reach to evaporator which resulted in sudden spike in the evaporator temperature.

In case of filling ratio 150%, 175 % and 200 % (Fig. 4.4 (d-e-f)), sufficient quantity of working substance was available to handle high heat load. However, excess quantity of liquid in the heat pipe restricted the path of vapour which subsequently resulted in local temperature rise that happened in case of 175% and 200 % filling ratio.

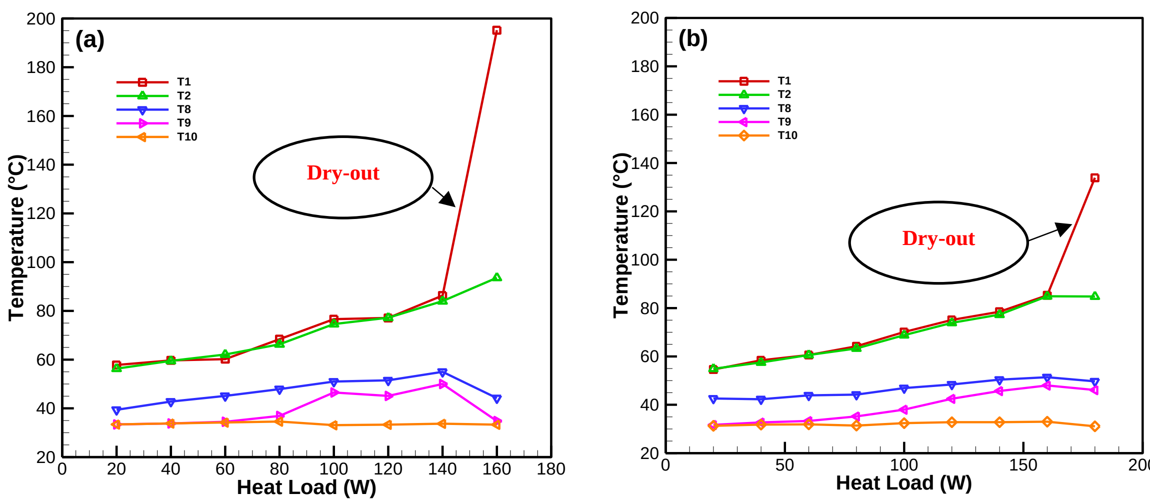

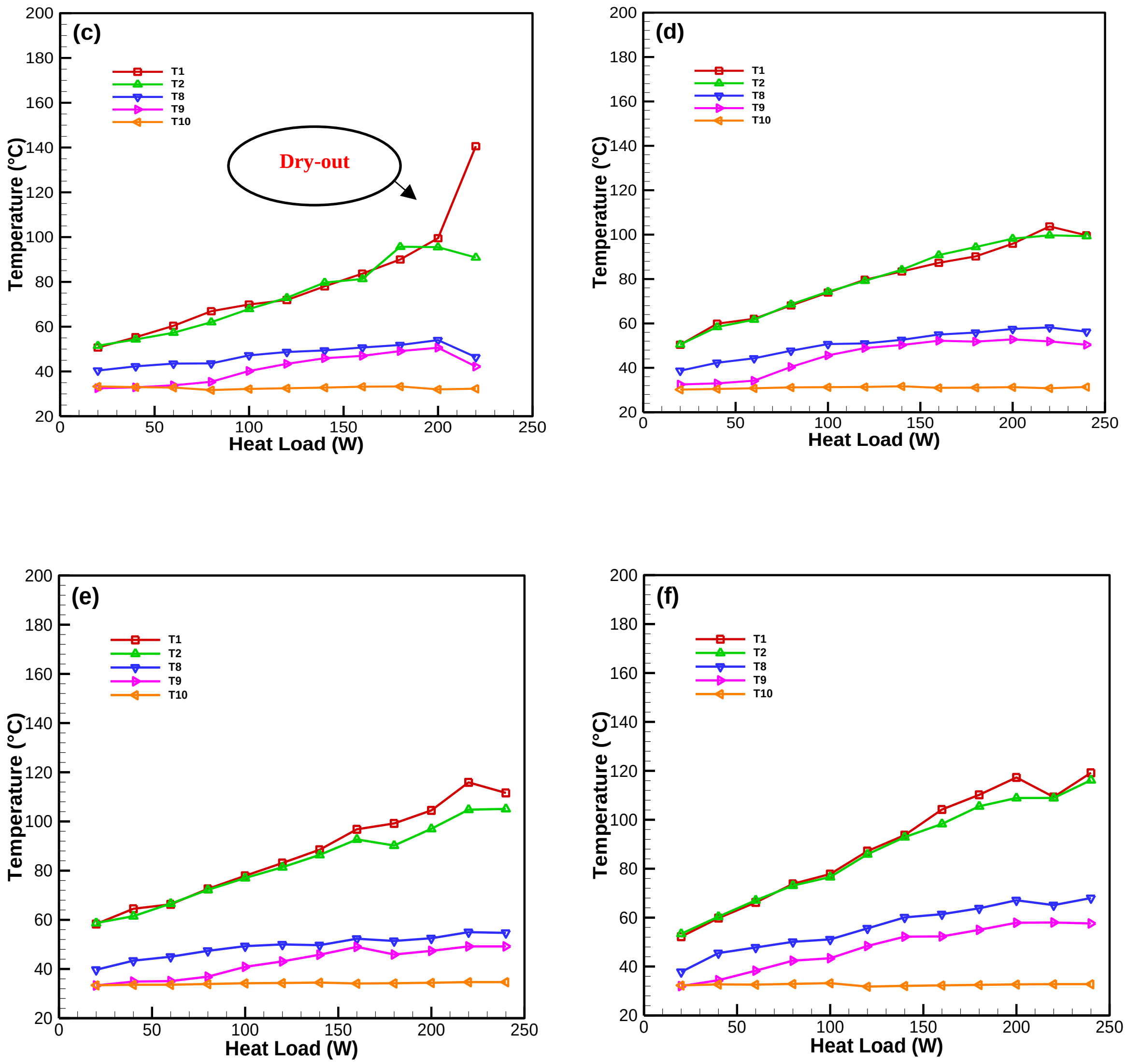

Fig. 4.4 Thermal performance of AGMBHP with different filling ratios: (a) 75% (b) 100% (c) 125% (d) 150% (e) 175% (f) 200%.

4.4.2 Variation in the thermal resistance

One of the methods of studying the effect of the filling ratio on the heat pipe performance is to evaluate the total thermal resistance between evaporator and the condenser. Total thermal resistance of heat pipe was calculated using eq. (4.7). The separate thermal resistances of evaporator and condenser sections were calculated using eq. (4.5) and (4.6) respectively. Variation in total thermal resistance with respect to the heat load at different filling ratios are shown in Fig. 4.5.

The values of maximum and minimum thermal resistances were found to be in the range of 1.02 to 0.23 °C/W, 0.88 to 0.21 °C/W, 0.72 to 0.20 °C/W, 0.89 to 0.19 °C/W, 1.09 to 0.23 °C/W and 0.89 to 0.21 °C/W for 75%, 100%, 125%, 150%, 175% and 200% filling ratio respectively. It was observed that for lower filling ratio (75% and 100%) the range of thermal resistance is large. In the range of 125% to 150 % FR, average thermal resistances were comparatively lower and again for higher filling ratio (175% and 200%), average thermal resistance increased. The overall total thermal resistance varied from 1.09 °C/W (maximum) to 0.19 °C/W (minimum) for all the filling ratios. For 125 % FR, average thermal resistance was minimum for majority of heat loads but this filling ratio led to dry-out at 220 W heat load. However, the minimum thermal resistance was found out to be at 150% FR and 240 W heat load where the performance of heat pipe can be considered optimum.

From the above observations, it was understood that the optimum filling ratio for the proposed geometry of heat pipe lies in between 125-150 % which would transport the representative heat load up to 240 W and results in comparatively lower thermal resistance. However, this is only true for the present geometry, given number of grooves and selected heat load range. Moreover, it was observed that at lower value of heat loads, thermal resistances were comparatively large. This was due to the fact that at lower heat loads, less quantity of vapour generation might not produce sufficient pressure in the heat pipe, resulted in slow vapour velocity and so did the slow evaporation-condensation cycle.

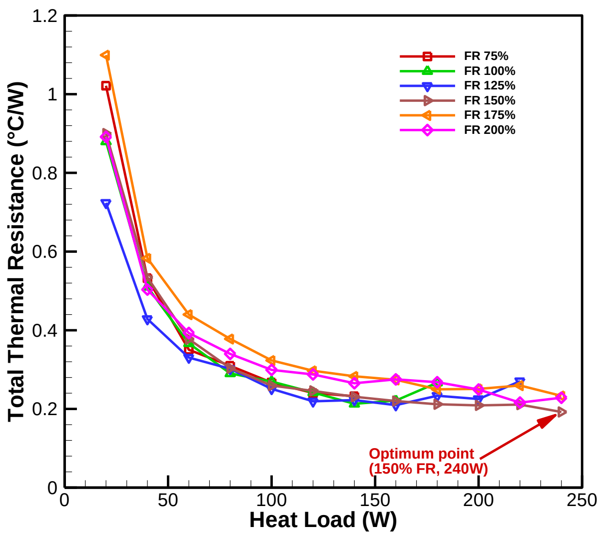

Fig. 4.5 Thermal resistance variation at various heat loads with different filling ratios.

4.4.3 Temperature distribution along the length

Temperature distribution along the length is an important criterion as far as performance of heat pipe is concerned. Kim et al. [92] used the same in his work on cylindrical conventional heat pipe. However, due to "T" shape of AGMBHP, the respective temperatures on similar locations on both the evaporators were averaged and temperature distribution was obtained as shown in Fig. 4.6 (a-b-c-d-e-f). The average of T_1-T_2, T_3-T_4 and T_5-T_6- T_7 were considered as a single point along the length of heat pipe. Here, it should be noted that temperature distribution was obtained at equal heat loads on both the evaporators and under the steady state condition.

Ideally, it was desirable to have horizontal temperature distribution i.e., constant temperature along the length of heat pipe which would indicate zero thermal resistance. However, in practical devices it was not possible to achieve the same. As shown in Fig. 4.6 (a-b-c) for 75%, 100% and 125% filling ratio, dry-out was clearly visible. It was observed that in case of 75% FR, dry-out caused temperature rise in large length of heat pipe (length covered by sensors T_1, T_2, T_3, and T_4) whereas in case of 100 % and 125 % FR, only evaporator was getting dried-out. This tendency of temperature distribution gave an intuition that the heat pipe was approaching optimum performance as filling ratio was increased. For 150% FR, it was seen that the large portion of heat pipe resulted in minimum temperature variation (length covered by sensors T_3, T_4, T_5, T_6 and T_7). Further, for 175% and 200 % FR, it was observed that temperature distribution along the length was getting scattered with respect to heat load with more temperature difference.

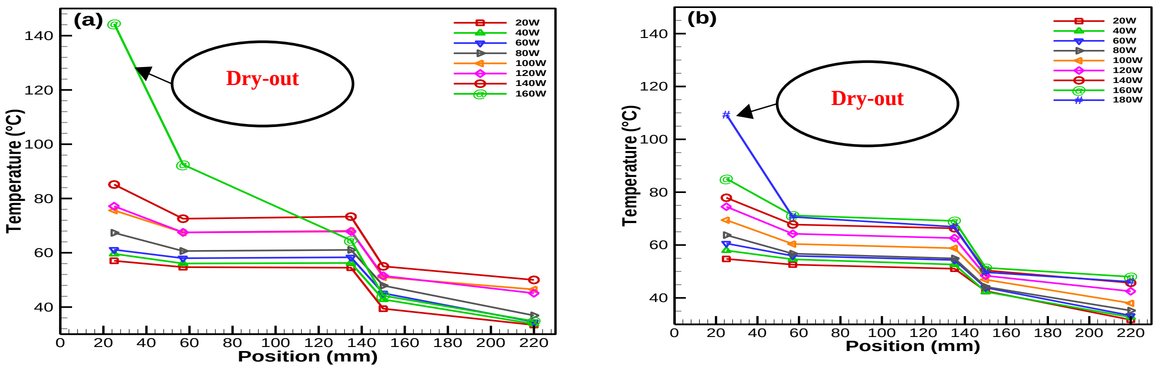

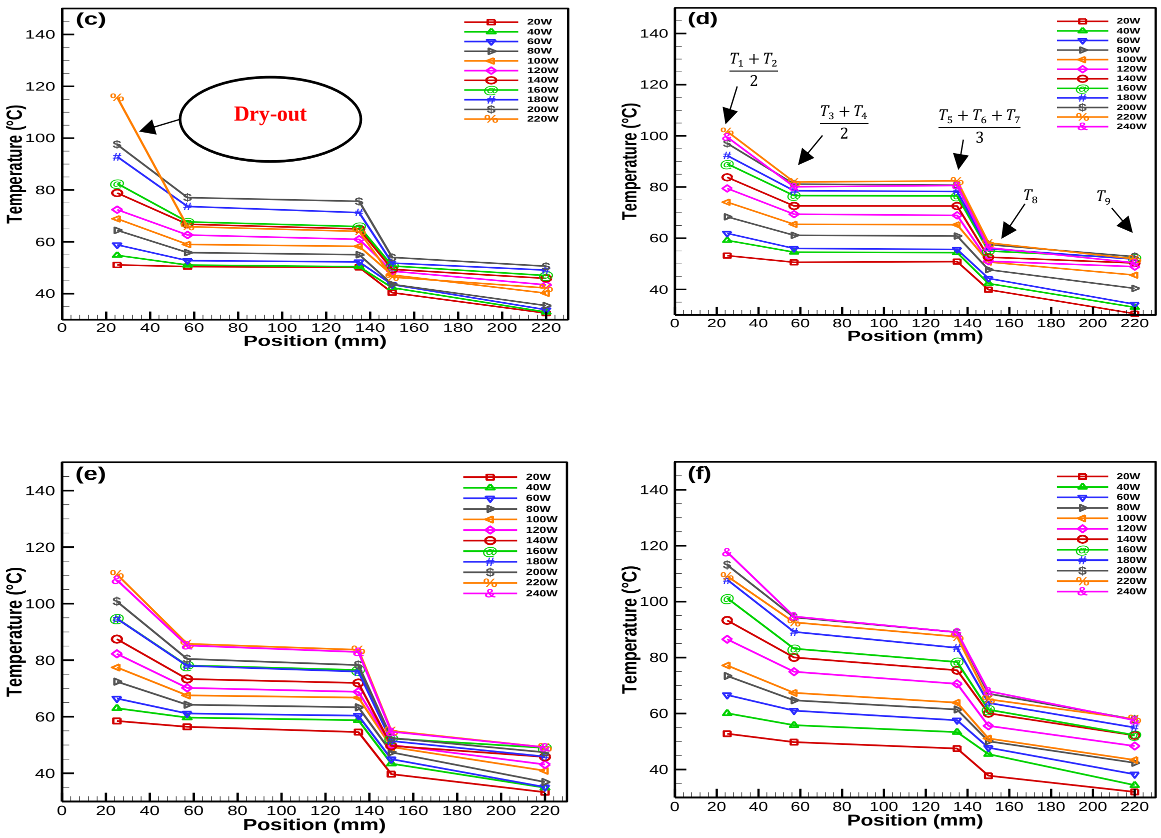

Fig. 4.6. Temperature distributions along the length at different heat loads with filling ratio of (a) 75% (b) 100% (c) 125% (d) 150% (e) 175% (f) 200%.

4.4.4 Start-up characteristic

(a) With equal heat loads on the evaporators at different filling ratios

Start-up characteristics are the response of heat pipe before it reaches to steady state when heat load is applied to evaporator. It is a transient response of heat pipe while heating. Figure 4.7 shows the start-up characteristics of heat pipe for some selective heat loads and filling ratios. It was observed that in all the cases heat pipe reaches to steady state within 45 minutes. It should be noted that when variation in temperature was negligible with respect to time, steady state was considered to be reached. In this study, both the evaporators were applied with equal heating loads.

Figure 4.7 (a-b) shows the start-up characteristics of 75% and 100% filling ratio for 140 W heat load. For the same heat load, 100% filling ratio resulted in quick starting and lower steady temperature. It was seen that at moderate value of heat load, moderate quantity of working substance was required to avoid overheating of heat pipe. Steady temperatures and start-up time were found to be T_1 = 86.3 ˚C, T_2 = 84 ˚C, 40 min and T_1 = 78.5 ˚C, T_2 = 77.3 ˚C, 31.6 min for 75% and 100% filling ratio respectively. Figure 4.7 (c-d) shows the start-up characteristics of 125% and 150% filling ratio for 200 W heat power. Almost identical results were obtained for both the filling ratios. Steady temperatures and start-up time were T_1 = 99.5 ˚C, T_2 = 95.5 ˚C, 28.3 min and T_1 = 95.9 ˚C, T_2 = 98.2 ˚C, 28.3 min for 125% and 150% filling ratio respectively. Figure 4.7 (e-f) shows the start-up characteristics of 175% and 200% filling ratio for 240 W heat load. Steady temperatures and start-up time were T_1 = 104 ˚C, T_2 = 97 ˚C, 25 min and T_1 = 117.3 ˚C, T_2 = 108.9 ˚C, 30 min for 175% and 200% filling ratio respectively. For 240 W heat load and 150% filling ratio (point of minimum thermal resistance), steady temperatures and start-up time were T_1 = 99.7 ˚C, T_2 = 99.3 ˚C, 24.8 min respectively. At maximum representative load of 240 W, it was clear that 150% filling ratio resulted in lower steady temperature and quick start-up compared to others. Maximum evaporator temperature was observed to be lower than 100 °C which is a common requirement in electronics cooling [94]. However, steady characteristics obtained for 125% filling ratio, resulted in comparable and better performance in many cases before dry-out at 220 W. This was again an indication of optimum filling ratio lied in between 125 % to 150%.

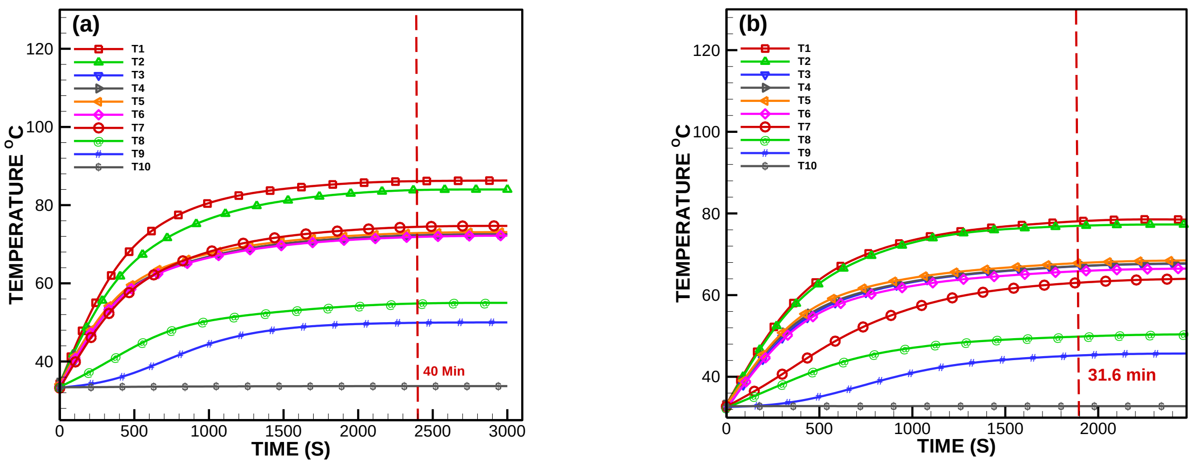

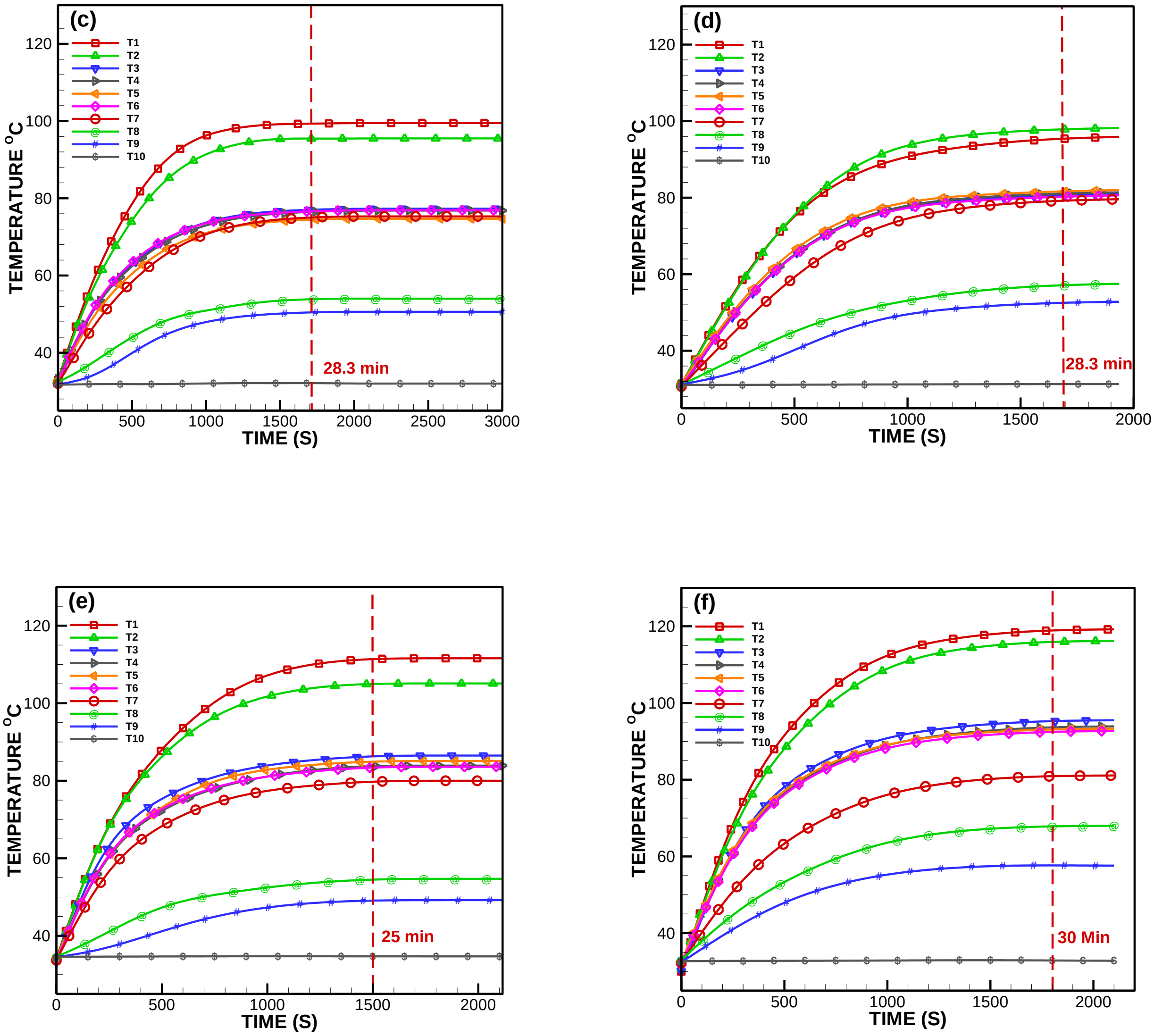

Fig. 4.7 Start-up characteristics for various filling ratios and heat loads (a) 75% and 140 W (b) 100% and 140 W (c) 125% and 200 W (d) 150% and 200 W (e) 175% and 240 W (f) 200% and 240 W.

Initially heat pipe was in ambient condition from where heating started and it reached to the steady state condition. Start-up temperature rise is the temperature difference of evaporator at steady state and at starting. It is desirable to have minimum start-up temperature rise for given heat load to have minimum wall conduction compared to phase change. Figure 4.8 shows the summary of start-up temperature rise for different filling ratios for all the heat loads. It was observed that for heat loads up to 200 W, 125% filling ratio resulted in minimum temperature rise for majority of the heat loads, indicating reasonably better performance.

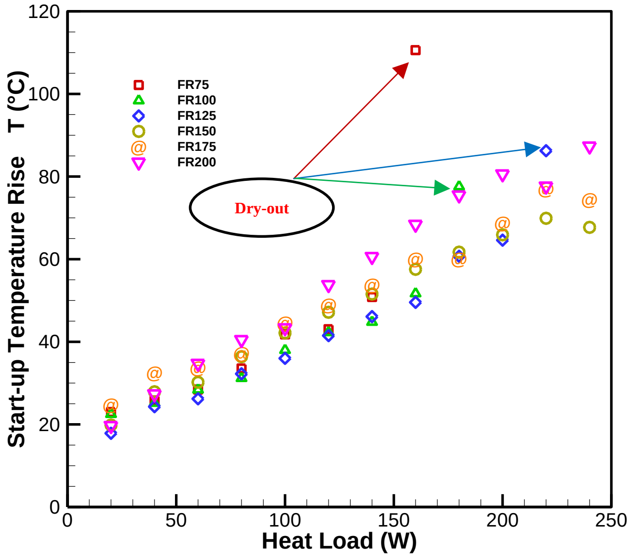

Fig. 4.8. Summary of final and initial temperature difference of evaporator at different heat loads and filling ratios.

(b) With unequal heat loads on the evaporators at 125 % filling ratio

In this section, start-up characteristic was studied with an unequal heat load on two evaporators such that the total heat load remained constant equals to 120 W. This study was done with a constant filling ratio of 125%. In this experimental study, heat load was supplied in the set-of (a) 120-0 W (b) 100-20 W and (c) 80-40 W (d) 60-60 W and their results are shown in Fig. 4.9 (a-b-c-d) for comparison.

It was clear from Fig. 4.9(a-b-c-d), that heat pipe under unequal heat load condition, reached to steady state within 45 minutes. However, it was clear that evaporator with higher heat load resulted in high temperature comparatively. The maximum evaporator temperatures were found to be 107.6 ˚C and 57.3 ˚C, 82.3 ˚C and 60.2 ˚C, 75.8 ˚C and 62.9 ˚C, 71.9 ˚C and 72.9 ˚C for (a) 120-0 W (b) 100-20 W and (c) 80-40 W (d) 60-60 W respectively. It was seen that, as the heat load distribution between the two evaporators became more and more even, the maximum temperature as well as the temperature difference between the two evaporators also decreased.

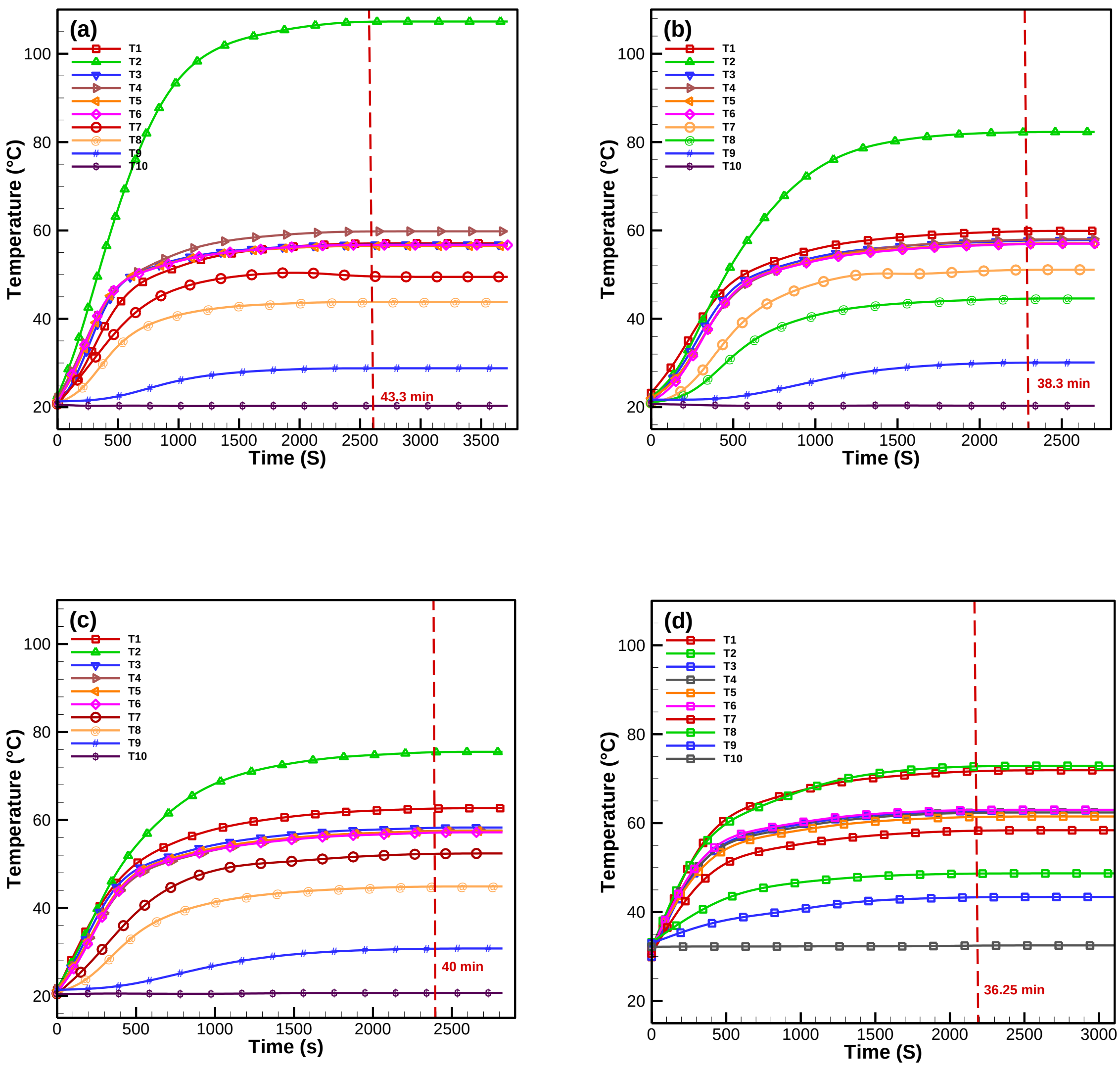

Fig. 4.9 Start-up characteristics of AGMBHP with 125 % filling ratio with variable heat load on evaporator (a) 120-0 W (b) 100-20 W (c) 80-40 W (d) 60-60 W.

4.4.5 Variation in the heat transfer coefficient

Total heat transfer coefficient is an important performance parameter in the working of heat pipe. Total heat transfer coefficient for AGMBHP was calculated by using eq. (4.8) and its values are plotted in Fig. 4.10 with respect to different heat loads. The sudden reduction in heat transfer coefficient indicated dry out of heat pipe at given heat load for 75%, 100% and 125% filling ratio respectively. The maximum and minimum value of heat transfer coefficient were found to be 2.71 kW/m^2°C to 0.44 kW/m^2°C respectively. It was observed that the maximum heat transfer coefficient for heat pipe was obtained where thermal resistance was minimum. Moreover, the results obtained here for variation of heat transfer coefficient also validated the thermal resistance results described in Fig. 4.5.

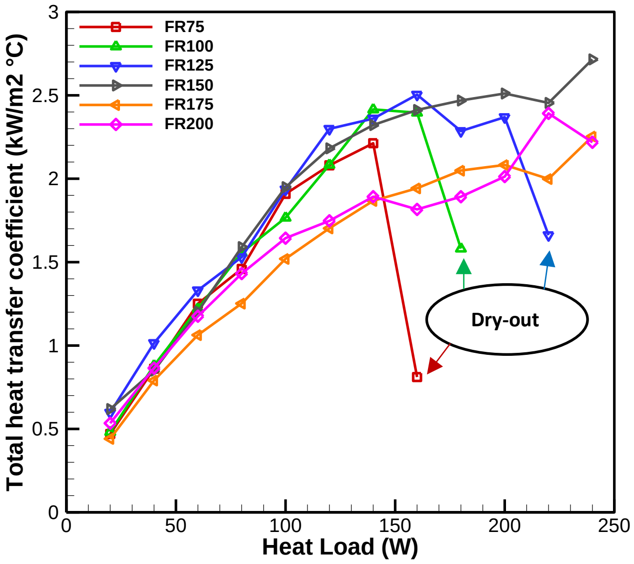

Fig. 4.10 Variations in total heat transfer coefficients with heat loads for different filling ratios.

4.4.6 Dynamic characteristics

When heat pipe is subjected to continuous progressive heating or cooling by increasing or decreasing the heat load immediately after achieving the steady state, the response of the heat pipe is known as dynamic characteristics [58]. Figure 4.11 and Fig. 4.12 show dynamic characteristics of heat pipe during heating, cooling and combined heating and cooling for 125% and 150% filling ratio respectively. For this study, the heat load was increased at an interval of 40 W in both the cases. However, the maximum heat load applied was 200 W and 240 W for 125 % and 150 % filling ratio respectively. It was seen that the maximum temperature remained below 90 ˚C and 100 ˚C for 125% and 150% filling ratio respectively. This could be considered as common working range for high performance electronics cooling[93], [94].

For both 125 % and 150 % FR, the heating, cooling as well as combined characteristics were found to be smooth, indicating stable performance of AGMBHP under dynamic condition. Similar dynamic characteristics were obtained by authors in their previous work [97] for multi-branch thermosiphon heat pipe. The phenomena like temperature jump were not observed in any of the cases which is a comparatively improved sign of performance of AGMBHP.

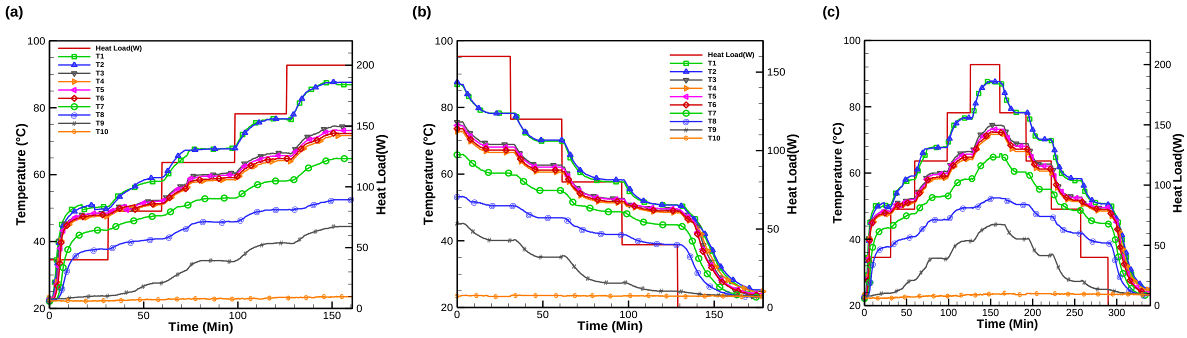

Fig. 4.11 Dynamic characteristics with heat load ranging from 0 to 200 W for 125 % filling ratio during (a) Heating (b) Cooling (c) Combined heating and cooling.

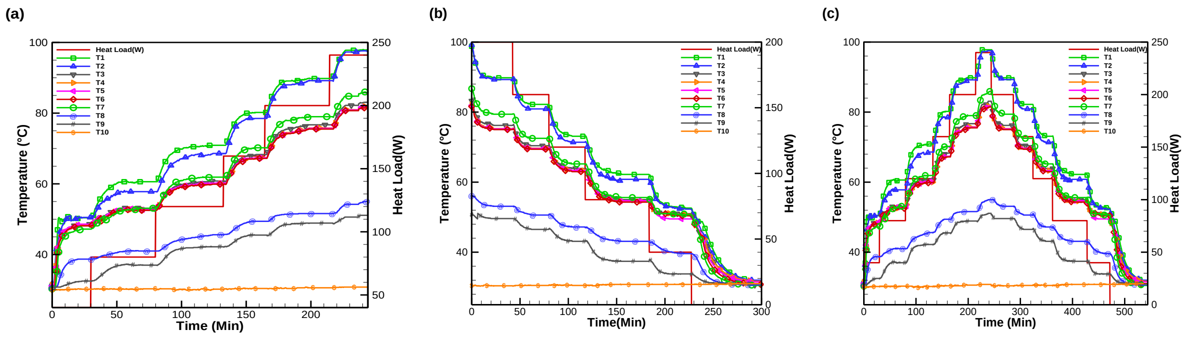

Fig. 4.12 Dynamic characteristics with heat load ranging from 0 to 240 W for 150 % filling ratio during (a) Heating (b) Cooling (c) Combined heating and cooling.

4.4.7 Effect of cooling water flow rate in horizontal orientation (150% FR)

It is a well-established fact that the performance of heat pipe is largely dependent on the cooling water flowrate of condenser [32], [33]. In the present study, experiments were performed with three different flowrates in the water-cooled condenser viz. 2.5 ml/s, 5 ml/s and 10 ml/s.

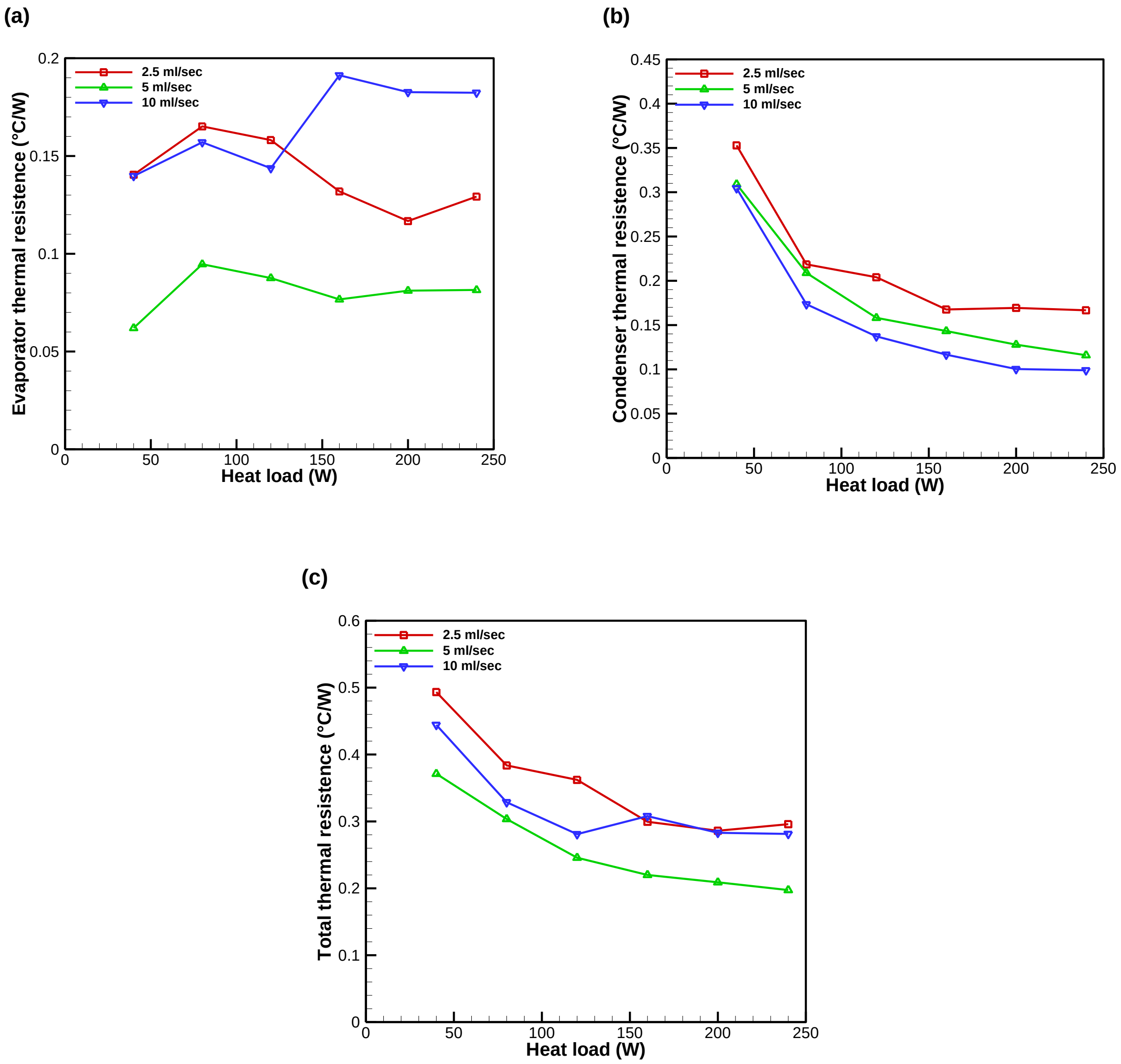

Fig. 4.13 Thermal resistance at different cooling water flow rates
(a) Evaporator (b) Condenser (c) Total.

Investigation was carried out with different flowrates for 150% filling ratio and horizontal orientation of heat pipe. The results were compared in terms of evaporator thermal resistance, condenser thermal resistance and total thermal resistance of heat pipe calculated as per eqs. (4.5), (4.6) and (4.7) respectively. Figure 4.13 shows the variation of thermal resistances of evaporator, condenser and total heat pipe with different water flowrates with increase in heat load. It is always desirable to have optimum cooling requirements for heat pipe in view of power saving opportunities. Insufficient cooling may lead to dry-out of heat pipe and an excess cooling may increase the power usage for condenser flow.

Figure 4.13(a) shows the variation of evaporator thermal resistance for different flowrates at different heat loads. For 5 ml/s cooling flowrate, evaporator thermal resistance was found to be minimum. Upto 120 W heat load, thermal resistance for cooling flowrate of 10 ml/s was observed to be lower compared to cooling flowrate of 2.5 ml/s. At higher heat loads (above 120 W), evaporator resistance increased for higher cooling flowrate. Evaporator resistance basically depended on temperature difference between evaporator and adiabatic section. The adiabatic section remained comparatively colder for higher cooling flowrate. At lower heat load, where evaporator temperatures were also low, it resulted in lower evaporator resistance for high cooling flowrate. For high heat load values, evaporator temperatures tended to increase, but the adiabatic temperatures were still low due to high cooling flow rate [32]. This resulted in increment in evaporator resistance for heat load above 120 W for 10 ml/s cooling flowrate.

Variation in condenser resistance is shown in Fig.4.13 (b) where, cooling flowrate of 10 ml/s provided minimum resistance. It was basically dependent on the temperature difference between condenser inlet to outlet. It was obvious from the figure that for higher cooling flow rate, condenser as well as adiabatic temperatures were comparatively low and so did the thermal resistance [32].

However, from Fig. 4.13 (c), it was clear that the total thermal resistance was minimum in case of 5 ml/s cooling flowrate. For cooling flowrate of 2.5 ml/s, heat pipe attained comparatively higher temperature differences due to insufficient cooling. In case of 10 ml/s flowrate, the excess cooling of condenser increased the temperature difference between the heat source and heat sink due to colder condenser. In case of lower cooling flowrate, evaporator temperatures were dominating and in case of higher cooling flowrate, condenser temperatures were dominating. The above results showed that cooling flowrate of 5 ml/s is optimum for AGMBHP.

4.4.8 Comparison of axially grooved multi-branch heat pipe (AGMBHP) with multi-branch thermosiphon heat pipe (MBTHP)

A heat pipe with similar specifications was tested by author in his previous work [97] in thermosiphon mode without any wick structure. In their study, the cooling water flowrate was kept as 52 ml/s in condenser. A brief comparison of multi-branch thermosiphon heat pipe (MBTHP) with axially grooved multi-branch heat pipe

(AGMBHP) in horizontal orientation in terms of thermal resistance and effective thermal conductivity at different heat loads is shown in Fig. 4.14. Thermal resistance and effective thermal conductivity of heat pipe are those performance parameters which are used to compare two different heat pipes irrespective of their design parameters, wick structure, working range and dimensions. Both the heat pipes had similar geometry but different working parameters. Authors suggest both the heat pipes in the application of electronics cooling with multiple heat loads. Hence, the following comparison is made between these two heat pipes in terms of above-mentioned performance parameters. In MBTHP, 50% and 60% filling ratios were taken into comparison as it led to minimum thermal resistance and maximum effective thermal conductivity [97]. In case of AGMBHP, as described earlier, optimum range of filling ratio was found to be 125-150% which was taken into consideration. Effective thermal conductivity was calculated using eq. (4.12) [4], [6].

$$k_e = \frac{Q\,L_{eff}}{A_C\,\Delta T}\text{, where } L_{eff} = \frac{L_{evap}+L_{cond}}{2} + L_{adia} \tag{4.12}$$

It is observed from Fig. 4.14 that AGMBHP at 240 W heat load provided minimum thermal resistance of 0.19 ℃/W in comparison with MBTHP which resulted 0.21 ℃/W at 160 W heat load under the tested condition. Moreover, maximum effective thermal conductivities were found to be 34.2 kW/m K and 31.8 kW/m K for MBTHP and AGMBHP at 160 W and 240 W respectively. However, the major and the most significant advantage of AGMBHP over MBTHP was found to be its cooling requirement. AGMBHP used 5 ml/s cooling water flowrate compared to 52 ml/s for MBTHP. Cooling requirement of AGMBHP was found to be almost 10 times lesser with slightly less effective thermal conductivity and thermal resistance. In electronics cooling, it is always desirable to have minimum cooling requirement for lower operating cost of equipment [24].

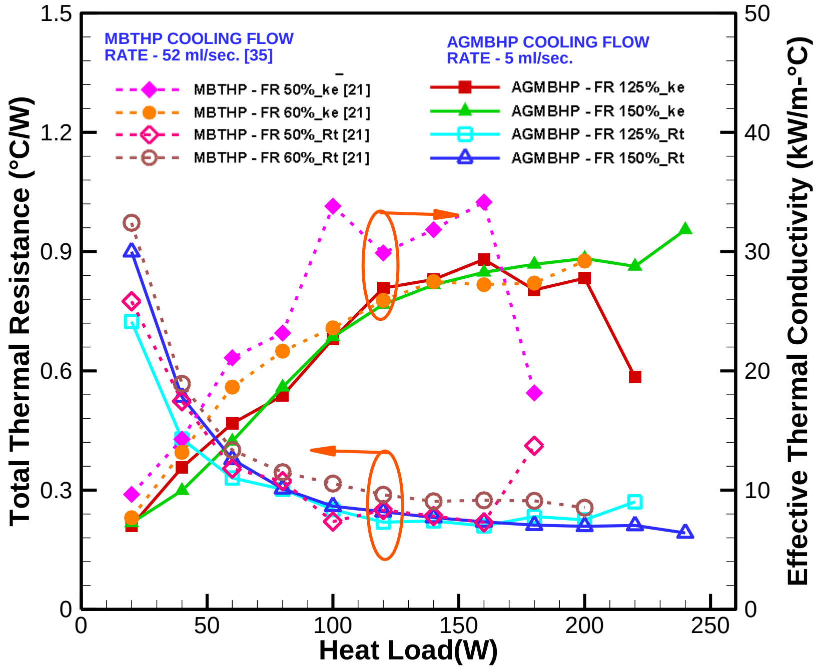

Fig. 4.14 Total thermal resistance (R_t) and effective thermal conductivity *(k_e)* comparison of MBTHP [97] with AGMBHP.

From the above results, it was understood that both the heat pipes could be used in the cooling of multiple heat sources. However, the operating parameters in both the heat pipes were quite different. In a gravity assisted thermosiphon, condensate return was dependent on cooling rate and gravity. In order to provide sufficient liquid return at large value of heat load, sufficiently high cooling duty of condenser was necessary because the vapour bubbles tended to accumulate at vertical branch (near to condenser) in MBTHP. Larger the heat load, higher would be the temperature of vapour bubble near to heat sink. It was found that the working of MBTHP became pulsating in nature in case of lower cooling rates. At lower cooling rates, condensation of vapor bubbles was delayed which resulted in rise in overall temperature which further suddenly decreased once the bubble was collapsed due to condensation and chunk of liquid fell down due to gravity and reached to evaporator. In order to avoid such pulsating working of MBTHP, high cooling rates were required for the condenser. In case of AGMBHP in horizontal orientation, sufficient liquid return was available due to capillary pressure even at high heat loads. Accumulation of high temperature vapour at condenser end was not possible due to proper distribution of liquid return through channels and vapour space.

4.5 Closure

In the present study, experimental investigations were carried out on the axially grooved multi-branch heat pipe (AGMBHP) with different filling ratios in the wide range of heat loads. Steady characteristics with equal and unequal heat loads were applied on both the evaporators. Performance parameters like thermal resistance, heat transfer coefficient and effective thermal conductivity were evaluated. Dynamic response of heat pipe was studied along with the effect of condenser cooling flow rate. Heat pipe was tested for different orientations and temperature distribution along the length was studied. From the above study, following observations are made.

The optimum fluid filling ratio for the given design of AGMBHP, was found to be in the range of 125% to 150% as the average thermal resistance was minimum in this range for the representative heat load. However, 150% FR, provided 240 W heat transport capacity which was more than that for 125% FR (200 W) and the minimum thermal resistance was found to be 0.192 °C/W at 240 W. Moreover, when the heat pipe was operated under optimum condition, the start-up time reduced significantly. The maximum heat transfer coefficient obtained for AGMBHP was 2.72 kW/m^2°C at 150% filling ratio and 240 W heat load. The results obtained for heat transfer coefficient are in-line with the thermal resistance results. The minimum thermal resistance of AGMBHP was found to be lower compared to MBTHP. Moreover, the cooling requirement of AGMBHP is ten times reduced compared to MBTHP for comparatively higher heat transport capacity. This is the most significant advantage in case of electronics cooling application.

The following paper is based on this chapter:

Bhatt, A.A., Jain, S.V., Patel, R.N, Vaghela, D., 2023, "Parametric Study on Axially Grooved heat pipe with two heat sources and one heat sink with multiple branches". ASME J. Therm. Sci. Eng. Appl., doi: https://doi.org/10.1115/1.4062155

Chapter 5

Orientation Study of Axially Grooved Multi-Branch Heat Pipe (AGMBHP)

This chapter describes the experimental investigation carried out on axially grooved multi-branch heat pipe (AGMBHP) having 20 number of grooves with different orientations. The performance parameters and experimental set-up and its specifications are elaborated while performing the orientation study.

This chapter elaborates the investigation of T-shaped multi-branch heat pipe with 20 numbers of axial grooves and various novel type of orientations i.e., (a) horizontal orientation (HO) (b) gravity assisted orientation (GAO) (c) Anti-gravity orientation (AGO) and (d) compound orientation (CO). Optimum water filling ratio of 150% is considered for the experimentations. A water-cooled condenser is used with constant flow rate (5 ml/s) of water. Results are analyzed in terms of start-up characteristics, heat transfer co-efficient, thermal resistance and effective thermal conductivity.

5.1 Experimental Set-up and Specifications

The setup included "T" shaped axially grooved multi-branch heat pipe (AGMBHP), two copper blocks inserted with cartridge heaters, tube in tube heat exchanger over condenser portion, two independent variable auto-transformers, ring type temperature sensors, data logger etc. Figure 4.1 illustrates the schematic diagram of the experimental setup along with temperature sensor locations. The same experimental set-up was used in the orientation study as discussed in chapter 4. The orientation study was carried out by considering all the parameters in optimum condition of AGMBHP as discussed in chapter 4 on parametric study. The filling ratio and condenser cooling flowrate were kept optimum as 150% and 5 ml/s respectively. The remaining parameters were kept constant for the study.

The image of the experimental setup with the heat pipe oriented anti-gravity is shown in Fig. 5.1. The anti-gravity position of the heat pipe model with heater blocks and condenser is depicted in Fig. 5.2(a). The positions of the heat pipe in the horizontal, gravity-assisted, and compound orientations are depicted in figures 5.2 (b), (c), and (d), respectively. Table 5.1 lists the primary specifications of the AGMBHP setup. Two different variable auto-transformers were employed in order to individually manage the heat input for both evaporators. To reduce heat loss to the environment while conducting the experiments, the complete heat pipe testing assembly was covered with glass wool insulation.

In order to measure the temperatures at various locations along the heat pipe, nine numbers of resistance temperature detector (RTD) sensors were used as shown in Fig. 4.1. The temperatures of evaporator branches were measured at two locations on either side along the length (T_1, T_3 and T_2, T_4) and three sensors were provided on the adiabatic section (T_5, T_6, T_7). Two sensors (T_8, T_9) were provided to measure the temperature of the condenser section at inlet and outlet. Two sensors (T_{11}, T_{12}) were used to measure cooling water temperature at inlet and outlet respectively. One sensor (T_{10}) was used to measure the ambient temperature. Thermal conductive grease was applied on the temperature sensors before mounting them on the heat pipe to minimize the contact resistance. All the temperature readings were automatically recorded and stored by the temperature data logger.

Table 5.1

Specifications of Experimental Set-up and Heat Pipe

Component	Specifications
Heat pipe	Material: Copper OD: 9 mm ID: 7 mm Overall size: Horizontal branch: 210 mm Vertical branch: 110 mm
Wick Structure	Type: Axially grooved Size of groove: 0.6 mm width and 0.6 mm depth along the length No. of grooves: 20 Shape of grooves: Rectangular
Working fluid	Deionized water
Evaporator	Length: 25 mm Numbers: 2
Condenser	Length: 70 mm Number: 1
Water heat exchanger	ID: 50 mm Length: 65 mm
Filling ratio	150%
Cooling water flowrate	5 ml/s

5.2 Experimental Procedure

A high vacuum was initially created into the heat pipe. Due to the high value of latent heat, high vacuum offers lower boiling points of working substance as well as high heat pumping capacities. Heat pipe was evacuated when needed, then filled with deionized water and sealed at the predetermined filling ratio (i.e., 150%). The filling ratio was regarded as 100% when all of the axial grooves (liquid channels) within the heat pipe were entirely filled with water. As a result, the 150% filling ratio was precisely determined and used to experiments. A steady initial vacuum level of -700 mm of Hg was fixed after the required charging procedure and maintained throughout all of the trials.

The heaters and all of the temperature sensors were attached on the heat pipe once it had been installed in the configuration. In the current investigation, experiments were conducted using various heat inputs between 20 W and 240 W. By placing heater blocks on it, multiple heat inputs were provided to the evaporator portions depending on the requirement needed. A steady flow rate of 5 ml/s of cooling water was kept up throughout the experiment. The heat exchanger's connections were examined for leaks.

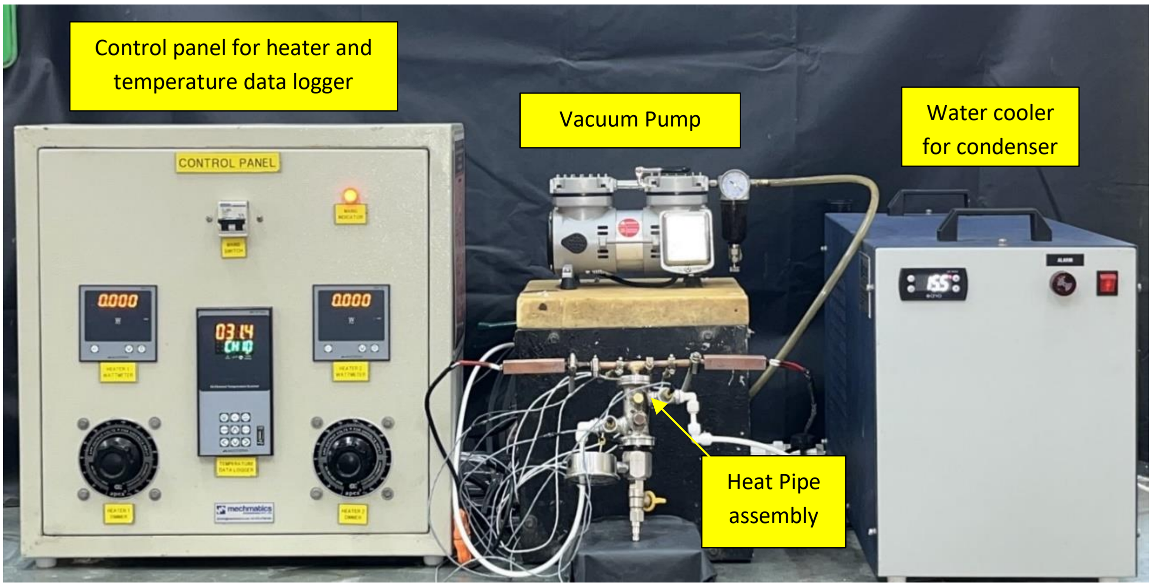

Fig. 5.1 Photograph of Experimental set-up.

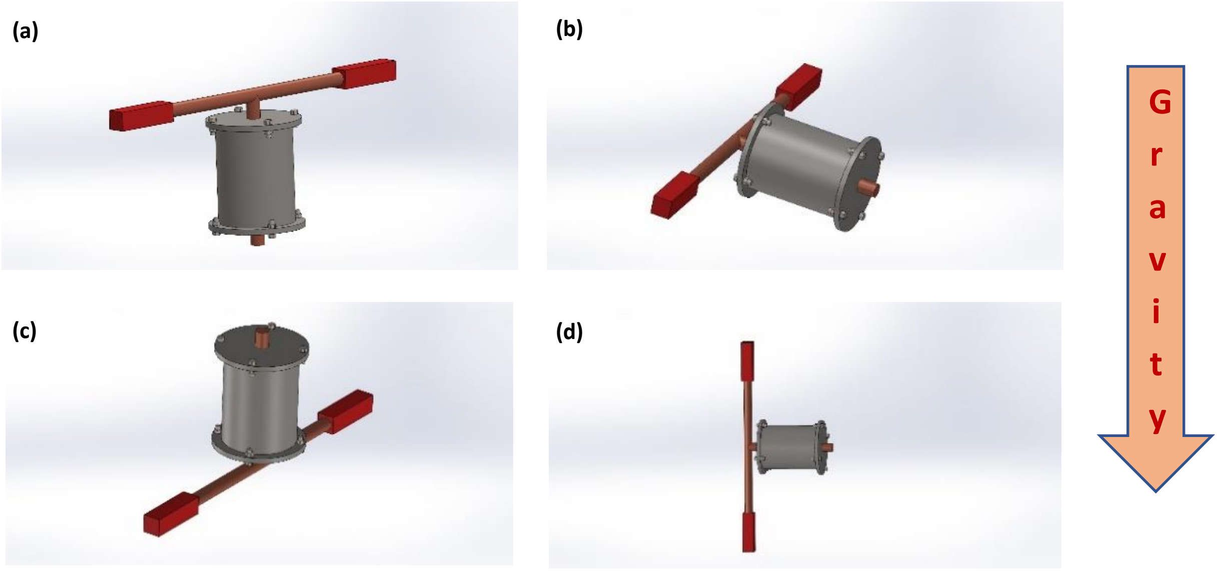

Fig. 5.2 Different type of Orientations (a) Anti-gravity orientation (AGO) (b) Horizontal Orientation (HO) (c) Gravity assisted orientation (GAO) (d) Compound orientation (CO).

All the temperature readings were recorded in the data logger at an interval of 15 seconds. All the measuring instruments were calibrated before putting in use. In order to obtain the total uncertainty in temperature measurement, various parameters like (a) accuracy of temperature sensor PT-100 (b) resolution of temperature data logger (c) accuracy of cartridge heater and its digital indicator and (d) heat loss through glass wool insulation were considered [97]. Calculating all the uncertainties for the total experimental uncertainty in temperature measurement was estimated maximum 5.5 % in accordance with the procedure given by Kline et al. [91] using square formula. Relative uncertainty of convective heat transfer coefficient was also calculated. Maximum relative uncertainty in convective heat transfer coefficient were found to be 5.1 % by considering an accuracy in temperature sensor as $\pm$ 0.1ºC.

5.3 Performance Parameters

Different parameters used to evaluate the performance of heat pipe are described in this section.

The fluid filling ratio (η) of working substance was defined as per eq. (5.1)

$$\eta = \frac{20\ (v_g)}{v_w} \times 100\ \% \tag{5.1}$$

where, v_w = volume of water to be filled inside the heat pipe for required filling ratio (ml), v_g = volume of water that can be filled in one groove (ml) and No. of grooves = 20

The total convective heat transfer coefficient (h_T) and evaporator convective heat transfer coefficient for heat pipe (h_e) were calculated as per eq. (4.8) and (5.2) respectively [92] under the steady state condition of heat pipe.

$$h_e = \frac{Q}{A_{se}\ (T_e - T_a)} = \frac{Q}{A_{se}\left[\left(\frac{T_1+T_2}{2}\right)-\left(\frac{T_5+T_6+T_7}{3}\right)\right]} \tag{5.2}$$

where, Q = total heat power (W), A_{se} = total surface area of evaporator heat transfer surface (m^2) A_{se}=20 $(w + 2h)\ 2l_e$ where, T_e And T_c are evaporator and condenser temperatures (°C) respectively. T_a is adiabatic temperature (taken as average of T_5, T_6, T_7)

The thermal resistances (R_1 and R_2) of individual evaporators (EV_1 and EV_2) were calculated as per eqn. (4.3) and (4.4) respectively.

An equivalent resistance for two evaporators (R_{evap}) was calculated as per eqn. (4.5)

The condenser resistance (R_{cond}) was determined as per eqn. (4.6)

The uncertainty in temperature (U_T) was calculated using the square formula as per eq. (4.9) [91]

The relative uncertainty in thermal resistance of heat pipe was calculated as per eq. (4.10)

The relative uncertainty in convective heat transfer coefficient was calculated as per eq. (4.11).

5.4 Results and Discussion

In this section, the start-up characteristic is described with equal heat loads on the evaporators for different orientations. Total and evaporator heat transfer coefficients and its variation are elaborated. Evaporator and condenser thermal resistances for different orientations are described. Temperature variation along the length is plotted for all the orientations. It is to be noted that the presented orientation study is performed at an optimum filling ratio of 150% for AGMBHP [56].

5.4.1 Start-up characteristics

(a) Anti-gravity orientation

In the anti-gravity orientation (AGO), condenser was located below the plane of both evaporators as shown in Fig. 5.2 (a). Initially heat pipe was applied with nominal heat load of 20 W without any working substance in it to allow pure conduction and temperatures were matched with the temperatures obtained from various orientations. This activity gave the idea about the contribution of boiling in the working of heat pipe. Such comparison was very much useful in AGO. In anti-gravity orientation, as capillary action through the wick was minimum due to anti-gravity direction, it was possible that evaporator might not receive liquid and boiling-condensation cycle would stop. In that case, heat pipe would transfer heat by pure conduction and temperature of heat pipe would increase beyond a certain level. These temperatures when compared with the temperatures obtained from heat pipe without working substance, gave the idea whether phase change was present or not. Authors have observed very high temperatures of heat pipe in case of pure conduction. AGO temperatures were found to be lower than those temperatures under pure conduction which proves that in AGO, boiling-condensation cycle is working but availability of liquid is low compared to other orientations.

The steady state temperature rise is shown in Fig. 5.3 (a-b-c-d-e) for heat loads of 20, 40, 60, 80 and 100 W. Even at nominal load of 20 W, evaporator temperature reached above 90°C. However, this temperature was lower than the temperature obtained from heat pipe without working substance. This showed that the heat pipe in anti-gravity orientation, undergoes at least some non-zero phase change. If the heat load on evaporator increased, temperature also increased and reached to more than 275°C for 100 W heat load. Such a high temperature in electronics cooling is not suitable. Maximum evaporator temperature should be lower than 100 °C which is a common requirement in electronics cooling [93], [94]. Moreover, it was observed that the temperatures in one of the branches of evaporator was higher in all the cases for similar locations. This was due to the fact that the return of liquid in evaporator could be uneven in both the branches at very high temperature and elevated vapour pressure inside the heat pipe. Another important observation was that the temperature difference between all the sensors (i.e., T_1, T_2, T_3….) was significant. This indicated the dominance of wall conduction over boiling and condensation during operation of heat pipe in AGO.

(a)

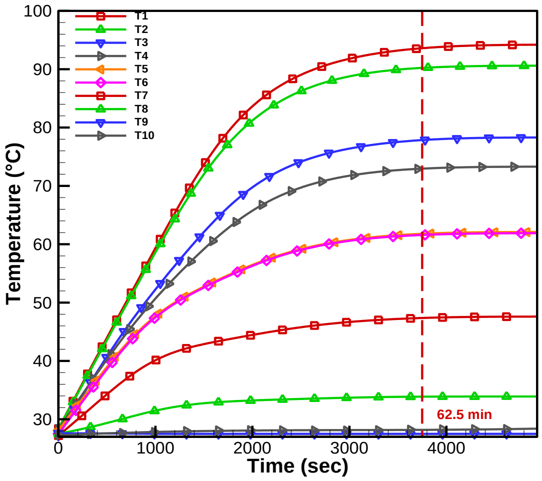

(b)

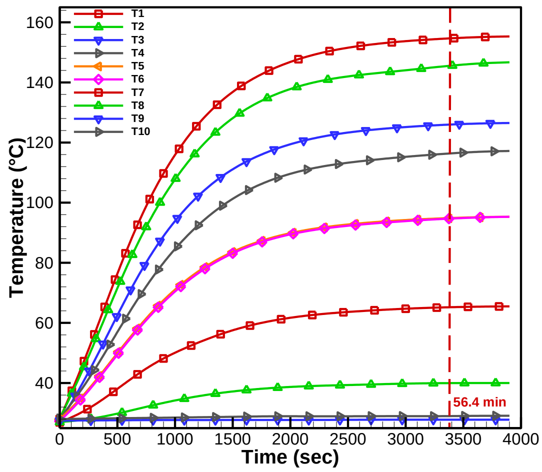

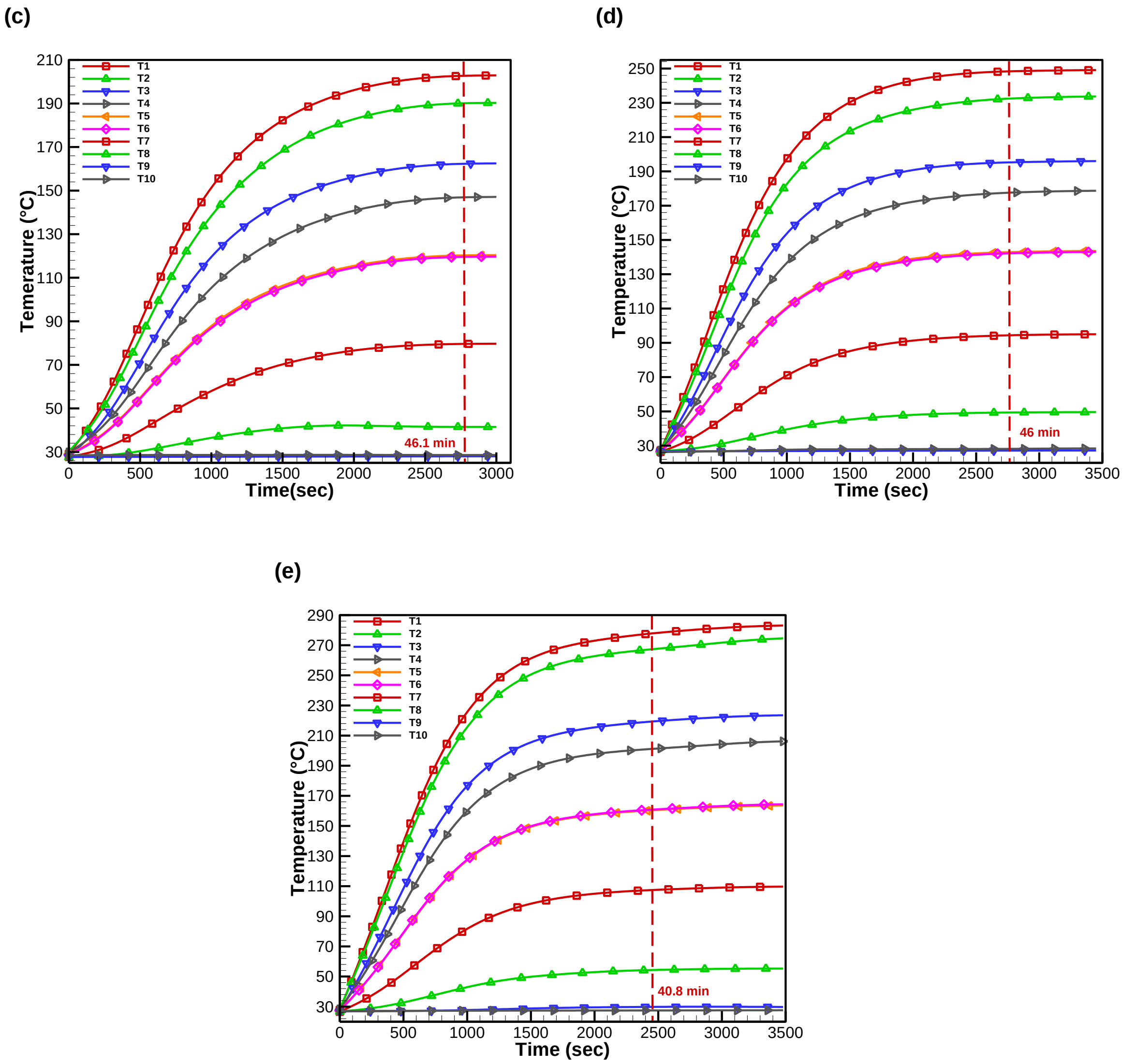

Fig. 5.3 Start-up characteristics for AGO (a) 20 W (b) 40 W (c) 60 W (d) 80 W (e) 100 W.

(b) Horizontal orientation

The steady state temperature rise in the horizontal orientation (HO) for AGMBHP is shown in Fig. 5.4 (a-b-c-d-e-f) for 40, 80, 120, 160, 200 and 240 W respectively. It was observed that heat pipe reached to steady state within 30 minutes of starting in all the cases of heat load. In HO, heat pipe was found to be working at much higher heat load with steady operation compared to other orientations. The reason being the sufficient capillary force to adjust the wide range of heat load in horizontal position. Evaporator temperatures were comparatively lower in horizontal orientation which makes it suitable for electronics cooling. The difference between maximum temperature (T_1

and/or T_2) and minimum temperature (T_9) was comparatively low for horizontal orientation. This lower difference makes the heat pipe more or less isothermal in its operation and near to ideal working condition. In this case, contribution of boiling was more compared to wall conduction. As the applied heat load increased, vapour generation in a heat pipe increased and so did the pressure. Subsequently, at higher pressure, condensation temperature (T_9) also increased. Moreover, it was observed that as the heat load increased, variation in temperatures T_3, T_4, T_5, T_6 and T_7 became narrow as shown in Fig. 5.4. This observation implies that the large length of heat pipe behaves as an adiabatic length at higher heat load and so does the reduced thermal resistance of heat pipe at 240 W.

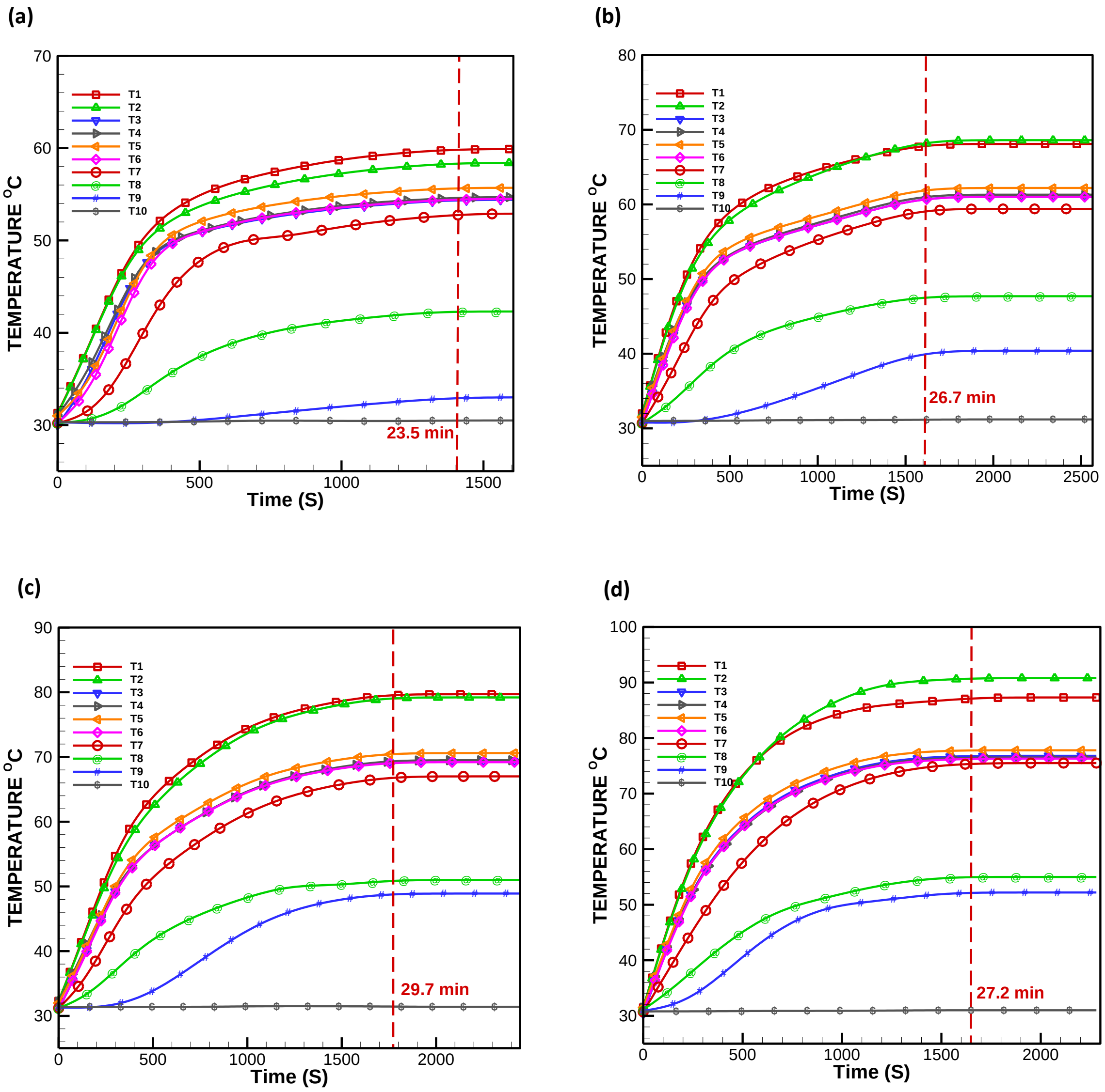

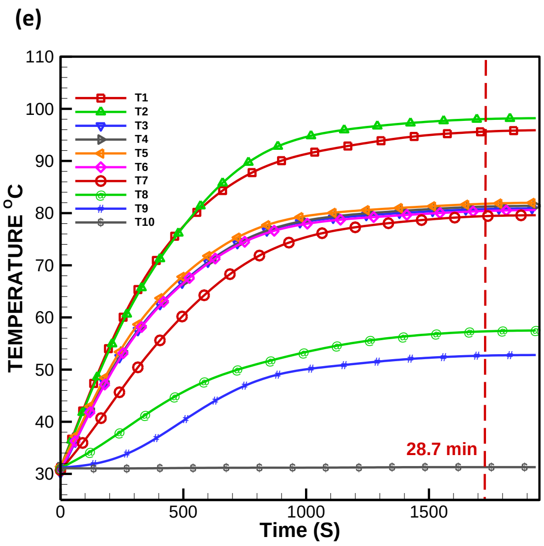

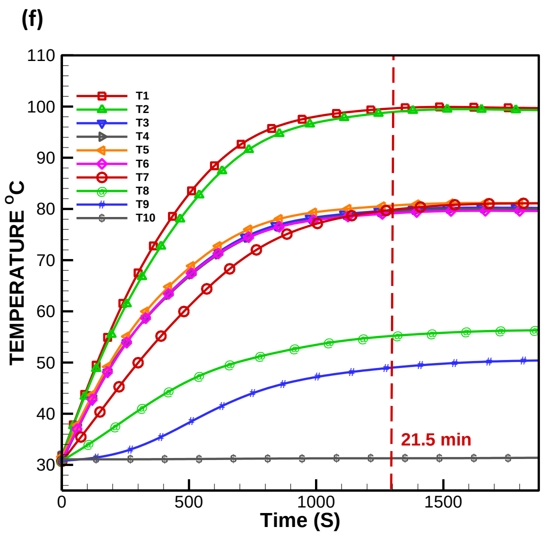

Fig. 5.4 Start-up characteristics for HO at heat loads of (a) 40 W (b) 80 W (c) 120 W (d) 160 W (e) 200 W (f) 240 W.

(c) Gravity assisted orientation

In case of gravity assisted orientation (GAO), condenser plane is upper than the plane of both the evaporators as shown in Fig. 5.2 (c) hence gravity also contributes in condensate return in addition to capillary action. The start-up characteristics for gravity assisted orientation is shown in Fig.5.5 (a-b-c-d-e) for 40,80,120,160 and 200 W respectively. Up to 160 W heat load, heat pipe reached to steady state within 32 minutes after starting. Maximum evaporator temperatures were lower in GAO than HO up to 160 W heat load, which may be due to better condensate return by gravity. However, for higher heat load (at 200 W) heat pipe dried out and temperature increased up to 168 °C. At higher heat load, superheated vapour generation in evaporator caused very high pressure in a constant volume body. The tendency of vapour was to accumulate at top near the condenser section and increased the temperature of fresh condensate gradually. This caused disturbances in condensation process and effective length of condenser gradually decreased. Moreover, overall temperature increased and liquid return from condenser subsequently ceased and heat pipe got dry out. The above-mentioned explanation is also supported by observing the variation in T_9 (i.e., condenser outlet temperature) in Fig. 5.5. In horizontal orientation (Fig. 5.4), condenser inlet temperature (T_8) was always higher than condenser outlet temperature (T_9) which was the usual case. In GAO, as the heat load increased T_9 also increased sharply and above 80 W heat load, condenser outlet temperature was found to be higher than condenser inlet temperature at steady state. This variation in temperature proves the accumulation of high temperature vapour at the top near the condenser end.

Moreover, it is to be noted that when T_9 overtakes T_8, temperature T_9 gradually increased as the heat load was increased (i.e., for 80 W-32 °C, for 120 W-32.5 °C, for 160 W-38 °C, for 200 W-44 °C). From the above observations, GAO is suggested up to 160 W heat load for steady operation in electronics cooling. However, thermal resistance of heat pipe was found to be affected to higher temperature at condenser outlet.

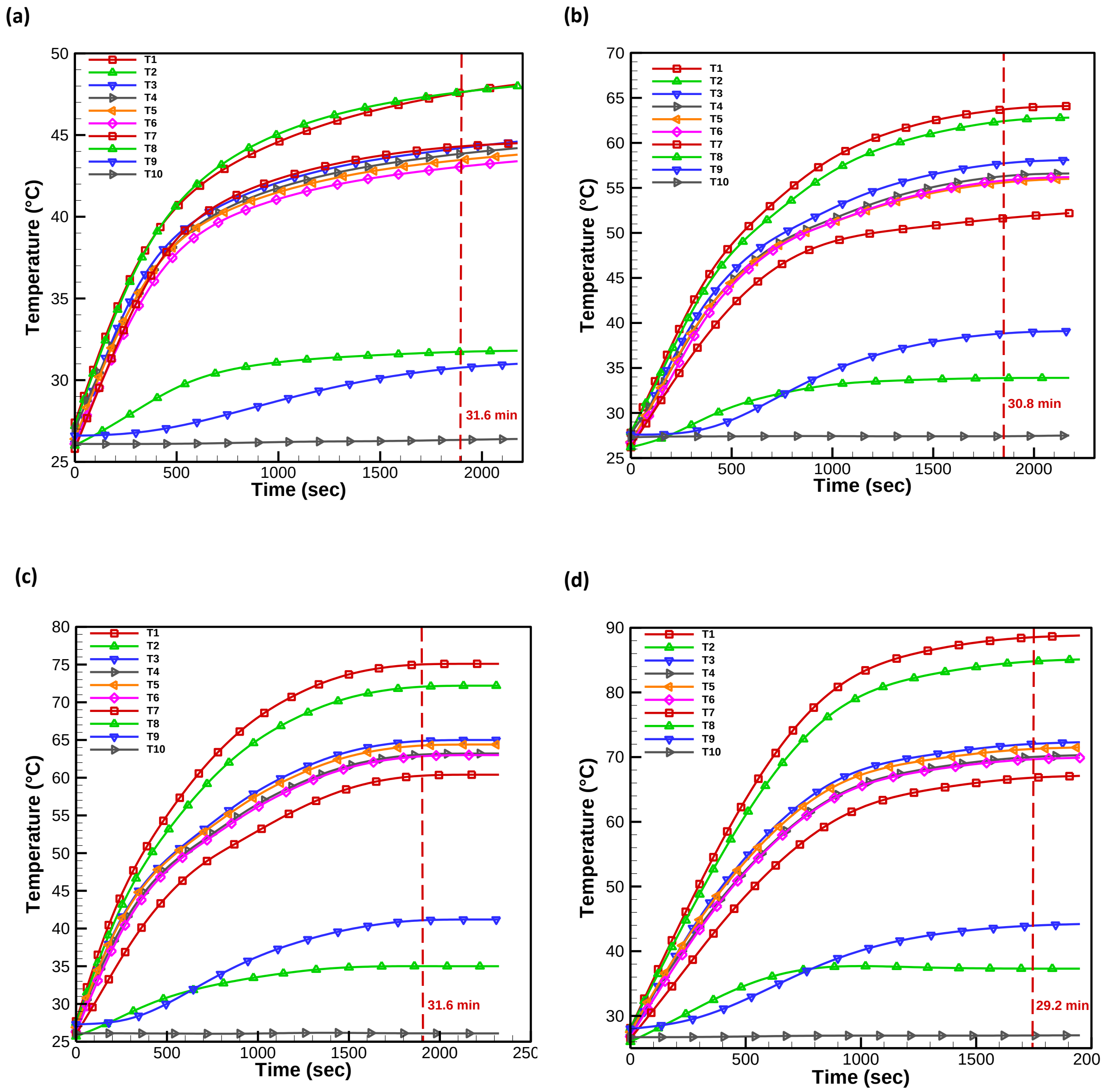

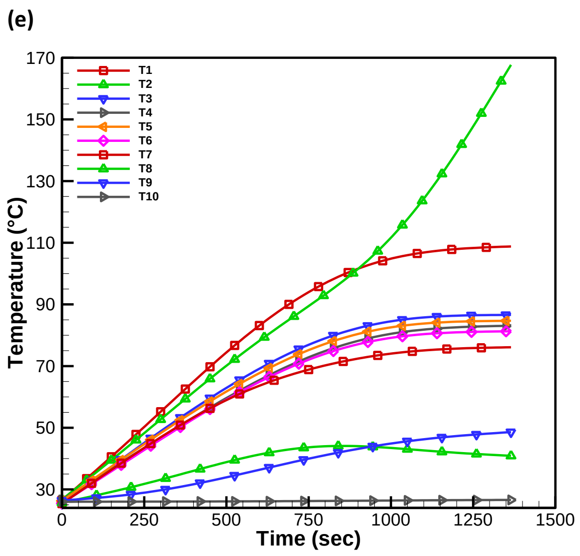

Fig. 5.5 Start-up characteristics for GAO at heat loads of (a) 40 W (b) 80 W (c) 120 W (d) 160 W (e) 200 W.

(d) Compound orientation

In a compound orientation (CO), one evaporator is kept under the effect of gravity influence and another one is kept under the effect of anti-gravity direction as shown in Fig. 5.2 (d). The start-up characteristics for compound orientation is shown in Fig. 5.6 (a-b-c-d). In CO, heat pipe was capable to transmit heat load up to 80 W only. Frequent and multiple temperature jumps were observed in steady characteristics of heat pipe before it gets dried out at 80 W. It was observed that these temperature jumps were as high as 12 to 15 °C for different heat loads. As the heat load increased, frequency of temperature oscillation decreased. For 20 W heat load, majority of temperature sensors indicated jumps multiple times. However, it was observed that the evaporator which was under the effect of anti-gravity influence (T_2), experienced more frequent and high temperature oscillations. After 40.3 minutes, all the sensors in heat pipe showed nearly steady state, but anti-gravity evaporator (T_2) resulted in continuous fluctuations.

Moreover, it was observed that the temperature jumps with higher degrees were observed in T_2, T_4, and T_6 at a same time after the start-up of heat pipe. This behavior of heat pipe gives an intuition of sudden break of vapour bubble and receiving of liquid in evaporator which is in anti-gravity influence. Moreover, as the heat load increased, the frequency and intensity of temperature jump decreased. This is due to the fact that at high heat load, vapour pressure in heat pipe was high enough to splash and supply the liquid to be reached into anti-gravity evaporator which reduced the scarcity of liquid in evaporator and so did the temperature jump. Higher the heat load, higher was the pressure and more would be the availability of liquid. Steady state time also decreased as the heat load increased. However, at a particular value of heat load (80 W), the vapour pressure in a heat pipe was not found to be sufficient enough to execute splashing to overcome vapour accumulation in anti-gravity evaporator. The effect of vapour and its temperature on evaporator was more dominating than the quantity of returning liquid to overcome and avoid dry-out of evaporator by absorbing heat.

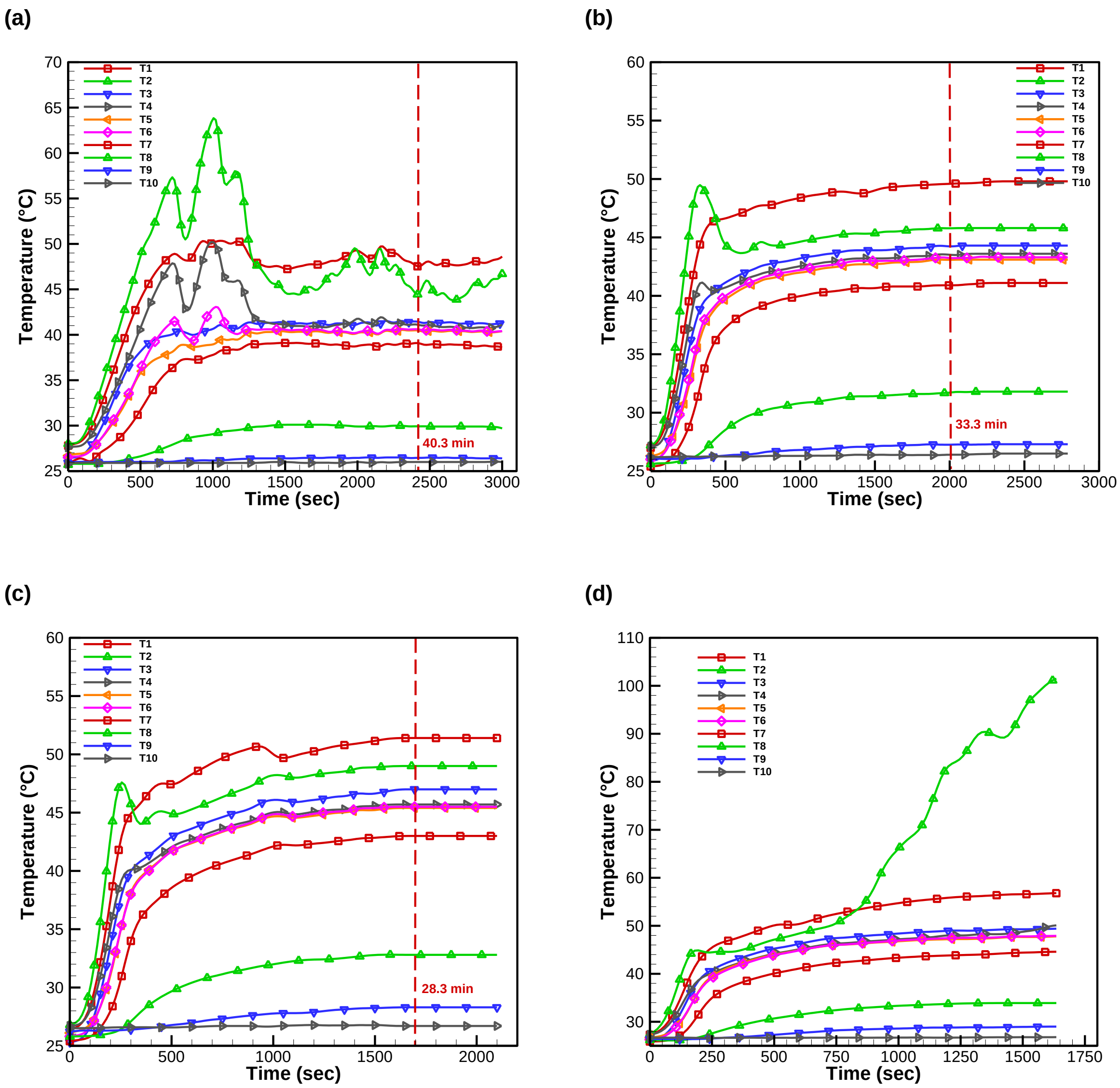

Fig. 5.6 Start-up characteristics for CO at heat loads of
(a) 20 W (b) 40 W (c) 60 W (d) 80 W.

5.4.2 Heat transfer coefficient analysis

Convective heat transfer coefficient of heat pipe is a useful parameter to determine and predict the performance of heat pipe. The variation of evaporator and total heat transfer coefficient with respect to heat load for different orientations were calculated by eq. (5.2) and (4.8) respectively and described in Fig. 5.7 (a-b) for the proposed axially grooved multi-branch heat pipe.

Evaporator heat transfer coefficient (h_e) was calculated by considering temperature difference between evaporator and adiabatic section whereas total heat transfer coefficient (h_t) was calculated by considering temperature difference between evaporator and condenser. These values were calculated at temperatures when heat pipe reached at steady state. Variation in h_e and h_t with respect to different heat loads for a particular orientation suggests the effectiveness of heat pipe as a heat transport device. Maximum values of h_e and h_t for AGO, CO, GAO and HO were found to be 0.228 and 0.223 kW/m^2°C, 2.56 and 1.69 kW/m^2°C, 1.85 and 2.16 kW/m^2°C and 2.06 and 2.72 kW/m^2°C respectively. In AGO, the convective heat transfer coefficient was found to be very low due to very high wall surface temperatures. It was the direct indication of highly dominating part of wall conduction and a very little contribution of boiling. Moreover, it was observed that the convective heat transfer coefficient was found to be almost constant at different heat loads which indicated that anti-gravity orientation is independent from the heat load and gave very high resistance in heat flow due to reduced capillary force.

In case of horizontal orientation, the variation in convective heat transfer coefficient was steady and it increased with increase in the heat load. At 240 W heat load, its value was found to be maximum (2.72 kW/m^2°C). Kim et.al. [92] obtained maximum 0.62 kW/m^2°C of overall heat transfer coefficient in their heat pipe with nano fluids. Similar trend was found for the gravity assisted orientation. In fact, GAO provides higher h values up to 100 W heat load than the horizontal orientation. However, the sudden reduction in h_e *and* h_t value indicates the dry-out of heat pipe at 200 W heat load in GAO.

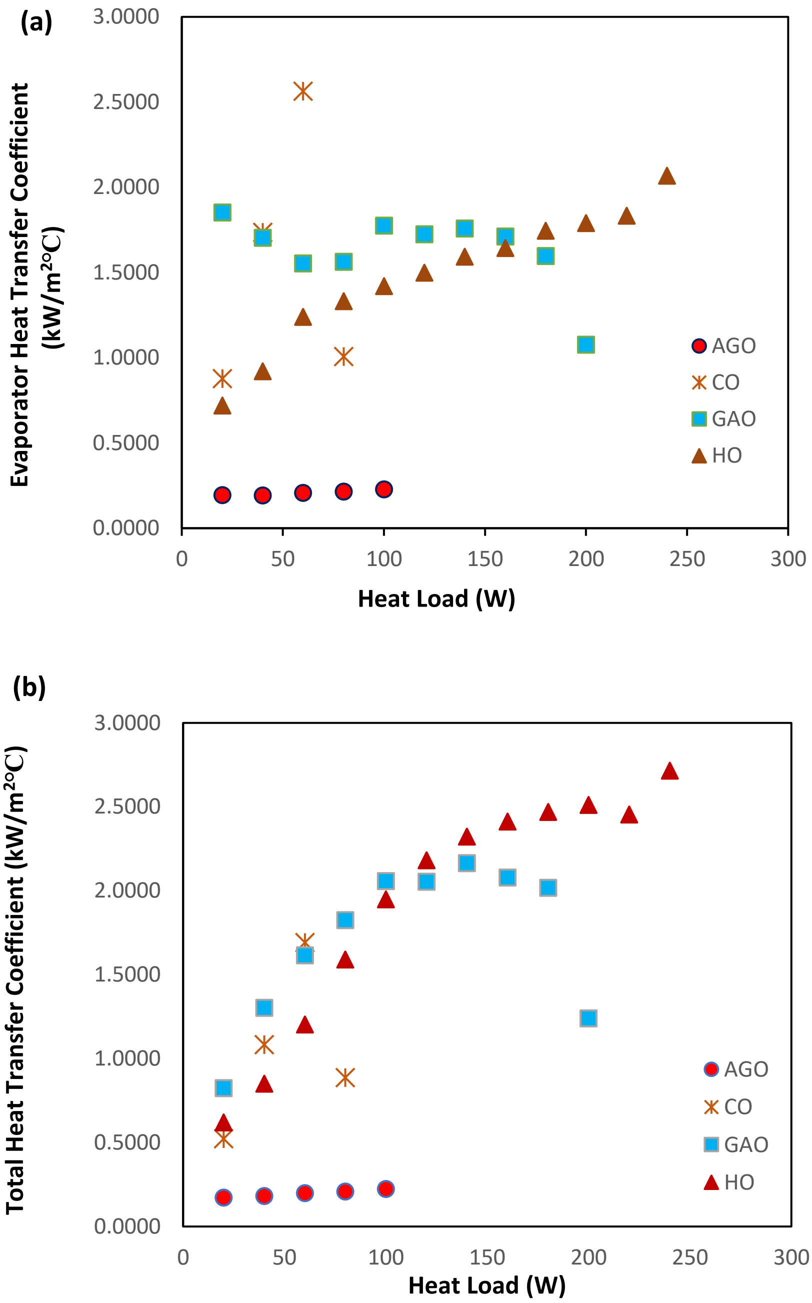

Fig. 5.7 Heat transfer coefficient vs heat load for (a) Evaporator (b) Total.

Moreover, variation in the convective heat transfer coefficient for compound orientation was quite interesting. In CO, h_e value was found to be maximum at 60 W heat load. Also, 60 W heat load is sufficient enough to generate vapour pressure which can splash the liquid towards evaporator and vapour towards condenser. Splashing of liquid from condenser to evaporators was such that only a few drops of liquid may reach to anti-gravity evaporator and larger quantity may reach to gravity assisted evaporator due to gravity. As the total heat load in both the evaporators was equally distributed, an imbalance in the liquid return quantity creates turbulences. This results in lower temperature difference between evaporator and adiabatic section as well as evaporator and condenser section which subsequently gives higher value of heat transfer coefficient at 60 W. It is to be noted that at 60 W heat load, the frequency of temperature jump reduces as well compared to lower heat loads. However, at 80 W, heat pipe undergoes dry-out in compound orientation and results in sudden reduction in heat transfer coefficient.

5.4.3 Thermal resistance analysis

Thermal resistance of heat pipe is the most valuable parameter to evaluate the performance of heat pipe as well as comparison of two heat pipes with different specifications. In the present study, the geometry of heat pipe is non-conventional. There are two evaporators in "T" shape heat pipe in parallel connection to each other and condenser is in series connection. Individual resistances of each evaporator were evaluated by equation (4.3) and (4.4). Their equivalent resistance was calculated using equation (4.5) and plotted in Fig. 5.8 (a) with respect to different heat loads for different orientations. Condenser resistance was calculated by equation (4.6) and described in Fig. 5.8 (b). In the calculation of evaporator and condenser resistances, it was assumed that the temperature variation in adiabatic section of heat pipe was negligible (i.e., section between T_5, T_6 and T_7). The minimum value of evaporator and condenser resistances for AGO, CO, GAO and HO were found to be 2.65 and 1.03 °C/W, 0.15 and 0.19 °C/W, 0.18 and 0.18 °C/W and 0.15 and 0.11 °C/W respectively.

It was clear from Fig. 5.8 (a) that anti-gravity orientation resulted in maximum resistance due to large temperature different between T_1/T_2 and T_5/T_6 in evaporator. Higher thermal resistance in evaporator was the indication of poor capillary action and insufficient supply of working substance towards evaporator. However, evaporator resistance gradually decreased as the heat load increased in AGO. This can be understood as heat power increases, temperature and pressure of the working substance increases in a closed volume which subsequently resulted in better water circulation and enhanced boiling in evaporator. Moreover, AGO resulted in higher condenser resistance (5.8 (b)) as well due to large temperature difference between T_8 and T_9. This was the indication of poor condensation in condenser due to elevated temperatures and insufficient utilization of condenser length due to migration of high temperature vapour towards condenser.

Moreover, in the evaporator resistance analysis, two separate calculations were performed in case of compound orientation (CO) i.e., one for the evaporator which was under the effect of gravity (EV1) and other for the evaporator which was in anti-gravity position (EV2). As in case of compound orientation, both the evaporators experience different capillary, different phase change and different temperatures, it became more important to describe their resistance behavior separately. It was obvious that the evaporator EV2 got dry-out at 80 W heat power due to anti-gravity direction. However, it was somewhat surprising that the EV2 resulted in lower evaporator resistance up to 60 W than EV1. It was observed from Fig. 5.6 (a-b-c) that the temperatures of EV2 (T_2) were lower compared to EV1(T_1) at steady state for 20, 40 and 60 W heat power respectively. Whereas T_5 and T_6 were almost identical. It was understood that the evaporator branch which undergoes temperature jump, resulted in lower steady temperature. This is due to the fact that initially due to insufficient pressure and liquid return, local dry-out occurred which increased the temperature for a small time period. Once the liquid return was regulated after sometime, frequency of local dry-out (temperature jump) decreased and temperature dropped below the temperature of EV1. However, at 80 W heat power, return of working substance was not sufficient enough to avoid permanent dry-out of evaporator EV2.

Evaporator resistances in case of HO and GAO were found to be almost identical except for 200 W, where gravity assisted orientation (GAO) resulted in dry-out. For their normal working range, both HO and GAO resulted in almost constant evaporator resistance for wide range of heat power. This was the indication of steady temperature rise of evaporator with respect to heat load. Such a steady operation of evaporator was desirable in a heat pipe when applied in cooling of electronics and space application [56].

From the condenser resistance (5.8 (b)), it was observed that the average value of condenser resistance was lower than the evaporator resistance. This was due to the fact that the condensation was more effective with sufficient cooling water flow rate. It was found that there is no indication of evaporator dry-out in the condenser resistance. The condensation process was effective with the sufficient cooling water flow rate but the migrating high temperature vapour when encountered the liquid condensate, there occurs evaporation of liquid before it reached to load center (evaporator). Entrainment of liquid particles in the vapour could be the reason behind dry-out. Moreover, condenser resistance gradually decreased with respect to heat load in all the cases. At comparatively lower value of heat loads, low vapour pressure in heat pipe kept the flowrate of working substance lower. As the heat load and vapour pressure increased, the boiling and condensation cycle rate increased and resistance decreased. For heat loads above 80 W, horizontal orientation resulted in minimum condenser resistance which represents its ideal condition of operation.

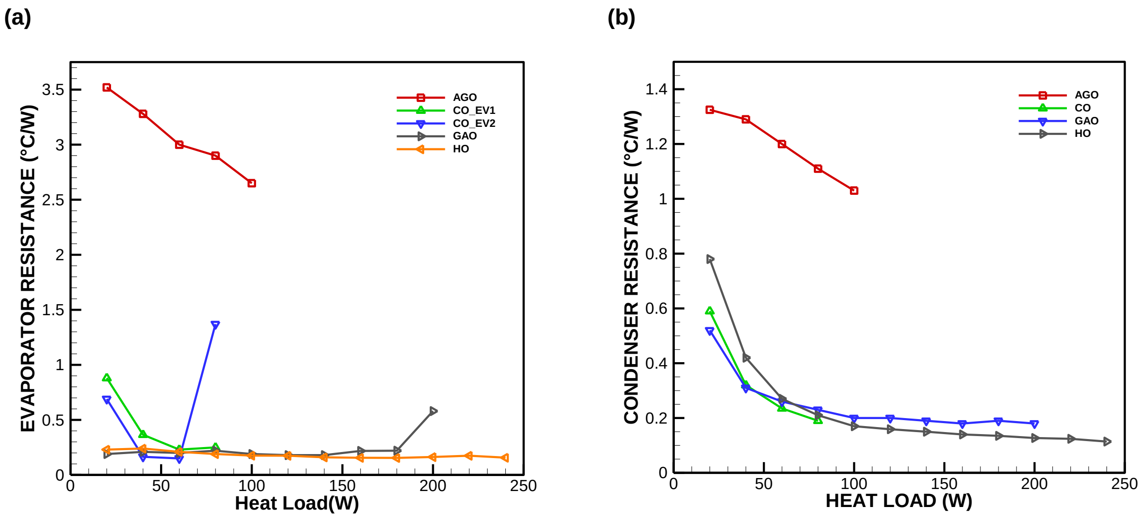

Fig. 5.8 Thermal resistance vs heat load for (a) Evaporator (b) Condenser.

5.4.4 Temperature distribution along the length of heat pipe

Temperature distribution along the length is an important criterion as far as performance of heat pipe is concerned. Kim et al.[92] used similar approach in his work on conventional heat pipe. However, due to “T” shape of AGMBHP, the respective temperatures on similar locations on both the evaporators were averaged and temperature distribution was obtained as shown in Fig. 5.9 (a-b). The average of T_1-T_2, T_3-T_4 and T_5-T_6- T_7 were considered as a single point along the length of heat pipe. Here, it is to be noted that temperature distribution was obtained at equal heat loads on both the evaporators and under the steady state condition. Moreover, for all the orientations, maximum heat load was considered (Fig.5.9(a)) through which heat pipe reached at steady state without dry-out (i.e., for AGO-100 W, HO-240 W, GAO-160 W and CO-60 W). Figure 5.9 (b) represents the temperature distribution at equal heat load (60 W) for all orientations.

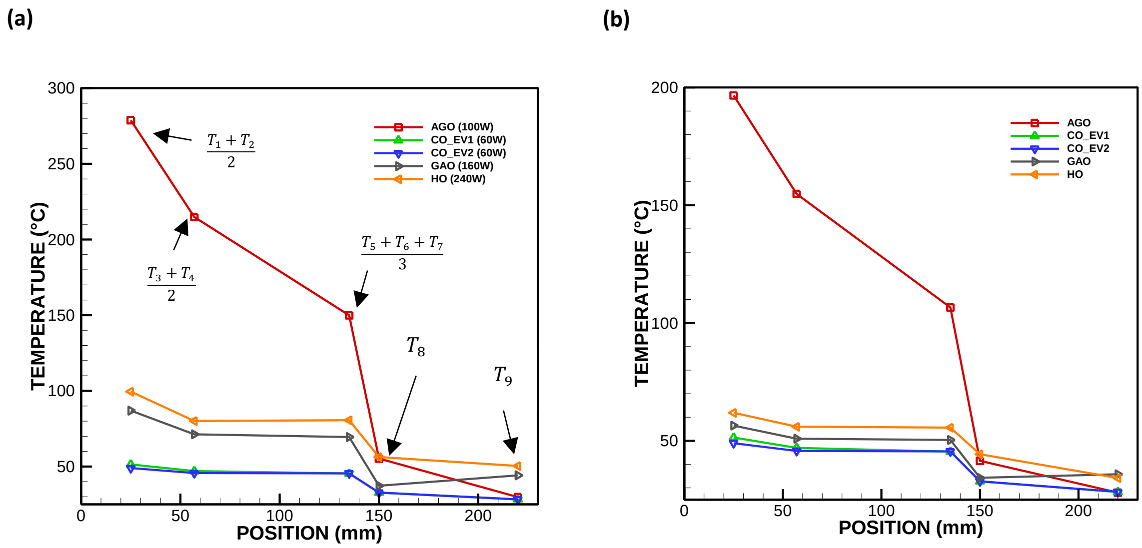

Fig 5.9 Temperature distribution along the length for different orientations for (a) Maximum load capacity (b) 60 W heat load.

In case of compound orientation, both the evaporators and their respective temperatures were considered separately in the graph to understand the temperature variation.

Ideally, it is desirable to have temperature distribution line completely horizontal i.e., constant temperature along the length of heat pipe which indicates zero thermal resistance [56]. However, in practical devices it is not possible to achieve the same. It was observed that the temperature variation along the length was the highest in case of anti-gravity orientation due large thermal resistance. For HO and GAO, it was moderate and identical in nature without temperature jump. However, T_9 is higher than T_8 in case of gravity assisted orientation. This was due to the fact that vapour accumulated at top near neck of heat pipe due to gravity effect as discussed earlier. Moreover, negligible temperature variation was observed in adiabatic section of heat pipe (between T_3/T_4 and T_5/T_6/T_7) for all the orientations except AGO which was a desirable condition.

5.4.5 Effective thermal conductivity

Effective thermal conductivity of heat pipe is a performance parameter which is used to compare two different heat pipes irrespective of their design parameters, wick structure, working range, orientation and dimensions. Effective thermal conductivity basically represents the effectiveness of a heat pipe as a heat transport device including combined conduction and phase change of working substance.

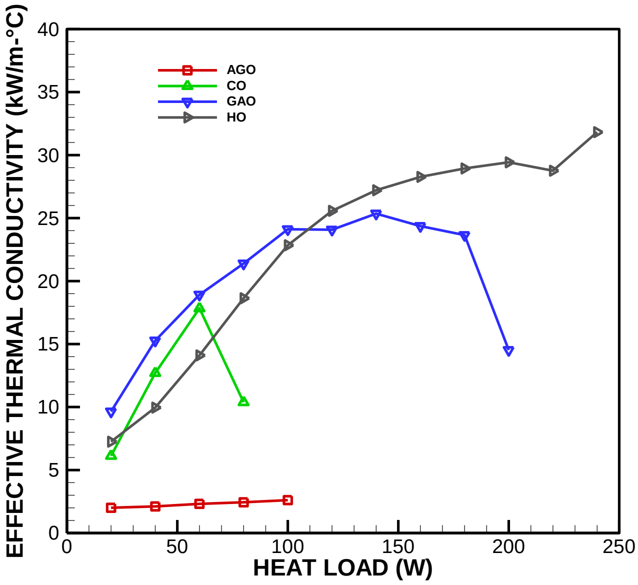

Fig. 5.10 Effective thermal conductivity of heat pipe at different heat loads.

The major contributor of heat transfer in a heat pipe is boiling and condensation as wall conduction is limited due to finite value of thermal conductivity of wall material. Effective thermal conductivity is calculated by using equation (5.3) as per following [4], [6] and its variation is plotted in Fig. 5.10.

$$k_e = \frac{Q\, L_{eff}}{A_C\, \Delta T}\text{, where } L_{eff} = \frac{L_{evap}+L_{cond}}{2} + L_{adia} \tag{5.3}$$

From the above equation, effective thermal conductivity is the indication of amount of heat transport due to temperature difference between evaporator and condenser by a heat pipe for given cross section and effective length. The maximum value of effective thermal conductivities for AGO, CO, GAO and HO were found to be 2.61, 17.84, 25.35 and 31.82 kW/m °C respectively. Heat loads below 100 W, GAO resulted in higher k_{eff} whereas for the heat loads above 100 W, HO resulted highest effective thermal conductivities. The results shown in Fig. 5.10 also validated the results obtained in convective heat transfer coefficient and thermal resistance data presented earlier.

5.5 Closure

From the novel orientation study of axially grooved multi branch heat pipe (AGMBHP), following points were observed based on the start-up characteristics, analysis of heat transfer coefficient, thermal resistance and temperature distribution along the length.

In horizontal orientation, heat pipe is capable to transmit 240 W heat load with maximum total heat transfer coefficient. Evaporator and condenser thermal resistance analysis also validates the above finding as at 240 W heat load, thermal resistance of HO is the lowest. Gravity assisted orientation is comparable to horizontal orientation up to 160 W heat load in terms of temperatures, convective heat transfer coefficient and thermal resistance but the maximum heat transport capacity is found to be lower than HO. Anti-gravity orientation is not suggested in the applications of electronics cooling as it results in very high wall surface temperatures. Compound orientation results in temperature shocks with high frequency and high resonance due to uneven liquid distribution. This orientation is not suggested in the heat pipe application. Temperature distribution study along the length, suggests lower temperature variation for both horizontal and gravity assisted positions. However, in condenser region, temperature variation is negative in case of GAO.

Chapter 6

Comparative Investigation on Different Numbers of Axial Grooves

This chapter describes the comparison of the experimental investigation carried out on axially grooved multi-branch heat pipe (AGMBHP) having 20, 16 and 12 numbers of grooves. The performance parameters involved in the comparative study are analyzed and some important conclusions are drawn.

This chapter elaborates the comparative investigation on "T"-shaped multi-branch heat pipe with 20, 16 and 12 numbers of axial grooves. For all three heat pipes, remaining parameters are kept constant i.e., level of vacuum, cooling water flow rate and horizontal orientation. Results are analyzed in terms of thermal resistance; convective heat transfer coefficient and start-up temperature rise for the optimum filling ratio of each individual heat pipe.

6.1 Experimental Set-up and Different Heat Pipes

As described in previous chapters, the same experimental set-up was used in the comparative study on number of grooves of AGMBHP. Total three heat pipes were manufactured with 20, 16 and 12 numbers of axial grooves with same external dimensions as described in chapter 4. Moreover, internal dimensions of individual grooves were also same with 0.6 mm width and 0.6 mm height of each groove. However, the pitch between two subsequent grooves was kept different in each heat pipe. As defined earlier, the filling ratio was decided by the total groove volume for a heat pipe [56]. The volume of water was different for each heat pipe for a specific filling ratio. Table 6.1 describes the volume of water filled inside a heat pipe for a given filling ratio and for a prescribed number of grooves. Figure 6.1(a) shows the closer view of heat pipe assembly in horizontal position and Fig. 6.1 (b), (c) and (d) shows the internal view of three heat pipes having 20,16 and 12 numbers of axial grooves. Figure 6.1 (e) shows the cross section of groove geometry and its dimensions.

The level of vacuum was kept constant of -700 mm of Hg gauge for entire comparative investigation. Moreover, cooling flow rate of water was maintained at 5 ml/s through condenser throughout the study. Each experiment was conducted in horizontal orientation for all the heat pipes as it provided the optimum performance as discussed earlier in chapter 5.

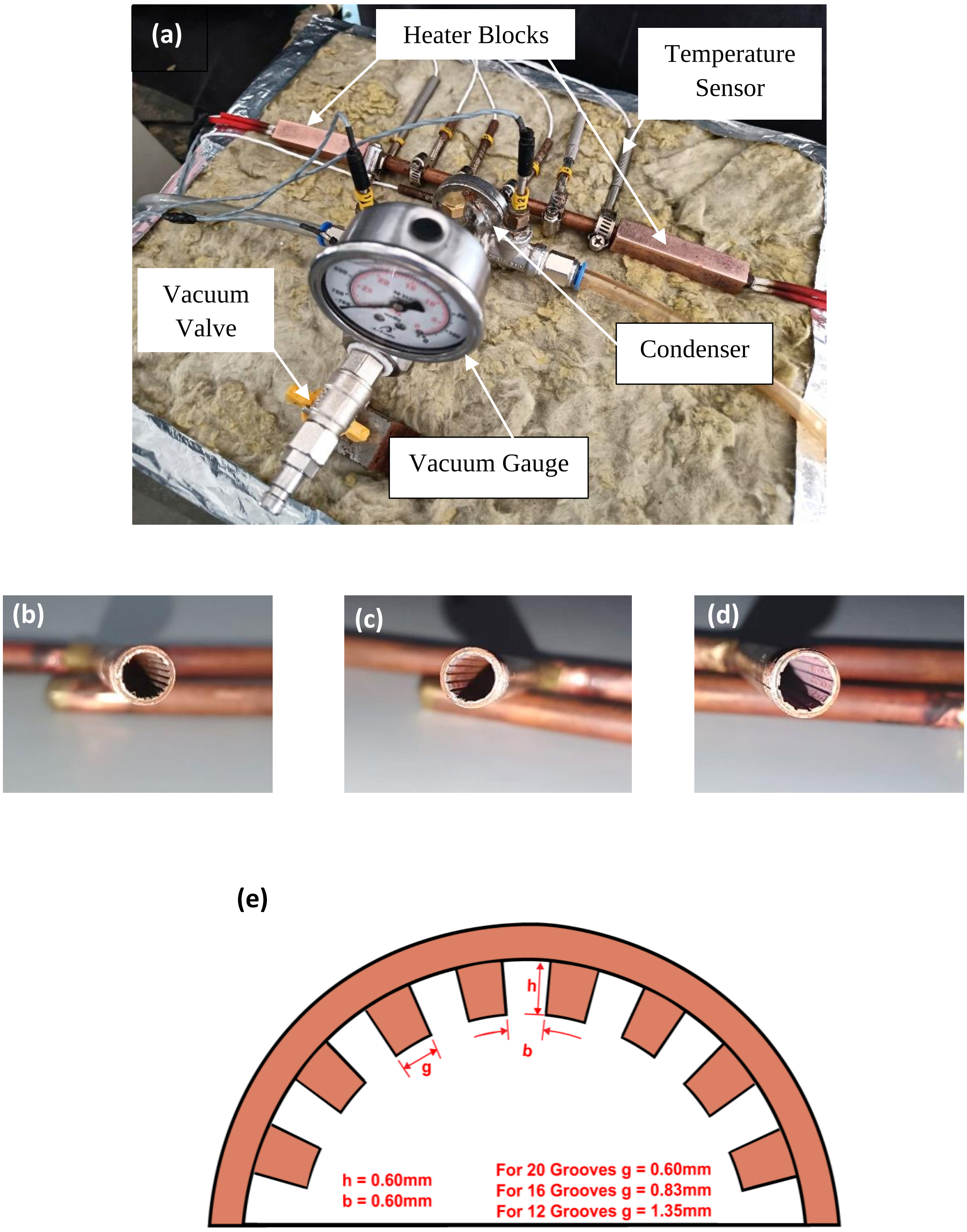

Fig. 6.1 (a) Photograph of heat pipe and sensor assembly (b) 20 grooves (c) 16 grooves (d) 12 grooves heat pipes (e) Cross section of pipe with groove dimensions.

Table 6.1

Filling ratio for different heat pipes with 20, 16 and 12 numbers of grooves

Filling Ratio (%)	Approx. Volume of distilled water (ml)		
	20 Grooves	16 Grooves	12 Grooves
75	1.63	1.29	0.98
100	2.18	1.72	1.31
125	2.72	2.15	1.64
150	3.26	2.58	1.97
175	3.81	3.01	2.30
200	4.36	3.44	2.62
225	-	-	2.96

The specifications of experimental set-up and dimensions of heat pipes were same as discussed in chapter 4 earlier. The locations of different temperature sensors were also similar in the entire investigation. The heat pipe was applied with the heat load in the range of 20 W each up to maximum 240 W and start-up temperature characteristics were recorded at an interval of 15 seconds. Once steady state condition was obtained, the steady temperatures were used to calculate various performance parameters.

6.2 Performance Parameters

Different parameters used to evaluate the comparative performance of heat pipe are described in this section.

The fluid filling ratio (η) of working substance was defined as per eq. (6.1) for heat pipes with 20, 16 and 12 numbers of grooves respectively.

$$\eta = \frac{n\,(v_g)}{v_w} \times 100\ \% \tag{6.1}$$

where, v_w = volume of water to be filled inside the heat pipe for required filling ratio (ml), v_g = volume of water that can be filled in one groove (ml) and n = number of grooves = 20, 16 and 12

The thermal resistances (R_1 and R_2) of individual evaporators (EV_1 and EV_2) were calculated from eqn. (4.3) and (4.4)

An equivalent resistance for two evaporators (R_{evap}) was calculated from eqn. (4.5)

The condenser resistance (R_{cond}) was determined from eqn. (4.6)

Total thermal resistance of heat pipe was calculated as per eq. (4.7)

However, for the calculation of thermal resistances, it was assumed that the temperatures T_1 and T_2 were the evaporator temperatures, as they were located nearest to the heater block on heat pipe. Due to curvature effect of heat pipe surface, it was difficult to insert temperature sensors exactly on the evaporator inside the heater block. This could have resulted in slightly lower value of thermal resistance than the actual value. Moreover, thermal resistance in adiabatic section was considered negligible due to almost identical values of temperatures of T_5, T_6 and T_7.

The total convective heat transfer coefficient (h_T) was calculated as per eq. (6.2) [92] under the steady state condition of heat pipe.

$$h_T = \frac{Q}{A_{se}\,(T_e - T_c)} = \frac{Q}{A_{se}\left[\left(\frac{T_1+T_2}{2}\right) - T_9\right]} \tag{6.2}$$

where, Q = total heat load (W), A_{se} = total surface area of evaporator heat transfer surface (m^2)

$A_{se} = n\,(w + 2h)\;\; 2l_e$ for a heat pipe with n number of grooves,

where, T_e And T_c are evaporator and condenser temperatures (°C) respectively.

The uncertainty in temperature (U_T) was calculated using the square formula as per eq. (4.9) and the relative uncertainty in convective heat transfer coefficient and thermal resistance was calculated as per eq. (4.11) and eqn. (4.10) respectively as described earlier.

6.3 Results and Discussion

In this section, the start-up characteristics were performed for all the heat pipes for different heat loads (equal) on both the evaporators. From the steady temperatures of heat pipe, using above discussed equations, various performance parameters were calculated and compared. Thermal resistance, total heat transfer coefficient and start-up temperature rise were plotted for heat pipes with different numbers of grooves in order to study the performance of heat pipe and effect of number of grooves.

6.3.1 Thermal resistance analysis

Thermal resistance of heat pipe is the direct indication of heat pipe performance as a phase change heat transport device. Figure 6.2 (a), (b) and (c) shows the thermal resistance of heat pipes at different heat loads and filling ratios for 20 grooves (20G), 16 grooves (16G) and 12 grooves (12G) respectively. For a 20G heat pipe, the optimum filling ratio was observed in the range of 125% to 150% as already discussed in chapter 4. However, 150% filling ratio provided better heat transport capacity and minimum thermal resistance was also obtained at 150% FR. From Fig. 6.2 (b), it is also clear that the 150% filling ratio provided minimum thermal resistance for a wide range of heat loads for 16G heat pipe. However, for low value of heat loads (below 80 W), 75% and 100% FR resulted in lower thermal resistance. This was obvious as for low filling ratio and low value of heat load, immediate phase change occurred and wall conduction decreased and so did the thermal resistance. At higher heat loads, larger quantity of working substance was required to handle high heat loads and so did the higher filling ratio. However, up to representative load of 240 W, 150% FR provided lower thermal resistance for wide range so it was considered the optimum filling ratio for 16G heat pipe.

The dependency of heat load on filling ratio was clear in case of 12G heat pipe as shown in Fig. 6.2 (c). At 20 W heat load, 75% FR provided minimum thermal resistance. For 60 W heat load, 100% FR resulted in minimum thermal resistance and for higher heat loads, higher filling ratios were found better in terms of thermal resistance. However, it should be noted that for 12G heat pipe, the dry-out occurred at 75% FR at 60W, 100% FR at 80W, 125% FR at 100 W, 150% FR at 200W 175% FR at 200 W and 200% FR at 220 W respectively. So, it was clear that the 12G heat pipe was not capable to convey representative heat load of 240 W at majority of filling ratios under consideration. However, 225% FR transported 220 W heat load without dry-out but it resulted in maximum thermal resistance. For a moderate heat load range of 40 to 160 W, 150% FR resulted in lower thermal resistance and it was considered to be optimum in case of 12G heat pipe. However, 12G heat pipe was not suggested in electronics cooling applications due to very high evaporator temperatures and frequent dry-out due to poor capillary forces. Moreover, its comparison with 16G and 20G heat pipes made the picture very clear about optimum number of grooves.

The performance of three heat pipes (i.e., 20G, 16G and 12G) was compared at an optimum filling ratio of 150% in terms of total thermal resistance at various heat loads is shown in Fig. 6.3. It was observed that the thermal resistance of 12G heat pipe was found the lowest up to 60 W heat load. From 60 W to 180 W heat load, 16G pipe resulted in the lowest thermal resistance and above 180 W, 20G pipe was found more superior in terms of the lowest value of thermal resistance.

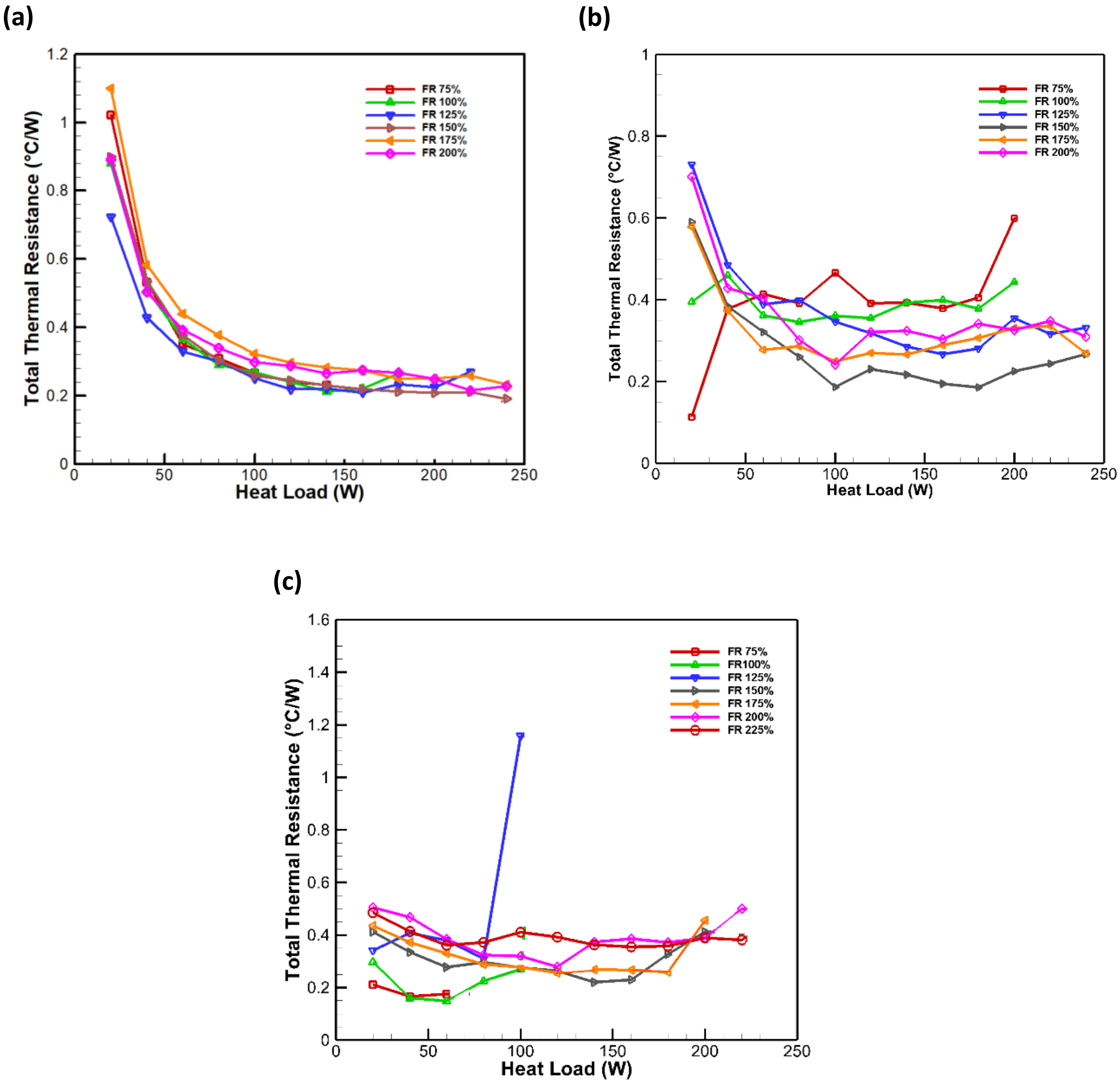

Fig. 6.2 Total thermal resistance for heat pipes (a) 20 grooves (b) 16 grooves (c) 12 grooves at different filling ratio and heat load.

Moreover, the trend of thermal resistance curves for 16G and 20G were such that at lower heat loads, thermal resistance was high and it gradually decreased by increasing heat load, reached to minimum and then increased at higher heat loads. However, for 20G heat pipe, the trend of thermal resistance was continuously in decreasing manner. So, it was possible that minimum thermal resistance could not be achieved up to the representative heat load of 240 W.

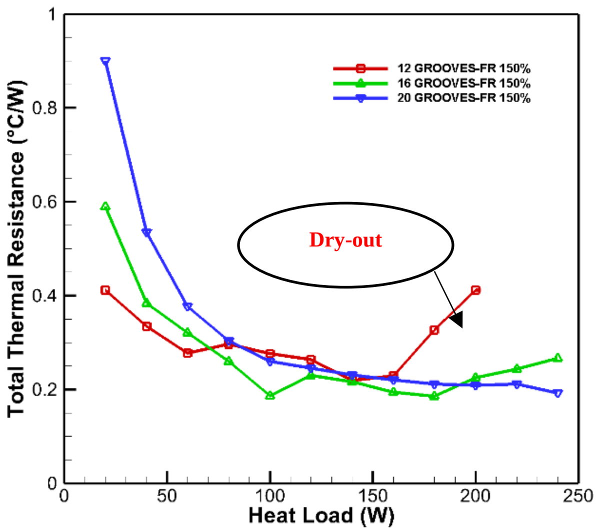

Fig. 6.3 Total thermal resistance of 20G, 16G and 12G heat pipes at optimum filling ratio of 150%.

6.3.2 Total heat transfer coefficient

Total heat transfer coefficient of heat pipe indicates effectiveness of the heat transfer from the evaporator end to the condenser end for a given heat load. [99]. The variation of total heat transfer coefficient for 20G, 16G and 12G heat pipe is shown in Fig. 6.4 (a), (b) and (c) respectively. Sudden fall in the curve indicated dry-out of heat pipe at respective heat load. The maximum value of total heat transfer coefficient was found to be 2.72 kW/m^2°C for 20G, 2.07 kW/m^2°C for 16G and 2.43 kW/m^2°C for 12G heat pipe respectively corresponding to 150% filling ratio. Moreover, the maximum value of convective heat transfer coefficient was found at 240 W for 20G, 180 W for 16G and 140 W at 12G respectively. These results also validated the fact that the optimum filling ratio of heat pipe depended on the amount of heat load to be transmitted.

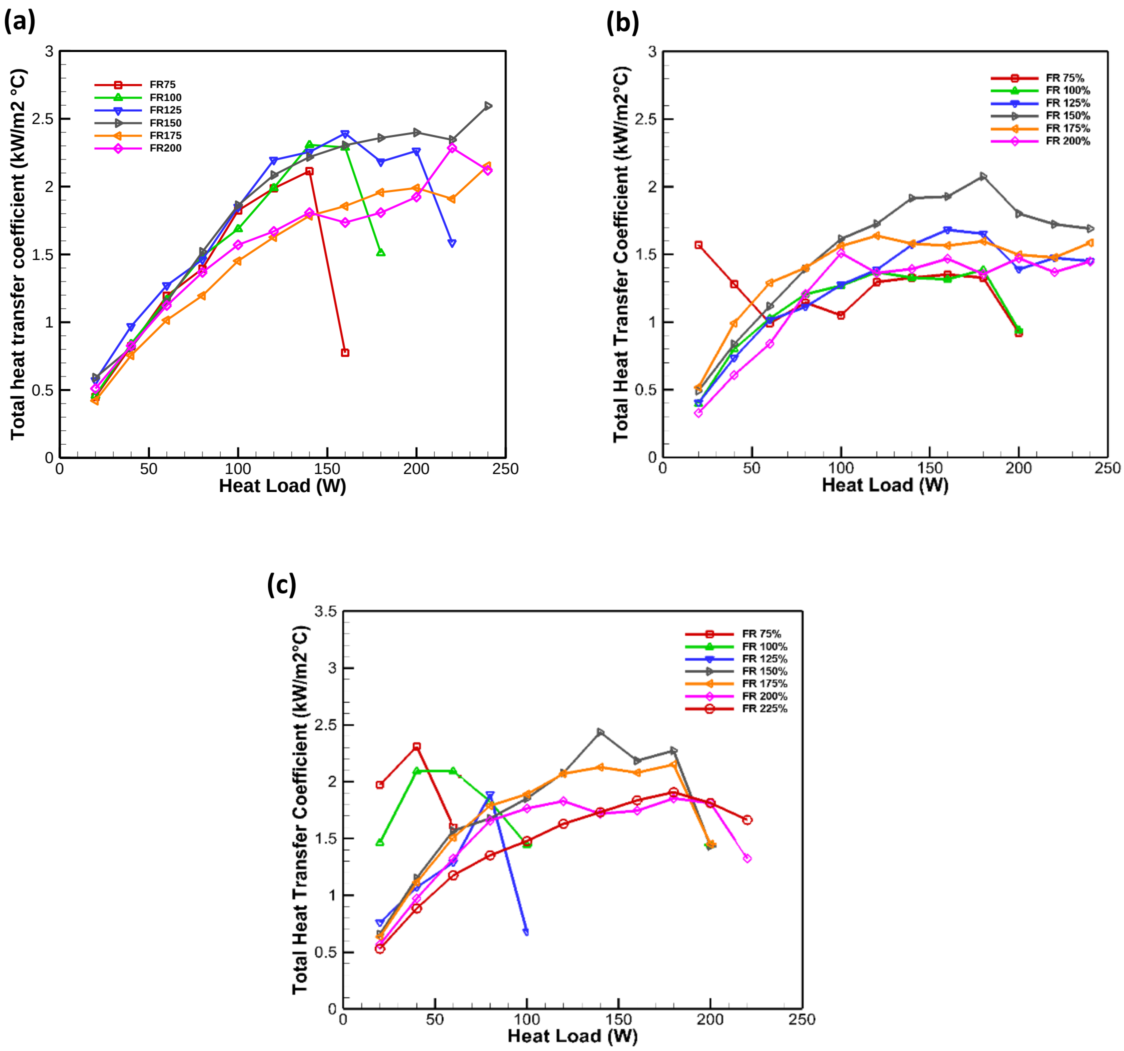

Fig. 6.4 Total heat transfer coefficient for heat pipes with (a) 20 grooves (b) 16 grooves (c) 12 grooves.

Moreover, the comparison of total heat transfer coefficients is done for three heat pipes i.e., 20G, 16G and 12G corresponding to an optimum filling ratio of 150% in Fig. 6.5. It was seen that the total heat transfer coefficient increased as the heat load increased, reached to maximum and decreased at some high value of heat load for 16G and 12G heat pipes. For 20G heat pipe, the variation in total heat transfer co-efficient was such that the maximum value was not achieved up to 240 W heat load as discussed earlier. It should be noted here that the heat transfer surface area of evaporator was taken into account for the calculation of total heat transfer coefficient as per eqn. 6.7, which was different in all three cases and it was dependent on numbers of grooves.

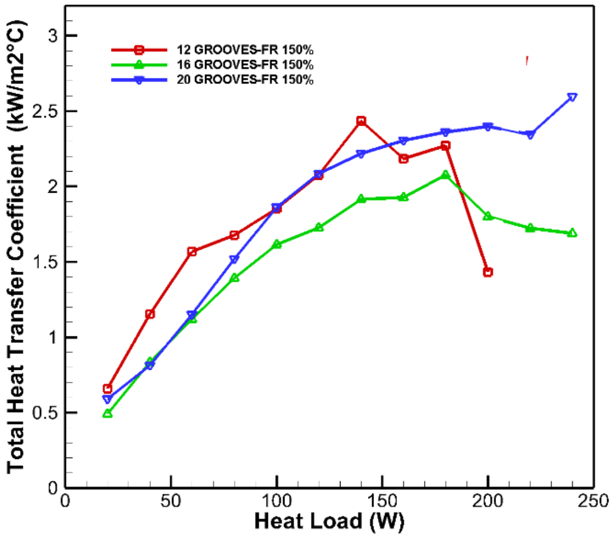

Fig. 6.5 Total heat transfer coefficient for 20G, 16G and 12G heat pipes at optimum filling ratio of 150%.

6.3.3 Start-up temperature rise

Start-up temperature rise is the temperature difference of evaporator obtained at steady state condition and at starting. Figure 6.6 shows the startup temperature rise for 20G,16G and 12G heat pipes. Evaporator temperature rise for a given heat load, depends on many parameters. If insufficient quantity of working substance is filled in the heat pipe for given amount of heat load, heat pipe results in higher temperature rise due to superheating of working substance. Excessive amount of working substance in heat pipe may obstruct the vapour path to move towards condenser. This may cause the local dry-out or pulsating behavior of heat pipe and again the evaporator temperature may rise. However, in the current study, it was observed that 20G heat pipe, resulted in minimum startup temperature rise amongst all the heat pipes for majority of heat inputs. It was observed that the start-up temperature rise was directly associated with numbers of grooves and hence the capillary. The sufficient capillary pressure provided sufficient liquid to reach at evaporator and temperature increment ceased in the evaporator. In 12G heat pipe, due to lower capillary forces, the circulation of working substance was comparatively less. It resulted in ineffective boiling condensation cycle and wall conduction was dominated. This was the reason for the higher evaporator temperature difference at the same heat load for 12G and 16G heat pipes compared to 20G heat pipe.

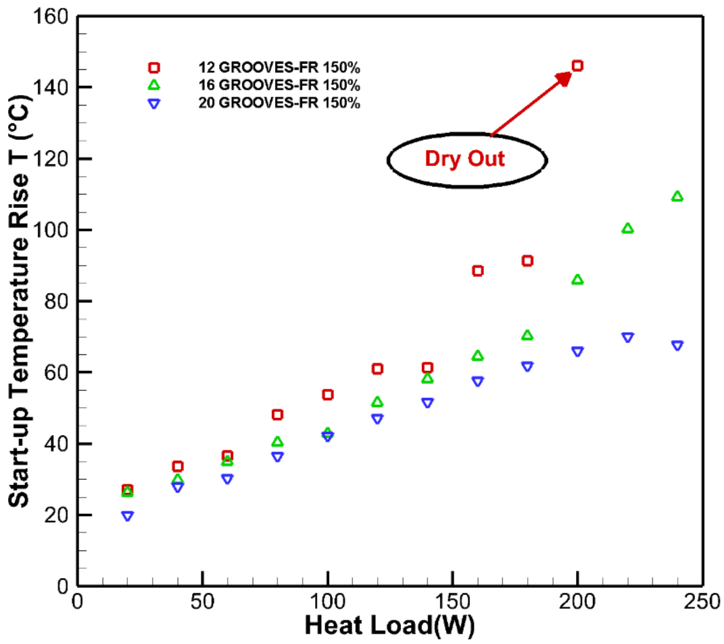

Fig. 6.6 Startup temperature rise at 150% FR for different numbers of grooves.

6.3.4 Temperature distribution along the length

As discussed in previous chapters, temperature distribution along the length of a heat pipe is the indication of how closely heat pipe is working to the ideal condition. Ideally it is desirable to have horizontal temperature profile along the length in order to have zero thermal resistance. However, practically it is not possible to obtain zero thermal resistance in heat pipe. The axial temperature distribution was obtained by averaging the temperatures of similar locations (on each evaporator) and unconventional "T" shape of heat pipe was considered as straight heat pipe to obtain linear temperature distribution. The axial temperature distribution for three heat pipes is shown in Fig. 6.6 (a), (b) and (c) for 40 W, 100 W and 200 W respectively. The heat loads were so selected that the thermal resistance data suggested the optimum working range of each heat pipe with different number of grooves. From Fig. 6.7 (a), it was clear that the temperature distribution along the length was almost similar in nature for all the cases. However, slightly higher condenser temperature was observed for 20G heat pipe for 40 W. Moreover, the adiabatic section (length covered by T_3, T_4, T_5, T_6, T_7) was almost horizontal indicating a large part of the heat pipe was close to the ideal condition.

At 100 W heat load, 20G heat pipe was superior in terms of temperature difference as it resulted in minimum temperature variation. However, overall temperatures were high compared to 16G and 12G heat pipe. In this case, 16G heat pipe resulted in lowest overall temperatures.

Moreover, in case of 200 W heat load, it was found that 20G heat pipe resulted in minimum temperature difference as well as lowest overall temperatures. These observations indicated that better capillary heat pipe (i.e., 20G) provided working conditions closer to an ideal heat pipe and a particular filling ratio suitable to given heat load would result in lower overall temperatures of heat pipe.

Both, heat load and overall temperatures are such parameters which depend on the type of application of heat pipe. If temperature of heat pipe is the focused parameter, excessive capillary is always not necessary. Same way, lower temperatures or lower thermal resistances are not always desirable when it comes to higher heat transport capacity for given area of application.

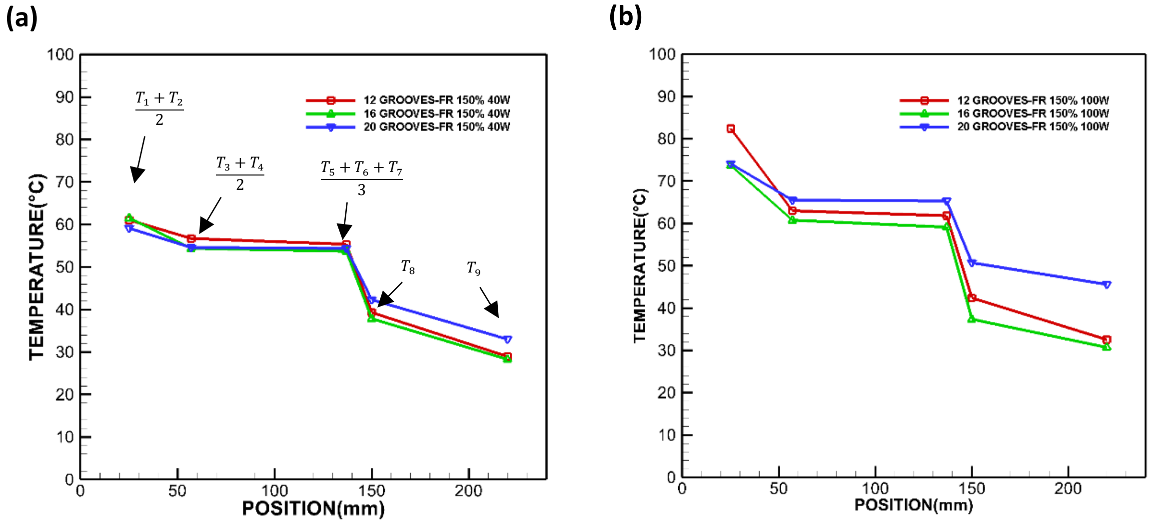

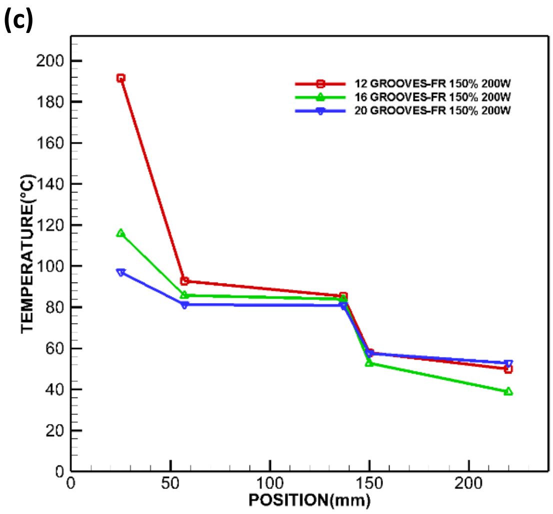

Fig. 6.7 Temperature distribution along the length of 20G, 16G and 12G heat pipe for (a) 40 W (b) 100 W (c) 200 W.

6.4 Closure

From the comparative investigation on different numbers of grooves on axially grooved multi-branch heat pipe, following points were observed based on the analysis of thermal resistance, total heat transfer coefficient, start-up temperature rise and axial temperature distribution.

For all three heat pipes with 20, 16 and 12 numbers of grooves, optimum filling ratio was found as 150%. 12G heat pipe resulted in the lowest thermal resistance up to 60 W heat load; 16G heat pipe resulted in the lowest thermal resistance from 80-180 W heat load; whereas, 20G heat pipe resulted in the lowest thermal resistance from 200-240 W heat load. Minimum evaporator temperature rise was obtained for 20G heat pipe for all the heat loads compared to 16G and 12G heat pipes. 20G heat pipe resulted in minimum temperature variation compared to other heat pipes. However, from the manufacturing limitations on number of grooves, it was not possible to manufacture more than 20 number grooves with [100] [101]0.6 mm width for the given diameter of heat pipe and given 0.6 mm pitch between the two subsequent grooves.

Annexure

Results of Uncertainty Analysis for Various Parameters

(1) Uncertainty in Temperature

Heat Load (W)	FR75%	FR 100%	FR 125%	FR 150%	FR 175%	FR 200%
20	0.050587968	0.050593705	0.050437569	0.050514768	0.050635199	0.050505737
40	0.025536277	0.025559151	0.025513711	0.025599865	0.025583427	0.025564308
60	0.017247199	0.017278793	0.017266054	0.017298526	0.01727676	0.017294993
80	0.013134685	0.013178492	0.01317324	0.013179696	0.01315447	0.013174297
100	0.010695963	0.010708137	0.010712121	0.010716413	0.010686067	0.010698177
120	0.009056795	0.009068288	0.009079905	0.009076642	0.009046239	0.009090473
140	0.00788321	0.007906261	0.007902528	0.007904207	0.007876368	0.007921322
160	0.007520403	0.007020431	0.007027178	0.007034849	0.007009332	0.007053665
180		0.006400208	0.006331725	0.006352369	0.006322702	0.006375683
200			0.005798088	0.005804515	0.005776823	0.005828253
220			0.005375677	0.00536164	0.005335664	0.005350498
240				0.004993229	0.004956676	0.004988827

Insulation Thickness 0.05 m

FR75%	FR 100%	FR 125%	FR 150%	FR 175%	FR 200%
5.0588	5.0594	5.0438	5.0515	5.0635	5.0506
2.5536	2.5559	2.5514	2.5600	2.5583	2.5564
1.7247	1.7279	1.7266	1.7299	1.7277	1.7295
1.3135	1.3178	1.3173	1.3180	1.3154	1.3174
1.0696	1.0708	1.0712	1.0716	1.0686	1.0698
0.9057	0.9068	0.9080	0.9077	0.9046	0.9090
0.7883	0.7906	0.7903	0.7904	0.7876	0.7921
0.7520	0.7020	0.7027	0.7035	0.7009	0.7054
	0.6400	0.6332	0.6352	0.6323	0.6376
		0.5798	0.5805	0.5777	0.5828
		0.5376	0.5362	0.5336	0.5350
			0.4993	0.4957	0.4989

% Temperature Uncertainity

Insulation Thickness 0.05 m

(2) Uncertainty in Thermal Resistance

Heat Load (W)	FR75%	FR 100%	FR 125%	FR 150%	FR 175%	FR 200%
20	0.0500	0.0500	0.0500	0.0500	0.0500	0.0500
40	0.0251	0.0251	0.0251	0.0251	0.0251	0.0251
60	0.0167	0.0167	0.0168	0.0167	0.0167	0.0167
80	0.0126	0.0126	0.0126	0.0126	0.0126	0.0126
100	0.0101	0.0101	0.0101	0.0101	0.0101	0.0101
120	0.0084	0.0084	0.0084	0.0084	0.0084	0.0084
140	0.0072	0.0073	0.0073	0.0072	0.0072	0.0072
160	0.0063	0.0064	0.0064	0.0064	0.0063	0.0063
180		0.0056	0.0057	0.0057	0.0057	0.0056
200			0.0051	0.0051	0.0051	0.0051
220			0.0046	0.0047	0.0046	0.0046
240				0.0043	0.0043	0.0043

Insulation Thickness 0.05 m

FR75%	FR 100%	FR 125%	FR 150%	FR 175%	FR 200%
5.0031	5.0033	5.0038	5.0039	5.0029	5.0036
2.5056	2.5059	2.5067	2.5057	2.5050	2.5055
1.6747	1.6748	1.6753	1.6745	1.6734	1.6734
1.2588	1.2598	1.2596	1.2585	1.2576	1.2574
1.0087	1.0103	1.0105	1.0091	1.0083	1.0084
0.8434	0.8441	0.8447	0.8428	0.8422	0.8413
0.7239	0.7257	0.7255	0.7242	0.7234	0.7223
0.6288	0.6360	0.6366	0.6350	0.6338	0.6328
	0.5630	0.5659	0.5660	0.5655	0.5632
		0.5104	0.5105	0.5098	0.5078
		0.4627	0.4651	0.4635	0.4637
			0.4286	0.4268	0.4252

% Resistance Uncertainity

(3) Uncertainty in Convective Heat Transfer Coefficient

Heat Load (W)	FR75%	FR 100%	FR 125%	FR 150%	FR 175%	FR 200%
20	0.0510	0.0510	0.0510	0.0510	0.0510	0.0510
40	0.0270	0.0270	0.0270	0.0270	0.0270	0.0270
60	0.0195	0.0195	0.0195	0.0195	0.0195	0.0195
80	0.0161	0.0161	0.0161	0.0161	0.0161	0.0161
100	0.0142	0.0142	0.0142	0.0142	0.0142	0.0142
120	0.0131	0.0131	0.0131	0.0131	0.0131	0.0131
140	0.0123	0.0124	0.0124	0.0123	0.0123	0.0123
160	0.0118	0.0119	0.0119	0.0118	0.0118	0.0118
180		0.0115	0.0115	0.0115	0.0115	0.0115
200			0.0112	0.0112	0.0112	0.0112
220			0.0110	0.0110	0.0110	0.0110
240				0.0109	0.0109	0.0109

Insulation Thickness 0.05 m

FR75%	FR 100%	FR 125%	FR 150%	FR 175%	FR 200%
5.1020	5.1023	5.1028	5.1029	5.1019	5.1025
2.6978	2.6981	2.6988	2.6979	2.6973	2.6977
1.9505	1.9506	1.9511	1.9504	1.9495	1.9494
1.6077	1.6084	1.6083	1.6075	1.6067	1.6066
1.4204	1.4215	1.4216	1.4206	1.4201	1.4201
1.3081	1.3086	1.3090	1.3078	1.3074	1.3068
1.2345	1.2356	1.2354	1.2347	1.2342	1.2336
1.1813	1.1851	1.1855	1.1846	1.1840	1.1834
	1.1476	1.1490	1.1491	1.1488	1.1477
		1.1227	1.1228	1.1224	1.1215
		1.1019	1.1029	1.1022	1.1023
			1.0880	1.0873	1.0867

% h Uncertainity

References

[1] R. S. Gaugler, "A Heat transfer Device," US2350348, 1944

[2] L. Trefethen, "On the surface tension pumping of liquids or a possible role of the candlewick in space exploration.," G. E. Tech. Info., Ser. No. 615 D114, 1962

[3] G. M. Grover, T. P. Cotter, and G. F. Erickson, "Structures of very high thermal conductivity," *J Appl Phys*, vol. 35, 1964.

[4] B. Zohuri, *Heat pipe design and technology: a practical approach*. CRC Press, 2011.

[5] S. W. Chi, "*Heat Pipe Theory and Practice- A Sourcebook*," Hemisphere publishing corp., 1976.

[6] D. A. Reay., "*Heat Pipes Theory, Design and Applications Sixth Edition*", Elsevier, 2014. [Online]. Available: http://store.elsevier.com/

[7] B. Zohuri, "*Heat Pipe Design and Technology Modern Applications for Practical Thermal Management Second Edition*." Springer, 2016.

[8] H. Jouhara, N. Khordehgah, S. Almahmoud, B. Delpech, A. Chauhan, and S. A. Tassou, "Waste heat recovery technologies and applications," *Thermal Science and Engineering Progress*, vol. 6. Elsevier Ltd, pp. 268–289, Jun. 01, 2018. doi: 10.1016/j.tsep.2018.04.017.

[9] M. Barbosa and H. Mantelli, "*Thermosyphons and Heat Pipes: Theory and Applications*." Springer, 2021.

[10] B. Zohuri, "*Functionality, advancements and industrial applications of heat pipes"*. Academic Press, 2020.

[11] S. Xu, W. Wang, Z. Guo, X. Hu, and W. Guo, "A multi-channel cooling system for multiple heat source," *Thermal Science*, vol. 20, no. 5, 2016, doi: 10.2298/TSCI140313123X.

[12] V. Guichet, S. Almahmoud, and H. Jouhara, "Nucleate pool boiling heat transfer in wickless heat pipes (two-phase closed thermosyphons): A critical review of correlations," *Thermal Science and Engineering Progress*, vol. 13. Elsevier Ltd, Oct. 01, 2019. doi: 10.1016/j.tsep.2019.100384.

[13] A. R. Anand, "Analytical and experimental investigations on heat transport capability of axially grooved aluminum-methane heat pipe," *International Journal of Thermal Sciences*, vol. 139, pp. 269–281, May 2019, doi: 10.1016/j.ijthermalsci.2019.01.028.

[14] G. Wang, Z. Quan, Y. Zhao, and H. Wang, "Performance of a flat-plate micro heat pipe at different filling ratios and working fluids," *Appl Therm Eng*, vol. 146, pp. 459–468, Jan. 2019, doi: 10.1016/j.applthermaleng.2018.10.014.

[15] A. Narayanan, "Thermal performance of internally grooved heat pipe with different flow rate and orientation," 2019. [Online]. Available: www.smenec.org

[16] S. C. Wu, D. Wang, J. H. Gao, Z. Y. Huang, and Y. M. Chen, "Effect of the number of grooves on a wick's surface on the heat transfer performance of loop heat pipe," *Appl Therm Eng*, vol. 71, no. 1, pp. 371–377, Oct. 2014, doi: 10.1016/j.applthermaleng.2014.06.042.

[17] T. W. (Johns H. P. Lab.) Wyatt, "Satellite temperature stabilization system. Early development of spacecraft heat pipes for temperature stabilization," 3,152,774, Oct. 13, 1963

[18] J. E. and K. J. E. Deverall, "High thermal conductance devices utilizing the boiling of lithium and silver, Los Alamos Scientific Laboratory report LA-3211," Oct. 1964.

[19] G. M. Grover, J. Bohdansky, and C. A. Busse, "The use of a new heat removal system in space thermionic power supplies," European atomic energy community, 1965.

[20] J. E. Kemme, "Heat pipe capability experiments," Proceed. of joint AEC/Sandia laboratories report, SCM66623, 1966.

[21] B. Zohuri "*Functionality, advancements and industrial applications of Heat Pipes",* Academic press, 2020.

[22] C. Tarau, W. G. Anderson, and C. J. Peters, "Thermal management system for long-lived venus landers," in *9th Annual International Energy Conversion Engineering Conference, IECEC 2011*, American Institute of Aeronautics and Astronautics Inc., 2011. doi: 10.2514/6.2011-5643.

[23] S. V. Garimella., A. S. Fleischer, J. Y. Murthi, A. Keshavarzi, R. Prasher, S. Patel, S. H. Bhavnani, et. al. "Thermal challenges in next-generation electronic systems," *IEEE Transactions on Components and Packaging Technologies*, vol. 31, no. 4, pp. 801–815, 2008, doi: 10.1109/TCAPT.2008.2001197.

[24] X. Chen, H. Ye, X. Fan, T. Ren, and G. Zhang, "A review of small heat pipes for electronics," *Applied Thermal Engineering*, vol. 96. Elsevier Ltd, pp. 1–17, Mar. 05, 2016. doi: 10.1016/j.applthermaleng.2015.11.048.

[25] Y. Wang, B. Wang, K. Zhu, H. Li, W. He, and S. Liu, "Energy saving potential of using heat pipes for CPU cooling," *Appl Therm Eng*, vol. 143, pp. 630–638, Oct. 2018, doi: 10.1016/j.applthermaleng.2018.07.132.

[26] W. Nakayama, "Heat in Computers: Applied heat transfer in information technology," *J Heat Transfer*, vol. 136, no. 1, 2014, doi: 10.1115/1.4025377.

[27] RR. Riehl, "Utilization of Passive Thermal Control Technologies for Electronics Cooling: A Brief Review," *J Appl Mech Eng*, vol. 5, no. 4, 2016, doi: 10.4172/2168-9873.1000214.

[28] V. G. Pastukhov, Y. F. Maidanik, C. V. Vershinin, and M. A. Korukov, "Miniature loop heat pipes for electronics cooling," in *Applied Thermal Engineering*, Elsevier Ltd, 2003, pp. 1125–1135. doi: 10.1016/S1359-4311(03)00046-2.

[29] S. M. Sohel Murshed and C. A. Nieto de Castro, "A critical review of traditional and emerging techniques and fluids for electronics cooling," *Renewable and Sustainable Energy Reviews*, vol. 78. Elsevier Ltd, pp. 821–833, 2017. doi: 10.1016/j.rser.2017.04.112.

[30] A. C. Kheirabadi and D. Groulx, "Cooling of server electronics: A design review of existing technology," *Applied Thermal Engineering*, vol. 105. Elsevier Ltd, pp. 622–638, Jul. 25, 2016. doi: 10.1016/j.applthermaleng.2016.03.056.

[31] P. Qu, J. Cheng, Y. Chen, Y. Li, W. Li, and H. Tao, "Numerical and experimental investigation on heat transfer of multi-heat sources mounted on a fined radiator within embedded heat pipes in an electronic cabinet," *International Journal of Thermal Sciences*, vol. 183, Jan. 2023, doi: 10.1016/j.ijthermalsci.2022.107833.

[32] H. Tang, Y. Tang, J. Li, Y. Sun, G. Liang, and R. Peng, "Experimental investigation of the thermal performance of heat pipe with multi-heat source and double-end cooling," *Appl Therm Eng*, vol. 131, pp. 159–166, Feb. 2018, doi: 10.1016/j.applthermaleng.2017.12.006.

[33] Y. Cai, Z. Li, J. Zhai, Y. Tang, and B. Yu, "Experimental investigation on a novel multi-branch heat pipe for multi-heat source electronics," *Int J Heat Mass Transf*, vol. 104, pp. 467–477, Jan. 2017, doi: 10.1016/j.ijheatmasstransfer.2016.08.080.

[34] L. Fourgeaud, V. Dupont, R. Mari, and C. Figus, "Experimental investigations of a Multi-Source Loop Heat Pipe for electronics cooling Cable cars safety items development View project SOCOOL (Solutions for Cooling) View project Experimental investigations of a Multi-Source Loop Heat Pipe for electronics cooling-phase flow; boiling in tube." [Online]. Available: https://www.researchgate.net/publication/326588649

[35] B. Xiao *et al.*, "Experimental investigation of loop heat pipe with a large squared evaporator for multi-heat sources cooling," *Renew Energy*, vol. 147, pp. 239–248, Mar. 2020, doi: 10.1016/j.renene.2019.08.142.

[36] C. Liu *et al.*, "Experimental study on temperature uniformity and heat transfer performance of nitrogen loop heat pipe with large area and multi-heat source," *Appl Therm Eng*, vol. 210, Jun. 2022, doi: 10.1016/j.applthermaleng.2022.118344.

[37] J. H. Boo and H. G. Kim, "Experimental study on the performance characteristics of a cylindrical heat pipe having a screen wick subject to multiple heat sources," *Appl Therm Eng*, vol. 126, pp. 1209–1215, Nov. 2017, doi: 10.1016/j.applthermaleng.2017.02.097.

[38] X. Han, Y. Wang, and Q. Liang, "Investigation of the thermal performance of a novel flat heat pipe sink with multiple heat sources," *International Communications in Heat and Mass Transfer*, vol. 94, pp. 71–76, May 2018, doi: 10.1016/j.icheatmasstransfer.2018.03.017.

[39] S. Okutani, H. Nagano, S. Okazaki, H. Ogawa, and H. Nagai, “Operating Characteristics of Multiple Evaporators and Multiple Condensers Loop Heat Pipe with Polytetrafluoroethylene Wicks,” *Journal of Electronics Cooling and Thermal Control*, vol. 04, no. 01, pp. 22–32, 2014, doi: 10.4236/jectc.2014.41003.

[40] E. Sedighi, A. Amarloo, and M. B. Shafii, “Experimental investigation of the thermal characteristics of single-turn pulsating heat pipes with an extra branch,” *International Journal of Thermal Sciences*, vol. 134, pp. 258–268, Dec. 2018, doi: 10.1016/j.ijthermalsci.2018.08.024.

[41] V. G. Pastukhov and Y. F. Maydanik, “Development and tests of a loop heat pipe with several separate heat sources,” *Appl Therm Eng*, vol. 144, pp. 165–169, Nov. 2018, doi: 10.1016/j.applthermaleng.2018.08.051.

[42] R. Zhang, L. Yan, and C. Wu, “Experimental study on the effect of various heat source configurations on the thermal performance of an axial swallow-tailed micro-grooved heat pipe,” *Heat and Mass Transfer*, vol. 56, no. 4, pp. 1237–1248, Apr. 2020, doi: 10.1007/s00231-019-02761-4.

[43] R. Zhang, “Evaporation thermal analysis of Swallow-tailed Axial-grooved Heat Pipe,” in *IOP Conference Series: Earth and Environmental Science*, Institute of Physics Publishing, Mar. 2018. doi: 10.1088/1755-1315/128/1/012124.

[44] P. R. Mashaei, M. Shahryari, H. Fazeli, and S. M. Hosseinalipour, “Numerical simulation of nanofluid application in a horizontal mesh heat pipe with multiple heat sources: A smart fluid for high efficiency thermal system,” *Appl Therm Eng*, vol. 100, pp. 1016–1030, May 2016, doi: 10.1016/j.applthermaleng.2016.02.111.

[45] J. Huang *et al.*, “Thermal performance of flexible branch heat pipe,” *Appl Therm Eng*, vol. 186, Mar. 2021, doi: 10.1016/j.applthermaleng.2020.116532.

[46] N. Phan, Y. Saito, N. Katayama, and H. Nagano, “Operating characteristics of a dual flat-evaporator loop heat pipe for single heat source cooling in any orientation,” *Int J Heat Mass Transf*, vol. 172, Jun. 2021, doi: 10.1016/j.ijheatmasstransfer.2021.121146.

[47] Z. Lataoui, C. Romestant, Y. Bertin, A. Jemni, and D. Petit, “Inverse thermal analysis of the drying zone of the evaporator of an axially grooved heat pipe,” *Exp Therm Fluid Sci*, vol. 34, no. 5, pp. 562–574, Jul. 2010, doi: 10.1016/j.expthermflusci.2009.11.009.

[48] G. Huang, W. Li, G. Zhong, A. A. Abdulshaheed, and C. Li, “Optimizing L-shaped heat pipes with partially-hybrid mesh-groove wicking structures,” *Int J Heat Mass Transf*, vol. 170, May 2021, doi: 10.1016/j.ijheatmasstransfer.2021.120926.

[49] L. Jiang, Y. Tang, M. Pan, W. Zhou, and L. Lu, “Phase change flattening process for axial grooved heat pipe,” *J Mater Process Technol*, vol. 212, no. 1, pp. 331–338, Jan. 2012, doi: 10.1016/j.jmatprotec.2011.09.019.

[50] B. Subedi, S. H. Kim, S. P. Jang, and M. A. Kedzierski, “Effect of mesh wick geometry on the maximum heat transfer rate of flat-micro heat pipes with multi-heat sources and sinks,” *Int J Heat Mass Transf*, vol. 131, pp. 537–545, Mar. 2019, doi: 10.1016/j.ijheatmasstransfer.2018.11.086.

[51] T. Wu, T. Wang, Z. Ma, Z. Zhang, W. Liu, and Z. Liu, “Experimental investigation on the start-up performance of a loop heat pipe with three flat disk evaporators combined,” *Appl Therm Eng*, vol. 216, Nov. 2022, doi: 10.1016/j.applthermaleng.2022.119128.

[52] V. Guichet, B. Delpech, and H. Jouhara, “Experimental investigation, CFD and theoretical modeling of two-phase heat transfer in a three-leg multi-channel heat pipe,” *Int J Heat Mass Transf*, vol. 203, Apr. 2023, doi: 10.1016/j.ijheatmasstransfer.2022.123813.

[53] G. Zhong *et al.*, “Various orientations research on thermal performance of novel multi-branch heat pipes with different sintered wicks,” *Energy Convers Manag*, vol. 166, pp. 512–521, Jun. 2018, doi: 10.1016/j.enconman.2018.04.066.

[54] I. Saad, S. Maalej, and M. C. Zaghdoudi, “Modeling of the EHD effects on hydrodynamics and heat transfer within a flat miniature heat pipe including axial capillary grooves,” *J Electrostat*, vol. 85, pp. 61–78, Feb. 2017, doi: 10.1016/j.elstat.2016.12.004.

[55] L. L. Jiang, Y. Tang, and M. Q. Pan, “Effects of bending on heat transfer performance of axial micro-grooved heat pipe,” *Journal of Central South University of Technology (English Edition)*, vol. 18, no. 2, pp. 580–586, Apr. 2011, doi: 10.1007/s11771-011-0734-2.

[56] A. Bhatt, S. Jain, R. N. Patel, and D. Vaghela, “Parametric Study on Axially Grooved Heat Pipe with Two Heat Sources and One Heat Sink with Multiple Branches,” *J Therm Sci Eng Appl*, pp. 1–27, Mar. 2023, doi: 10.1115/1.4062155.

[57] W. I. A. Aly, M. A. Elbalshouny, H. M. Abd El-Hameed, and M. Fatouh, “Thermal performance evaluation of a helically-micro-grooved heat pipe working with water and aqueous Al2O3 nanofluid at different inclination angle and filling ratio,” *Appl Therm Eng*, vol. 110, pp. 1294–1304, Jan. 2017, doi: 10.1016/j.applthermaleng.2016.08.130.

[58] K. Zhu, X. Li, Y. Wang, X. Chen, and H. Li, “Dynamic performance of loop heat pipes for cooling of electronics,” in *Energy Procedia*, Elsevier Ltd, 2017, pp. 4163–4168. doi: 10.1016/j.egypro.2017.12.341.

[59] H. Alijani, B. Çetin, Y. Akkuş, and Z. Dursunkaya, “Experimental Thermal Performance Characterization of Flat Grooved Heat Pipes,” *Heat Transfer Engineering*, vol. 40, no. 9–10, pp. 784–793, Jun. 2019, doi: 10.1080/01457632.2018.1442395.

[60] J. Jose and T. Kumar Hotta, “A comprehensive review of heat pipe: Its types, incorporation techniques, methods of analysis and applications,” *Thermal Science and Engineering Progress*, vol. 42. Elsevier Ltd, Jul. 01, 2023. doi: 10.1016/j.tsep.2023.101860.

[61] W. Yao, C. Liu, X. Kong, Z. Zhang, Y. Wang, and W. Gao, "A systematic review of heat pipe applications in buildings," *Journal of Building Engineering*, vol. 76. Elsevier Ltd, Oct. 01, 2023. doi: 10.1016/j.jobe.2023.107287.

[62] D. M. Weragoda, G. Tian, A. Burkitbayev, K. H. Lo, and T. Zhang, "A comprehensive review on heat pipe-based battery thermal management systems," *Applied Thermal Engineering*, vol. 224. Elsevier Ltd, Apr. 01, 2023. doi: 10.1016/j.applthermaleng.2023.120070.

[63] A. A. Pesaran, "Battery thermal models for hybrid vehicle simulations." *Journl. Of Power Sources*, vol 110, issue 2, Elsevier, 2002.

[64] A. Driss, S. Maalej, and M. C. Zaghdoudi, "Experimentation and modeling of the steady-state and transient thermal performances of a helicoidally grooved cylindrical heat pipe," *Microelectronics Reliability*, vol. 62, pp. 102–112, Jul. 2016, doi: 10.1016/j.microrel.2016.03.022.

[65] H. Wang *et al.*, "An integrated heat pipe coupling the vapor chamber and two cylindrical heat pipes with high anti-gravity thermal performance," *Appl Therm Eng*, vol. 159, Aug. 2019, doi: 10.1016/j.applthermaleng.2019.113816.

[66] T. Tharayil, L. G. Asirvatham, C. F. M. Cassie, and S. Wongwises, "Performance of cylindrical and flattened heat pipes at various inclinations including repeatability in anti-gravity – A comparative study," *Appl Therm Eng*, vol. 122, pp. 685–696, 2017, doi: 10.1016/j.applthermaleng.2017.05.007.

[67] X. Wang *et al.*, "A review on data center cooling system using heat pipe technology," *Sustainable Computing: Informatics and Systems*, vol. 35, Sep. 2022, doi: 10.1016/j.suscom.2022.100774.

[68] K. Liang, Z. Li, M. Chen, and H. Jiang, "Comparisons between heat pipe, thermoelectric system, and vapour compression refrigeration system for electronics cooling," *Appl Therm Eng*, vol. 146, pp. 260–267, Jan. 2019, doi: 10.1016/j.applthermaleng.2018.09.120.

[69] K. Shailesh, Y. Naresh, and J. Banerjee, "Heat transfer performance of a novel PCM based heat sink coupled with heat pipe: An experimental study," *Appl Therm Eng*, vol. 229, Jul. 2023, doi: 10.1016/j.applthermaleng.2023.120552.

[70] S. R. Akhil Krishnan, S. Sivan, V. C. Midhun, and S. R. Behera, "Experimental and numerical investigation of solid-solid phase change material assisted heat sink with integrated heat pipe for electronic cooling," *J Energy Storage*, vol. 59, Mar. 2023, doi: 10.1016/j.est.2022.106494.

[71] K. Natesan and S. Karinka, "A comprehensive review of heat transfer enhancement of heat exchanger, heat pipe and electronic components using graphene," *Case Studies in Thermal Engineering*, vol. 45, May 2023, doi: 10.1016/j.csite.2023.102874.

[72] G. E. Moore, "Cramming More Components onto Integrated Circuits." Proceedings of IEEE, vol. 86, issue 1, 1998.

[73] Z. Zhang, X. Wang, and Y. Yan, “A review of the state-of-the-art in electronic cooling,” *e-Prime - Advances in Electrical Engineering, Electronics and Energy*, vol. 1. Elsevier Ltd, Jan. 01, 2021. doi: 10.1016/j.prime.2021.100009.

[74] L. Ling, Q. Zhang, Y. Yu, and S. Liao, “A state-of-the-art review on the application of heat pipe system in data centers,” *Appl Therm Eng*, vol. 199, Nov. 2021, doi: 10.1016/j.applthermaleng.2021.117618.

[75] J. Shen, J. Fang, H. Sips, and A. L. Varbanescu, “An application-centric evaluation of OpenCL on multi-core CPUs,” *Parallel Comput*, vol. 39, no. 12, pp. 834–850, Dec. 2013, doi: 10.1016/j.parco.2013.08.009.

[76] I. Gabsi, S. Maalej, and M. C. Zaghdoudi, “Thermal performance modeling of loop heat pipes with flat evaporator for electronics cooling,” *Microelectronics Reliability*, vol. 84, pp. 37–47, May 2018, doi: 10.1016/j.microrel.2018.02.023.

[77] S. K. Hota, K. L. Lee, B. Leitherer, G. Elias, G. Hoeschele, and S. Rokkam, “Pulsating heat pipe and embedded heat pipe heat spreaders for modular electronics cooling,” *Case Studies in Thermal Engineering*, vol. 49, Sep. 2023, doi: 10.1016/j.csite.2023.103256.

[78] C. Liu *et al.*, “Experimental study on temperature uniformity and heat transfer performance of nitrogen loop heat pipe with large area and multi-heat source,” *Appl Therm Eng*, vol. 210, Jun. 2022, doi: 10.1016/j.applthermaleng.2022.118344.

[79] W. Thepsut and N. Pratinthong, “Numerical and experimental investigation on heat transfer of multi-heat sources mounted on an array of printed circuit boards in a rectangular case,” *Appl Therm Eng*, vol. 156, pp. 156–167, Jun. 2019, doi: 10.1016/j.applthermaleng.2019.04.032.

[80] Y. Qu, S. Wang, and Y. Tian, “A review of thermal performance in multiple evaporators loop heat pipe,” *Applied Thermal Engineering*, vol. 143. Elsevier Ltd, pp. 209–224, Oct. 01, 2018. doi: 10.1016/j.applthermaleng.2018.07.070.

[81] H. Zhou, T. Tian, X. Wang, and J. Li, “Combining looped heat pipe and thermoelectric generator module to pursue data center servers with possible power usage effectiveness less than 1,” *Appl Energy*, vol. 332, Feb. 2023, doi: 10.1016/j.apenergy.2022.120539.

[82] L. Deng *et al.*, “Thermal study of the natural air-cooling using roll bond flat heat pipe as plate fin under multi-heat source condition,” *International Journal of Thermal Sciences*, vol. 183, Jan. 2023, doi: 10.1016/j.ijthermalsci.2022.107834.

[83] R. Li *et al.*, “Experimental investigation of the thermal performance of high-temperature flat heat pipe with a single heat source and a multi heat source,” *Thermal Science and Engineering Progress*, vol. 43, p. 101977, Aug. 2023, doi: 10.1016/j.tsep.2023.101977.

[84] M. A. Chernysheva and Y. F. Maydanik, “Analysis of the thermal resistance of a loop heat pipe based on the P-T diagram of the working fluid operating cycle.,” *Int J Heat Mass Transf*, vol. 209, Aug. 2023, doi: 10.1016/j.ijheatmasstransfer.2023.124157.

[85] M. Kim, K. H. Lee, D. I. Han, and J. H. Moon, “Numerical case study and modeling for spreading thermal resistance and effective thermal conductivity for flat heat pipe,” *Case Studies in Thermal Engineering*, vol. 31, Mar. 2022, doi: 10.1016/j.csite.2022.101803.

[86] L. Tao, D. Zhengyu, H. Hui, H. Xiaoqiang, Q. Wenhai, and X. Jinbiao, “Experimental investigation on effective thermal conductivity of powder-packed assembly gaps in heat pipe cooled reactor core,” *Nuclear Engineering and Design*, vol. 388, Mar. 2022, doi: 10.1016/j.nucengdes.2021.111611.

[87] M. Mohammadiun, H. Mohammadiun, R. Alizadeh, M. Mesgarpour, A. Younesian, and S. Jowkar, “The effect of variable temperature and location on relative thermal conductivity (RTC) on the heat pipe in the presence of AL_2O_3 nanoparticles: Numerical and optimization approaches,” *J Taiwan Inst Chem Eng*, vol. 124, pp. 132–149, Jul. 2021, doi: 10.1016/j.jtice.2021.04.050.

[88] C. Guo, T. Wang, C. Guo, Y. Jiang, S. Tan, and Z. Li, “Effects of filling ratio, geometry parameters and coolant temperature on the heat transfer performance of a wraparound heat pipe,” *Appl Therm Eng*, vol. 200, Jan. 2022, doi: 10.1016/j.applthermaleng.2021.117724.

[89] X. Liu *et al.*, “Effect of evaporation and condensation section length ratio on thermal performance of aluminum flat plate heat pipe with different micro grooved wicks,” *Appl Therm Eng*, vol. 233, Oct. 2023, doi: 10.1016/j.applthermaleng.2023.121115.

[90] Y. A. Cengel, “*Heat Transfer: A Practical Approach*”, second Edition, McGrow hill, 2019. Y. A. Cengel, “*Heat Transfer: A Practical Approach*”, second Edition, McGrow hill, 2019.

[91] S. J. Kline, “The Purposes of Uncertainty Analysis,” *Journal of Fluids Engineering*, vol. 107, pp. 153–160, 1985.

[92] K. M. Kim, Y. S. Jeong, I. G. Kim, and I. C. Bang, “Comparison of thermal performances of water-filled, SiC nanofluid-filled and SiC nanoparticles-coated heat pipes,” *Int J Heat Mass Transf*, vol. 88, pp. 862–871, Sep. 2015, doi: 10.1016/j.ijheatmasstransfer.2015.04.108.

[93] X. Sun, L. Zhang, and S. Liao, “Performance of a thermoelectric cooling system integrated with a gravity-assisted heat pipe for cooling electronics,” *Appl Therm Eng*, vol. 116, pp. 433–444, 2017, doi: 10.1016/j.applthermaleng.2016.12.094.

[94] H. Y. Zhang, Y. C. Mui, and M. Tarin, “Analysis of thermoelectric cooler performance for high power electronic packages,” *Appl Therm Eng*, vol. 30, no. 6–7, pp. 561–568, May 2010, doi: 10.1016/j.applthermaleng.2009.10.020.

[95] M. Mahdavi, S. Tiari, S. De Schampheleire, and S. Qiu, “Experimental study of the thermal characteristics of a heat pipe,” *Exp Therm Fluid Sci*, vol. 93, pp. 292–304, May 2018, doi: 10.1016/j.expthermflusci.2018.01.003.

[96] J. Seo and J. Y. Lee, “Length effect on entrainment limitation of vertical wickless heat pipe,” *Int J Heat Mass Transf*, vol. 101, pp. 373–378, Oct. 2016, doi: 10.1016/j.ijheatmasstransfer.2016.05.096.

[97] A. A. Bhatt, S. V. Jain, and R. N. Patel, “Experimental Investigations on Performance Analysis of a Wickless Thermosiphon Heat Pipe with Two Heat Sources and Multiple Branches,” *J Therm Sci Eng Appl*, vol. 14, no. 10, Oct. 2022, doi: 10.1115/1.4054163.

[98] C. Ömür, A. Bilge Uygur, İ. Horuz, G., and M. Müh Böl, “The effect of manufacturing limitations on groove design and its implementation to an algorithm for determining heat transport capability of heat pipes,” *J. of Thermal Science and Technology*, vol. 37, pp. 159–170, 2017.

[99] A. K. Mozumder, M. S. H. Chowdhury, and A. F. Akon, “Characteristics of Heat Transfer for Heat Pipe and Its Correlation,” *ISRN Mechanical Engineering*, vol. 2011, pp. 1–7, Apr. 2011, doi: 10.5402/2011/825073.

[100] C. Ömür, A. B. Uygur, İ. Horuz, H. G. Işık, S. Ayan, and M. Konar, “Incorporation of manufacturing constraints into an algorithm for the determination of maximum heat transport capacity of extruded axially grooved heat pipes,” *International Journal of Thermal Sciences*, vol. 123, pp. 181–190, Jan. 2018, doi: 10.1016/j.ijthermalsci.2017.09.016.

[101] A. L. S. Sudhan, A. B. Solomon, and S. Sunder, “Heat transport limitations and performance enhancement of anodized grooved heat pipes charged with ammonia under gravity and anti-gravity condition,” *Appl Therm Eng*, vol. 200, Jan. 2022, doi: 10.1016/j.applthermaleng.2021.117633.

List of Journal Publications

1. Bhatt, A.A., Jain, S.V., Patel, R.N, 2022, Experimental Investigation on Performance Analysis on Wickless Thermosiphon Heat Pipe with Two Heat Sources and Multiple Branches", ASME J. Therm. Sci. Eng. Appl., **14,** P. 101006.
   doi: https://doi.org/10.1115/1.4054163
2. Bhatt, A.A., Jain, S.V., Patel, R.N, Vaghela, D., 2023, "Parametric Study on Axially Grooved heat pipe with two heat sources and one heat sink with multiple branches". ASME J. Therm. Sci. Eng. Appl.,
   doi: https://doi.org/10.1115/1.4062155

3. **Accepted (Heat and Mass Transfer-Springer):** Bhatt, A.A., Jain., S.V., Patel, R.N, Vaghela, D., 2023, "Experimental Investigations on Novel Orientation Study on Axially Grooved Heat Pipe with Two Evaporators and one condenser with Multiple Branches"

Conference

4. **Accepted:** "*Experimental Investigation on axially grooved heat pipe with 16 number of grooves for determination of optimum filling ratio and heat load***. – Paper Submitted in 10th International conference in fluid mechanics and fluid power (FMFP 2023) to be organized by IIT, Jodhpur in December 2023.**"